Designing Models for the Dynamics of T-Cell Clones: Antigen Presentation and Ageing

D I S S E R T A T I O N

zur Erlangung des akademischen Grades
doctor rerum naturalium
(Dr. rer. nat.)
im Fach Biophysik

eingereicht an der
Mathematisch-Naturwissenschaftlichen Fakultät I
Humboldt-Universität zu Berlin

von
Dottore in Fisica
Fabio Luciani
geboren am 18.04.1974 in Lanciano, Italien

Präsident der Humboldt-Universität zu Berlin:
Prof. Dr. Jürgen Mlynek

Dekan der Mathematisch-Naturwissenschaftlichen Fakultät I:
Prof. Thomas Buckhout, PhD

Gutachter/innen:

1. Prof. Hans Georg Holzhütter
2. Dr. Michal Or-Guil
3. Dr. Alexej Zaikin

eingereicht am:	11. Juli 2005
Tag der mündlichen Prüfung:	6. Januar 2006

Abstract

The major tasks of the immune system are the protection of the body from undesired external pathogenic attack and the prevention of further and already experienced challenges, which are avoided by the establishment of immunological memory. At the top of the philogenetic tree, the evolution has developed a specific (adaptive) immunity which cooperates with the ancestral innate immunity to control the antigenic insults T-cells are the protagonist of the adaptive immune response in fighting against intracellular infections and in the maintenance of self-tolerance. The T-cell repertoire is characterized by high diversity and size. Moreover, they share and compete each others for resources such as cytokines, MHC-peptide complexes and immunological space. The proteasome machinery plays a crucial role in the maintenance of cell functionality by destroying undesired or unfunctional proteins. Moreover, the proteasome is an important step in the generation of antigenic peptides which, ones mounted on the MHC molecules, are responsible for the activation of T-cell during an immune response.

During ageing the immune system undergoes an extended reshaping of the T-cell repertoire, which is now characterized by a different diversity and composition. This phenomenon seems to be a major cause for the increase in the mortality rate for elderly people. In this PHD thesis the study of the T-cells dynamics and their homeostasis has been investigated. In particular we focused on the following questions

What is the immunological function of the intracellular protein degradation? And in particular, what is the immunological function of the proteasome?

What is the role of the chronic antigenic stimuli on the T-cell dynamics and homeostasis? Can the reshaping of the immune system during ageing influence the survival probability of individuals?

Chapter 1 offers an introduction to the immunological aspects which will be considered along this thesis.

The study presented in Chapter 2 evidenced that the length and the amount of fragments generated by the proteasome degradation fairly depend on the size of the gates regulating the flux of substrate through the proteasome. This model captures the known characteristics of proteasomal degradation, and can therefore help to quantify MHC antigen processing and presentation.

In Chapter 3 we reviewed several models based on ecological concepts like competitive exclusion and co-existence in the context of the T- and B-cell

repertoire. Based on this literature, in Chapter 4 we present a model dealing with the dynamics of cytotoxic T-cells and the role of the antigen presentation in shaping the T-cell repertoire. We propose that the replacement of constitutive proteasome with the immunoproteasome, a form of proteasome which is believed to play a role during an immune response, re-shapes significantly the T-cell clone repertoire and helps to mount a fast and effective immune response.

Chapter 5 has been devoted to the population dynamics of cytotoxic T-cells over a long timescale. A stochastic differential equation model describing the maintenance of T-cell memory clones has been proposed. The model suggests that the size and the conformation of the T-cell pool depends on the chronic stimulation impinging upon the system over long timescale.

Chapter 6, is an attempt to use T-cell dynamics to understand demographic data. We test the hypothesis that the shrinkage of the naive T-cell repertoire over the lifespan is a major cause of mortality for human individuals. A model describing the demographic data is proposed and a comparison with the standard theory of survival curve has been developed.

The conclusions are: the kinetics of the antigen presentation and its quantification are critical aspects for the understanding of the maintenance and the functionality of the T-cell repertoire. The Immune system takes advantage of the kinetics of proteasome and the competition for resources in the T-cell repertoire to develop a clever strategy to challenge infections without expensive production of new resources. Future works are needed to understand how T-cells are extremely efficient weapon against acute infections, but it seems to cause a reshaping of the immune system with detrimental effects during ageing.

Keywords:
Proteasome, Antigen Presentation, T cell, Ageing

Zusammenfassung

Die Hauptaufgabe des Immunsystems ist der Schutz des Körpers gegen den externen Angriff von Viren, Bakterien und sonstigen potentiellen Krankheitserregern, sowie die Vermeidung von weiteren Infektionen durch bereits erfahrene Pathogene, die durch die Errichtung eines immunologischen Gedächtnisses vermieden werden. Das Repertoire von T-Zellen ist charakterisiert durch hohe Diversität und grossem Umfang. Darüberhinaus konkurrieren T-Zellen um Ressourcen wie zum Beispiel Zytokine, MHC-Peptidkomplexe und immunologischen Raum. Das Proteasom spielt eine wichtige Rolle in der Instandhaltung von Zellfunktionalität, indem es unerwünschte und nicht funktionelle Proteine abbaut. Weiterhin stellt das Proteasom einen wichtigen Schritt in der Produktion von antigenischen Peptiden dar, die, sobald sie von MHC-Moleküle präsentiert werden, für die Aktivierung von T-Zellen in der Immunantwort verantwortlich sind. Während des Alterungsprozesses durchläuft das Immunsystem eine umfangreiche Veränderung des T-Zell-Repertoires in Diversität und Zusammensetzung. Diese Arbeit untersucht die Dynamik und die Homeostase von T-Zellen. Insbesondere beleuchtet diese Arbeit folgende Fragen:

- Was ist die immunologische Funktion von intrazellulärer Proteindegradation? Und was ist die immunologische Funktion des Proteasoms?
- Welche Rolle spielen chronisch antigenische Stimuli in der T-Zell-Dynamik und Homeostase? Kann die Veränderung des Immunsystems während des Alterungsprozesses die Überlebensratewahrscheinlichkeit von Individuen beeinflussen ?

Kapitel 1 bietet eine Einführung in grundlegende immunologische Aspekte, die im Verlaufe dieser Arbeit von Bedeutung sind.

Kapitel 2 präsentiert eine Studie, die belegt, dass die Länge und Grösse von Fragmenten, die während der Proteasomedegradation entstehen, sehr von der Grösse der Schranke abhängt, die den Substratfluss durch das Proteasom steuert. Das hier vorgestellte Modell reproduziert die bekannten Charakteristika von Proteosomedegradation sehr gut und kann daher in der Quantifizierung des antigenischen Umsatzes und deren Präsentation von grossem Nutzen sein.

Kapitel 3 bietet eine Übersicht über einige ökologisch basierte, bereits veröffentlichte Modelle wie zum Beispiel die kompetitive Exklusion und Koexistenz im Kontext des T- und B-Zell-Repertoires.

Im Kapitel 4 stellen wir die Vermutung an, dass die Ersetzung von konstitutivem Proteasom durch Immunoproteasom, die während einer Immunantwort in antigenpräsentierenden Zellen stattfindet, das T-Zell-Repertoire stark verändert und dabei hilft, eine schnelle und effektive Immunreaktion zu starten.

Kapitel 5 ist der Populationsdyamik von zytotoxischen T-Zellen über lange Zeitskalen gewidmet. Ein stochastisches Differentialgleichungsmodell wird vorgestellt, das die Dynamik von T-Zell-Gedächtnisklone beschreibt. Das Modell legt nahe, dass der Umfang und die Diversität des T-Zell-Pools von der chronischen Stimulation abhängt, die auf das System über lange Zeiträume hinweg einwirkt.

In Kapitel 6 wird ein Modell eingeführt, welches demographische Prozesse unter Berücksichtigung der T-Zell-Dynamik beschreibt. Wir testen die Hypothese, dass der Rückgang des naiven T-Zell-Repertoires über die Lebensspanne eine Hauptursache für die Sterblichkeit des Individuums darstellt. Ein Vergleich mit der Standardtheorie der Überlebenskurve wird entwickelt.

Die Schlussfolgerungen dieser Dissertation sind: Die Kinetik der antigenischen Präsentation und ihre Quantifizierung sind wichtige Aspekte für das Verstehen der Instandhaltung und Funktionalität des T-Zell-Repertoires. Das Immunsystem nutzt die Kinetik des Proteasoms und den Wettbewerb um Ressourcen zwischen den T-Zellen zur Entwicklung von cleveren Strategien gegen Infektionen aus, ohne dabei auf die Produktion von teueren neuen Ressourcen zurückgreifen zu müssen.

Schlagwörter:
Proteasome, Antigen Presentation, T Zell, Ageing

Contents

List of Figures

List of Tables

Chapter 1

Introduction

1.1 The adaptive immune system

The immune system (IS) preserves the integrity of the organism, continuously challenged by internal and external agents (antigens). The large variety of antigens ranging from mutated cells and parasites to viruses, bacteria and fungi requires a rapid and efficient antagonistic response of the organism. At the top of the philogenetic tree, evolution has developed a specific (clonotypic) immunity, which cooperates with the ancestral innate immunity to control antigenic insults [Lanzavecchia and Sallusto, 2000]. The innate system has a vast arsenal of dendritic cells and macrophages with a limited number of receptors, capable of recognizing and neutralizing classes of antigens. The increase of complexity in vertebrate organisms stimulated the development of a system based on two new types of cells, B- and T-lymphocytes, with three distinct tasks: to recognize the antigens, to destroy them and to keep track of their structure through a learning process. This kind of immunological memory paves the way for a more efficient response to any subsequent antigenic insult caused by an antigen that the organism has already experienced. This is also the immunological basis of vaccination strategies.

The diversity of the lymphocyte repertoire changes during the lifespan. The diversity of the naive pool decreases continuously since it undergoes an activation and differentiation process. Antigen experienced (AE) cells suffer clonal expansion, gradually filling the immunological space available. Competition phenomena were shown to play an important role in shaping the lymphocyte repertoire.

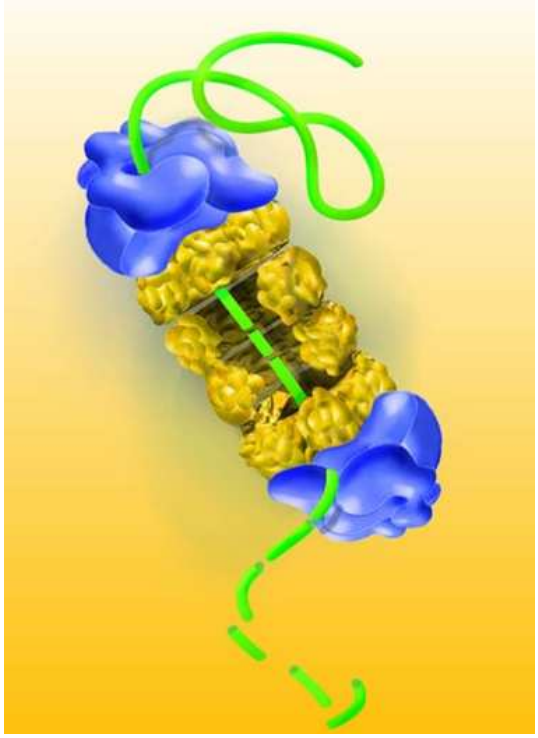

Figure 1.1: The proteasome is the major intracellular protease. It is involved in the maintenance of the cellular physiology and plays a significant role in the processing of intracellular antigenic peptides.

The lymphocyte repertoire

The adaptive immune system of vertebrate animals has evolved to respond to different types of perturbations (invading pathogens, stress signals), limiting self-tissue damage. Adaptive immunity evolved when gene rearrangements were employed to generate highly diverse lymphocyte repertoire. The adaptive IS is organized to fight both intracellular and extracellular pathogenic attacks. The lymphocyte repertoire is consists of approximately 10^{10} clones, with a variability of at least 3×10^7 different clones [Arstila et al., 1999]. B-cells are responsible for the recognition of antigens present in the extracellular environment and constitute the main players of the humoral immune response. B-cells produce antibodies, which are able to bind and destroy pathogens. In order to mount an effective IR, B-cells need help from a subset of T-cells which are called T-helper. The latter provides costimulatory signals which allow the activation and proliferation of B-cells. On the other hand, T-cells are involved in the recognition of intracellular peptides and are

responsible for the cellular immune response. Intracellular antigens are presented by the antigen presenting cell (APC), which displays the MHC-peptide complex (MHCp) on their surface. APCs can be simply infected cells or professional soldiers like dendritic cells, which possess the unique capacity to interact with cytotoxic T-cells and to stimulate their proliferation.

Cytotoxic T-cell activation is mediated by professional APCs. They proliferate and differentiate into effector cells, which kill infected cells presenting the specific antigen on their surface via MHC-class I molecules. MHC molecules can be envisaged as the identity-card of almost all cells of the organism. MHCs allow the IS to recognize the state and the origin of the cells present in the organism preventing unwanted attacks from the IS against healthy-self cells. T-cells, as well as B-cells, require two signals in order to be activated and to proliferate: the antigen as a primary signal, and a secondary more general costimulatory signal, which is typically provided by professional APCs, like dendritic cells (DC) and macrophages. DCs are the most important professional APCs that are seeded throughout peripheral tissues to act as sentinels that process and present antigen to mount adequate immune responses.

Depending on the type of antigen, and tissue localization, the IR is suppressed or activated. Indeed, self-antigens can be derived from their innocuous environment, such as necrotic and apoptotic cells that need to be scavenged before they disintegrate. Alternatively, non self-antigens are foreign products from invading pathogens that need to be eliminated. The main function of DCs is to capture antigen for processing and presentation as antigenic fragments on major histocompatibility complex for naive T-cell activation In a steady-state situation, prior to acute infection and inflammation, DCs are in an immature state and are not fully differentiated to carry out their known roles as inducers of immunity. They are not unresponsive as they actively circulate through tissues and into lymphoid organs, capturing self-antigens as well as innocuous environmental proteins. In a state of alarm such as a microbial invasion, or massive cell death, immature DCs receive simultaneous activation signals through the binding of conserved molecular motifs by pattern recognition receptors, such as Toll-like receptors or specific tumor necrosis factor (TNF) family members. This results in DC maturation and migration to secondary lymphoid organs, where DCs present the processed antigens to naive T-cells and induce antigen-specific immune responses.

At the turn of the last century, Ehrlich and Metchnikoff debated passionately over the relative importance of humoral versus cellular immunity in protecting hosts against pathogens and foreign substances. The delay in appreciating the importance of cellular immunity was due to its greater

complexity than humoral immunity. The role of the B-cell is to produce high-affinity protective antibodies. To succeed in this function, it attempts to increase the affinity of its receptors for the immunizing antigen by mutating its variable-region genes. Antigen recognition via T-cells, which is driven by the T-cell receptor (TCR) present on the surface of T-cells, is not simply based on TCR-antigen interaction as it occurs for the B-cell receptor (antibody) with extracellular antigens. The variable regions of T-cells cannot bind directly to antigen, and their genes do not mutate. Instead, an antigen-activated T-cell forms clusters of receptors with high avidity for the antigen presented on the cell surface via MHC class I or class II molecule [Janeway et al., 2001].

The selection mechanisms which define the specific T-cell over hundreds of different T-cell clones which receive a positive stimulus from the MHCp is still largely unknown. Cytotoxic (or CD8+) T-cells, which recognize MHC class I molecules, have a particularly important role in viral infections. MHC class I peptide ligands are generated from intracellular proteins that are synthesized by target cells, which can be any cell type in a vertebrate organism. The proteasome, an abundant and ubiquitous multi-catalytic protease, is responsible for the generation of most of these peptides in the cytosol (see Fig. 1.1). The proteasome activity is of outstanding importance in the process leading to the CD8+ T-cell response. After several decades we still don't have a clear picture. There are still many unanswered such as how specific T-cell clones are selected from the whole repertoire during an IR, or how their differentiation program from the naive to the memory state is established. Nevertheless, we now know that both the humoral and the cellular IR are fundamental weapons for the IS, and that they work conjointly, and not against each other. It could be worth to conclude with an interesting suggestion of a brilliant immunologist, Polly Matzinger (I was in one of her talks), stating that tolerance and IR are different masks of the same actor. It is just a matter of which face is displayed, and which has been kept covered because undesired. Sometimes these mechanisms become dysfunctional, and pathological conditions such as autoimmune disease rises.

1.2 The MHC class I processing pathway

The MHC-peptide complexes (MHCp) define the key for the IS to recognize bad from good, danger from non-danger, or self from non-self. The MHC class I presentation pathway opens up a window from the cell surface onto the entire repertoire of intracellular peptides. The cellular pathways involved in the generation of peptides, which are mounted on the MHC class I complexes,

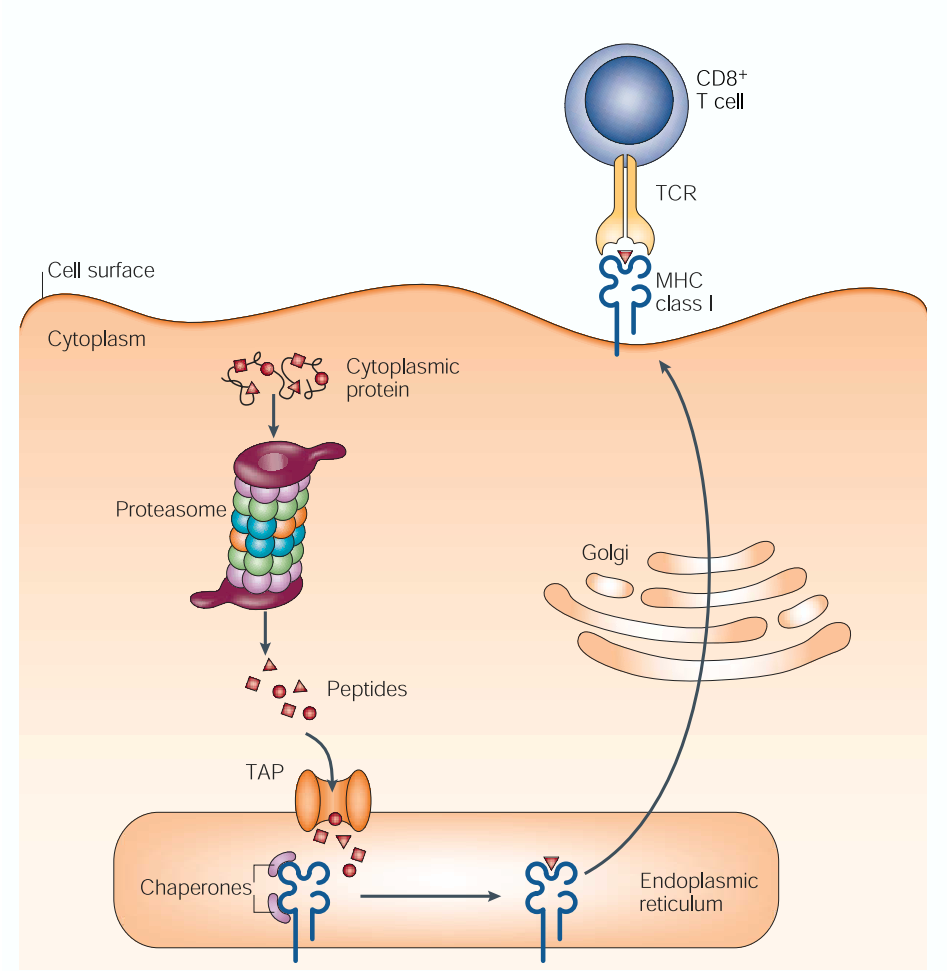

Figure 1.2: Antigen presentation pathway. Intracellular proteins are transported into the proteasome. Some of the peptides resulting from the degradation are transported via TAP (transport associated peptide) to the endoplasmatic reticulum. Here peptides ranging between 8 and 10 amino acids long are mounted into precursor of the MHC molecule. Successively MHC-peptide complexes are stabilized in the Golgi Apparatus and finally transported on the cell surface, where T-cell recognizes the peptide specificity of the MHC complex. Picture taken from Yewdell et al., 2003 (see also `www.nature.com`).

have been intensively studied, although still much has to be understood. As many viruses can replicate rapidly (progeny can be released as early as four hours after the entry of virus into cells), all cell types need a mechanism for rapidly generating peptides from viral proteins that are synthesized during infection. Moreover, there must be a way to transport peptides from the sites of antigenic protein synthesis in the cytoplasm to the site of MHC class I biogenesis in the endoplasmatic reticulum (ER). Finally, there must be a mechanism for MHC class I molecules to select peptides and carry them to the cell surface for perusal by cytotoxic T-cells. The generation of MHCp class I results from a multi-step process Fig. 1.2. Almost all of the MHC class-I-associated peptides are between eight and eleven residues in length, typically nine residues [Rock et al., 2004]. As most peptides have a limited capacity to diffuse across membranes, transport from the cytoplasm to the ER requires a transporter for antigen processing (TAP) an ER-resident, heterodimeric peptide transporter. TAP binds cytosolic peptides and drives the translocation of peptides into the ER lumen in the process (see Fig. 1.2). Successful peptide binding releases the MHC class I molecule from the MHC class-I-loading complex for delivery to the cell surface of the APC.

At the beginning of this new millennium, pathogens and cancer remain the leading causes of death world-wide. The development of vaccines to prevent diseases for which no vaccine currently exists, such as AIDS or malaria, or to treat chronic infections or cancers, as well as the improvement of efficacy and safety of existing vaccines, remains a high priority. In most cases, the development of such vaccines requires strategies capable of stimulating cytotoxic T lymphocytes and thus, to deliver antigen to MHC class I molecules. Several different pathways exist for loading viral or tumour antigenic peptides onto MHC class I molecules in order to stimulate the cellular immune response. We can summarize the antigen loading mechanisms in two families: the endogenous pathways and the cross-presentation pathways. The first family delivers the peptides which are mounted on the MHC class I complex. Endogenous pathway follow the phagocytosis of bacteria, or other amino acids sequences which are then processed intracellularly. The second family of pathways follow when immuno-complexes, chaperons or virus-like proteins, all of them carrying exogenous proteins, are captured by endocytosis inside the APC and pushed into the cytosolic classic pathway. This mechanism allows the processing of non-synthesized proteins (discovered in 1976, see Bevan [1976]). Significant redundancy exists between these two pathways (for a review see Norbury and Sigal [2003]). The prevailing pathways may depend on the localization, form and concentration of antigen itself. The proteasome seems to play a major role within both families.

1.3 The proteasome and the immune system

Two different forms of proteasome can be distinguished: the constitutive (CP) and the immunoproteasome (IP). Antigen processing has evolved dedicated mechanism to improve the presentation of antigenic peptides. Immune regulatory cytokines, IFN-γ and TNF-α, control the expression of several constituents of the proteasome system [Kloetzel, 2004a], suggesting a connection between the IS and the proteasome system. IP is a proteasome formed with replacement of the catalytic subunits by their IFN-γ-inducible homologs, LMP2 (β1i), MECL1 (β2i), and LMP7 (β5i), respectively. Historically, the location of LMP2 and LMP7 genes in the MHC class II locus was one of the first clues suggesting their involvement in antigen presentation [Glynne et al., 1991, Kelly et al., 1991, Martinez and Monaco, 1991]. In vitro studies performed with viral epitopes also showed that the IP is more efficient with respect to the CP in processing a number of antigenic peptides [Cerundolo et al., 1995]. For this reason, it was called immunoproteasome, as opposed to the constitutively expressed standard proteasome. Under non-inflammatory conditions many cell types lack expression of immuno-subunits or present them at low levels. This suggests that a continuous presence of IP in all tissues is either not required or desired. A possible function of the IP lies in the development of the CD8+ T-cell repertoire. In particular, the observation that in some cases immuno-subunits may differently influence the antigen processing of foreign and self-antigens appears indicative for this assumption. The expression of immuno-subunits in thymic cells may play an important role in the negative selection of T-cells reactive against peptides derived from self antigens. The presence of both CP and IP may be important in the shaping of the immune cell repertoire, Interestingly, Morel et al. [2000] reported that IPs are unable to produce several T-cell specific epitopes derived from self proteins. The authors suggest that APCs which contain IP present a different peptide distribution in the thymus, and therefore, the selected T-cell repertoire may not see some self peptides which are then highly presented in the peripheral tissue (maybe rich in CP expression). This would be an interesting way to escape autoimmune disease generated by ubiquitous self-proteins presented in the peripheral tissues. In Chapter 4 it will be discussed how the IP is involved in the peripheral maintenance of T-cell repertoire, and how the IP may improve the IR against viral challenges.

1.4 Homeostasis of the immune system

Homeostasis is the self-regulating process by which biological systems tend to maintain stability while adjusting to conditions that are optimal for survival. If homeostasis is successful, life continues; if unsuccessful, disaster or death ensues. (Encyclopedia Britannica)

The concept of homeostasis

A seminal contribution to medical science was the the definition of the meaning of the modern terms “stress" and “homeostasis". The physiologist Walter Cannon describes stress as any force which changes the physiological parameters of the organism, and homeostasis as the intrinsic ability of the organism to restore its original status [Cannon, 1939]. Improvements in the knowledge of intracellular mechanisms such as degradation pathways and regulatory gene networks allowed the extension of these concepts to the level of the cell. Stress is now broadly defined as any stimulus, whether internal or external, that disturbs the delicate but resilient cellular metabolism [Gleimer and Parham, 2003]. Claude Bernard was the first to realize that the body has control mechanisms able to maintain an internal equilibrium (like body temperature and the levels of nutrients and waste products) in spite of changes in the environment [Bernard, 1865]. This type of control was later called homeostasis [Cannon, 1939]. Homeostatic controls also determine the size and the number of cells in each organ of the body. The immune system is no exception; it reacts to changes in the environment to maintain internal balance; it tends to keep a steady constant number of its cells throughout the adult life of an individual. The concept of homeostasis implies that the introduction of a perturbation may modify the number of lymphocytes, but once the perturbation is removed, the number of cells tends to return to the previous level.

We can then ask: why do we need this complex homeostatic control of the lymphocyte repertoire? First, homeostasis prevents non-controlled lymphocyte accumulation. Moreover, it has a determinant role in shaping T-cell repertoires. Indeed, as the number of lymphocytes is kept constant, any newly produced cell can only survive if another resident cell dies. Because each lymphocyte may have a different antigen binding receptor, it is crucial which cell survives or which cell dies.

In conclusion, lymphocyte homeostasis is a highly dynamic process and homeostatic equilibrium may be reached at different levels depending on both T-cell properties and environmental clues. Two questions can be posed:

- What determines the number of peripheral lymphocytes?

- Which mechanisms contribute to the maintenance of steady state cell numbers?

In this thesis, these questions will be faced from different point of views and show how specific mechanisms, like antigen presentation, and non specific stimuli, such as chronic fluctuations of the environmental stimuli might both play an important role, maybe on different timescales.

Homeostasis of lymphocytes

The peripheral lymphocyte pool is under homeostatic control. Despite de novo production of lymphocytes in the bone marrow and the thymus, and proliferation of peripheral lymphocytes upon antigenic stimulation, the total number of peripheral lymphocytes remains at a steady state. A mouse transplanted with 10-20 ectopic thymuses may have a slightly increase in the number of peripheral T-cells [Berzins et al., 1998]. In this case the homeostatic equilibrium is set at a higher level due to increased T-cell generation. Once the transplants are removed, the number of T-cells returns to the level previous to transplant. In thymectomized mice the homeostatic number of peripheral T-cells is kept stable at a new lower level [Miller, 1965]. In contrast in Rag-deficient mice, which cannot produce any B- or T-cells, the homeostatic control of lymphocyte numbers can be said to be set at zero [Shinkai et al., 1992]. If a population of T-cells is introduced into this T-cell-deficient host, the T-cells expand to reach steady state numbers (homeostatic proliferation). Somehow, the homeostasis of T-cells is a complex system in which sources (thymic emigrants), local environment, and external stimuli work in concert to keep the repertoire at the right size.

A critical feature of lymphocyte homeostasis is that these cells compete against each other for filling the biological space through a variety of mechanisms. A well defined notion of biological space per se remains an area of intense investigation and debate, despite recent identification of several potential molecular mediators.

An equally important conceptual advance has been the general acceptance that these processes are intimately tied to the specificity-based selection and persistence of antigen experienced and non-experienced lymphocytes (see also Chapter 5 and 6). T-cells can sense the presence or the absence of sufficient numbers of others T-cells and adjust their division rate and numbers accordingly. In lymphopenic conditions massive proliferation of pre-existing T-cells occurs [Jameson, 2005, Surh and Sprent, 2002]. Once the cell number reaches a given level, the proliferation is likely terminated or strongly reduced.

The mechanisms behind immune homeostasis are not fully understood,

but there is increasing evidence that competition between lymphocytes plays an important role [Freitas et al., 1995, 1996]. Competition between (intra clonal) and within (inter clonal) T-cell compartments is observed [Tanchot and Rocha, 1995]. Typically T-cells compete for resources, such as space, cytokines antigens and physiological substances required for survival. It is accepted that T-cells require MHC-self peptide complexes to survive and to functionally stay in the peripheral system. Competition plays a role also in this case [Almeida et al., 2005]. How homeostatic processes react to perturbations in lymphocyte numbers during disease, therapy, or ageing are problems awaiting investigation.

T-cell homeostasis and ageing

Regardless of the exact molecular meaning of the void, changes in supply and demand of naive T-cells set the stage for the most profound changes in ageing. Thymic production declines at least 10-fold by the time of puberty; This induces an increase in the proliferation of the remaining cells. Meanwhile, naive T-cells over a lifetime are depleted by encounters with chronic persisting pathogens. This leads to a lifelong accumulation of memory cells that appear to be well preserved in ageing [Nikolich-Zugich, 2005, Fagnoni et al., 2000, Franceschi et al., 2000a], which could impare naive homeostasis. Lymphocytes can divide many times in response to antigen and in response to homeostatic stimuli, and although these cells are equipped with mechanisms to allow for intense division, such as the induction of telomerase [Hodes, 1999], the capacity of which may not be infinite [Effros and Pawelec, 1997].

Part I

The proteasome and the antigen presentation

Chapter 2

The kinetics of proteasome degradation

Introduction

The proteasome is a barrel-shaped multi-subunit protease involved in most cytosolic proteolysis. The role of the proteasome is to degrade (partially) unfolded and nonfunctional intracellular proteins. The 20S core particle is characterized by an internal chamber equipped with catalytic sites at the β subunits [Whitby et al., 2000, Groll et al., 1997, Forster and Hill, 2003, Lowe et al., 1995]. The α subunits, organized in a ring shaped structure, function as a gate by forming an axial channel that regulates the influx and efflux of proteins via the opening and closing of the entrance of the proteolytic chambers. The size of the axial channel can be controlled by regulatory particles like PA28 or its homologs, which can facilitate the substrate uptake and the release of fragments [DeMartino and Slaughter, 1999, Rechsteiner et al., 2000, Cascio et al., 2002, Dick et al., 1996, Groettrup et al., 1996, Kloetzel, 2004b, Van Hall et al., 2000, Kohler et al., 2001] and 19S [Groll et al., 2000, Cascio et al., 2001, Kisselev et al., 1999], which can bind substrates, unfold them and translocate them in to the internal chamber [Groll and Huber, 2003, Pickart and VanDemark, 2000]. The channel imposes constraints on the access of substrates into the proteolytic chamber and on the efflux of partially digested polypeptides [Akopian et al., 1997, Kisselev et al., 1998, Dorn et al., 1999, Groll et al., 1997, Groll and Huber, 2003]. Furthermore, the channel might favor the processive degradation of substrates by restricting the release of degradation products. Using open-channel eukaryotic proteasome mutants, Kohler et al. [2001] showed that the opening of the channel strongly influences the kinetics and the length distribution of the

fragments obtained *in vitro*. Opening the channel increases the degradation rate and increases the median length of resulting fragments by 40%. These results support the notion that the axial channel of the proteasome and its regulation play a pivotal role in the degradation of endogenous proteins. We develop a mathematical model of the proteasome degradation dynamics in order to get more insight into the effects of the gate size on the kinetics of degradation and products generation.

2.1 Mathematical models on the proteasome degradation

Few theoretical models describing the kinetics of proteasome degradation have been developed. Stein et al. [1996] report about experimental results on *in vitro* degradation of short fluorogenic peptides by mammal 20S proteasome. The reaction progress curves show a biphasic behaviour for high substrate concentrations. The velocity of fragment production at the very beginning of degradation is higher than at the steady state, and both velocities decrease with increasing substrate concentration. Fitting experimental results to a pseudo first-order model derived from a standard kinetic scheme, the authors show that this behavior can be explained by a slow conformational change of the proteasome due to substrate binding. Moreover, the presence of a second, inhibiting binding site has been proposed. A standard kinetic model has been proposed to fit experimental data on hydrolysis of small fluorogenic peptides by mammal 20S constitutive and immunoproteasome [Stohwasser et al., 2000]. It is showed that the cap subunit PA28 reduces the cooperative effect of the substrate binding, and increases the efficiency of the substrate uptake and the fragment exit, without considerably changing the cleavage specificity. Experiments conducted by Osmulski and Gaczynska [2002] and Hutschenreiter et al. [2004] showed that both the apertures of the 20S serve as influx and efflux with a reduced access for longer substrates, and that the rate limiting factor in the degradation kinetics is the substrate threading and transport, and not its cleavage. The authors propose a theoretical scheme in which the substrate binding shifts the equilibrium from a closed gate to an open gate conformation, which favors the uptake of substrate and the release of fragments from the COP (core particle). Schmidtke et al. [2000] relate to the fact that hydrolysis of short fluorogenic peptides by mammal 20S proteasomes can be either activated or inhibited, in dependence on the site specificity, by the presence of the protease inhibitor Ritonavir. Using rate equations derived from a kinetic scheme, they show that such kinetic

data can be explained by the existence of a non-catalytic modifier site, to which both the protease inhibitor and the substrate can bind, thus regulating degradation rates.

To our knowledge, only two theoretical works refer to the digestion of longer substrates. Both consider a length dependent transport rate of fragments either into or out of the proteasome cavity. In the first work, - Holzhutter and Kloetzel [2000] consider the digestion of $20 - 40$ aa (amino acids) long substrates by yeast 20S proteasome. Assuming an efflux rate decaying exponentially with the length, a maximum of two cleavages per substrate molecule, and a cleavage rate depending on the sequence specificity, the authors set up first-order differential equations describing the evolution of the probability with which fragments are generated during degradation process. By fitting the model parameters to experimental data on which fragments were produced, they show that the double cleavage products, namely fragments which are obtained by cutting twice the substrate, are generated with an asymmetric cleavage mechanism. The proteasome is shown to cut fragments of $7 - 13$ aa length first at the C terminus of the substrate and subsequently at the N terminus, while fragments of other lengths are cut predominantly first at the N, then at the C terminus. As in the present model, they suggests an optimal distance of nine amino acids between two cleavages, recalling the old molecular ruler hypothesis [Wenzel et al., 1994]. Upstream fragments are found to be released from the proteasome with higher rates then downstream fragments. In the second work, Peters et al. [2002] investigate quantitative kinetic data on the degradation of 25 and 27 aa long substrates by human 20S constitutive and immunoproteasome, as well as on fragment production. Here, a set of first-order differential equations describes the time evolution of fragment production probability assuming site specific cleavage probabilities. The authors investigate the effect of re-entry, which is shown to be responsible for changing the distribution of products during the time course of the degradation. The re-entry rate is assumed to be constant for long fragments but to decrease rapidly for fragments smaller then $12 - 15$ aa. Peters et al. [2002] suggest that the cleavage sites of the immunoproteasome are not modified (as reported by others [Cascio et al., 2001]), but instead that the kinetic rates and the amount of small fragments are increased. Also Hadeler et al. [2004] illustrate the influence of re-entry on the distribution of products with a toy model.

In the present work, we aim at investigating the influence of a length dependent cleavage process and of length dependent in- and efflux rates on the outcome of a digestion experiment. Unfortunately, these dependencies are not known explicitly. Therefore, we choose *ad hoc* terms do describe them. Moreover, we neglect any sequence specificity of the degradation process. As

a consequence, in contrast to the theoretical works cited above, we do not have the intent of fitting model parameters to data. Rather, we show how fairly simple assumptions about the degradation process lead to good agreement with experimental data. Thereby, the main focus of our investigation lies on i) the product length distribution and ii) the dependence of substrate degradation rates on its concentration.

The model describes the influx of the substrate, the cleavage process, and the efflux of the fragments. The proteasomal degradation exhibits Michaelis-Menten kinetics. The Michaelis-Menten constant K_m and the maximum velocity of degradation V_{max} are both decreasing functions of the substrate length, which is in agreement with experimental data Kisselev et al. [1998, 2000]. By tuning the parameters of the model, we can obtain a three-peak length distribution of products as observed experimentally [Kohler et al., 2001, Cascio et al., 2002, Saric et al., 2004, Wang et al., 1999]. The first peak corresponds to $2-3$ aa, the second to $8-10$ aa and the third is a wide peak around $20-30$ aa. The opening of the gate changes the residence time of fragments inside the COP and thereby changes the ratio of small over long fragments observed outside. Finally, we find that the re-entry of intermediate products does not strongly influence the initial dynamics unless the influx rate depends on the length of the peptides.

2.2 Model

The model describes the rates at which the concentrations of fragments of length k change over time. The concentrations change by proteasomal cleavage, making two short fragments out of a long one, and by the influx and efflux of fragments through the gates. A major characteristic of our model is that the dynamics do not depend on the actual amino acid sequence and orientation of the fragment. Influx, efflux, and cleavage only depend on the length of the fragment. Let n_k be the concentration of fragments of length k inside the proteolytic chambers, and let N_k be the fragments of length k

outside. The dynamics of n_k and N_k are given as:

$$\frac{dN_k}{dt} = -a(k)\Big[1 - v\sum_{j=1}^{L} jn_j\Big]N_k + e(k)n_k \ , \tag{2.1}$$

$$\begin{aligned}\frac{dn_k}{dt} &= a(k)\Big[1 - v\sum_{j=1}^{L} jn_j\Big]N_k - e(k)n_k \\ &\quad -c\sum_{i=1}^{k-1} F_{k,i}n_k + c\sum_{j=k+1}^{L}(F_{j,k} + F_{j,j-k})n_j \ ,\end{aligned} \tag{2.2}$$

for $k = 1, 2, \ldots, L$. The substrate N_L is an outside fragment of length $k = L$. The first term of Eq. (2.1) describes the influx of fragments into the proteasome. For the influx function $a(k)$ we will first consider the case where there is no re-entry of fragments other than the substrate, i.e., we set $a(k) = \hat{a}$ for $k = L$, and $a(k) = 0$ otherwise. Later (see Section 2.3.3) we also allow other fragments to enter. The influx of substrate into the proteolytic chambers is a rate limiting factor in protein degradation [Dorn et al., 1999, Liu et al., 2003, Lee et al., 2002, Huffman et al., 2003, Akopian et al., 1997]. Experimental works have suggested that the influx is limited by the maximum amount of amino acids that can be accommodated in the proteasome [Groll et al., 1997, Whitby et al., 2000, Forster and Hill, 2003] (see also Section 2.3.3). In our model the influx rate therefore decreases when the total amount of amino acids inside, $\sum_{k=1}^{L} kn_k$, increases. The maximum filling of the proteasome is normalized to one by a scaling parameter v determining the maximum number of amino acids that can be accommodated within the COP.

Proteasomes degrade a wide range of different substrates, including non protein substrates such as synthetic linear polymers, and a decreased degradation is observed with the increasing of the substrate length [Hortin and Murthy, 2002]. We assume that the influx does not strongly depend on the amino acid composition of the substrate. During *in vitro* digestion very large intermediate fragments can be observed [Cardozo and Michaud, 2002]. Based on the fact that the gates impose physical constraints to the in-going substrate, in this model we consider very long intermediate fragments (greater than 200 aa) as a new effective substrate. Very little is known about the efflux of fragments from the proteasome. Based on the intuition that each peptide binds with a probability p to the gate subunits, hence impairing the passage through the narrow pore, it has been proposed that the efflux rate is a negative exponent of the length $exp(-\gamma n)$ where $\gamma = \frac{1}{1-p}$ and n is the fragment's length [Holzhutter and Kloetzel, 2000]. On the other hand, the

Parameter	Description	Dimension	Default value
L	Length of the Substrate	amino acids	100
$N_L(0)$	Initial substrate concentration	mol	100
$\hat{a}$	Rate of influx	time^{-1}	0.1
$\hat{e}$	Rate of efflux	time^{-1}	1
c	Cleavage rate	time^{-1}	1
θ	Critical fragment length	amino acids	25
μ	Preferred cleavage position	amino acids	9
σ	Std of cleavage position	amino acids	3
v	Scaling factor	-	1/200

Table 2.1: Parameters values

analysis of *in vitro* digestion of 25 and 27 aa long substrates performed with the 20S proteasome suggests a length dependent reprocessing rate which decreases with the increase of the substrate length. These data suggest an increasing Hill function with high exponent to describe the reduced cleavage rate for short substrates [Peters et al., 2002]. Similar to the latter study, we describe the efflux rate with a phenomenological Hill function with high exponent and a critical length $\theta = 25$ aa. This function simply accounts for a high exit rate for short fragments which can be rescued from further degradation, while longer fragments hardly escape from the proteasome and are highly degraded. Although this assumption does not follow any mechanistic process, a simple biological rationale for this assumption can be given. Long fragments have, on average, a high probability to bend (or partially fold), and therefore their exit rate might be strongly reduced with respect to shorter fragments which can freely diffuse out (see also Section 2.4). Using the decreasing Hill function

$$e(k) = \frac{\hat{e}}{1 + (k/\theta)^{10}} \ , \tag{2.3}$$

the efflux rate switches at a fragment length of $k \simeq \theta$ from the maximal efflux rate $\hat{e}$ for short fragments to an efflux close to zero for long fragments. In Fig. 2.1A we depict this function for $\theta = 25$ and $\hat{e} = 1$.

The first two terms of Eq. (2.2) are the same influx and efflux terms as discussed above. The last terms describe the cleavage machinery located in the core of the proteasome. Fragments of length k are cut at a maximum rate c and with probability $0 < F_{k,i} < 1$ into two fragments of length i and $k - i$. Two terms account for the loss and for the gain of each fragment of

length k. The negative term corresponds to a loss for fragments of length k which are cut in shorter fragments, and the positive term is a gain because fragments of length $j > k$ can be cleaved into a fragment of length k. The standard parameters that are used in the simulations are given in Table 2.1, and will be discussed in more detail in Section 2.3.

2.2.1 Cleavage mechanism

Our main assumption for the cleavage mechanism is that the proteasome cleaves proteins starting around their N-termini or C-termini. To allow for cleavages, the protein has to bind into a groove close to a catalytic site [Lowe et al., 1995, Seemuller et al., 1995, Groll and Huber, 2003, Heinemeyer et al., 1997], and the minimal size of a binding motif is about 3-4 aa [Lowe et al., 1995, Seemuller et al., 1995, Groll and Huber, 2003, Heinemeyer et al., 1997, Kesmir et al., 2003]. During the maturation of proteasome, in which the catalytic sites are activated, intermediate fragments are cleaved inside the COP. Studies with mutant proteasome showed that these intermediate peptides possess a typical length of 7-9 aa [Heinemeyer et al., 1997]. It has been suggested that there is a preferred length of 7-9 aa for an optimal docking of the substrate with the binding grooves during the cleavage process inside the COP [Groll and Huber, 2003]. We therefore assume that the proteasome starts at a distance $m \simeq 9$ from one end of the protein/peptide, and scans the substrate chain in both directions until a cleavage site is found. Letting p be the probability to find a cleavage site, the chance to cut at site i has its maximum p at m, and is given by $P_i = p(1-p)^{|i-m|}$. Since possible cleavage sites are expected to be found on average once in 4 aa [Kesmir et al., 2002, 2003], we choose $p \simeq 0.25$. This probability distribution is depicted in Fig. 2.1B by the dashed lines. Using this cleavage function we were able to reproduce degradation kinetics found experimentally, but the fragment distribution had very sharp peaks (data not shown). Indeed it seems unrealistic that the cleavage probability has the sharp peak at $m = 9$ depicted in Fig. 2.1B. To round the peak one can model the cleavage probability with a phenomenological Gaussian distribution

$$g(i) = \frac{1}{\sqrt{2\pi\sigma}} \mathrm{e}^{-\frac{(i-\mu)^2}{2\sigma^2}} \ , \tag{2.4}$$

where the mean μ provides the most likely cutting position, and the standard deviation σ defines the range of likely cleavage positions. This distribution is similar to the previous one but it has a rounder peak (see Fig. 2.1B, where the solid line depicts Eq. (2.4) with $\mu = 9$ and $\sigma = 3$). Thus, the probability

of cutting a peptide of length k at position i is:

$$F_{k,i} = g(i) \quad \text{for} \quad i < k \tag{2.5}$$

The cleavage probability should be very low for the first $3-4$ residues of the protein due to the binding of the substrate prior to cleavage (see above). Hence the standard deviation, σ, should be small. Choosing $\mu = 9$ and $\sigma = 3$ implies that we expect at least one cleavage site in every $\mu + 2\sigma = 15$ consecutive residues, which seems a fair assumption. Because $\sigma < \mu$ we obtain that the proteasome has a low probability to cut in the very first positions (see Fig. 2.1). Note that this model does not address the question of the orientation of the sequence and thus the possibility to distinguish a cut at the N or at the C terminus. We consider a simple example: suppose the proteasome cuts with probability p_1 and p_2 at a distance d from the N terminus and from the C terminus, respectively. The fragments generated with this mechanism are the same of the case in which the proteasome cuts with probability $p_1 + p_2$ at distance d from only one side of the sequence.

2.3 Results

The model has three rate parameters: the cleavage rate c, the maximum influx rate $\hat{a}$, and the maximum efflux rate $\hat{e}$. A normal time scale of proteasome experiments is minutes. However, experimental results on proteasome degradation are typically compared for a certain level of substrate degradation, rather than at a specific point in time. Since time is not an important issue, and because we have three rate parameters in our model one can always rescale the time such that $c = 1$ per time unit. Increasing the cleavage rate will therefore be the same as decreasing the flux through the gates (i.e., as decreasing $\hat{a}$ and $\hat{e}$). Where not otherwise stated, the results of the model have been obtained numerically integrating Eqs. (2.1, 2.2) with a fourth order Runge-Kutta integrator.

2.3.1 Kinetics

Experimental data suggest that the *in vitro* degradation rate of substrates by the proteasome obeys Michaelis-Menten kinetics [Reidlinger et al., 1997, Djaballah and Rivett, 1992, Hortin and Murthy, 2002, Realini et al., 1997, Orlowski et al., 1991, Cardozo et al., 1999, 1994, Akopian et al., 1997, Kisselev et al., 2002]. For long substrates the maximum degradation rate and the Michaelis-Menten constant are known to decrease with the length of the substrate [Kisselev et al., 1999, 2000, Akopian et al., 1997, Cascio et al.,

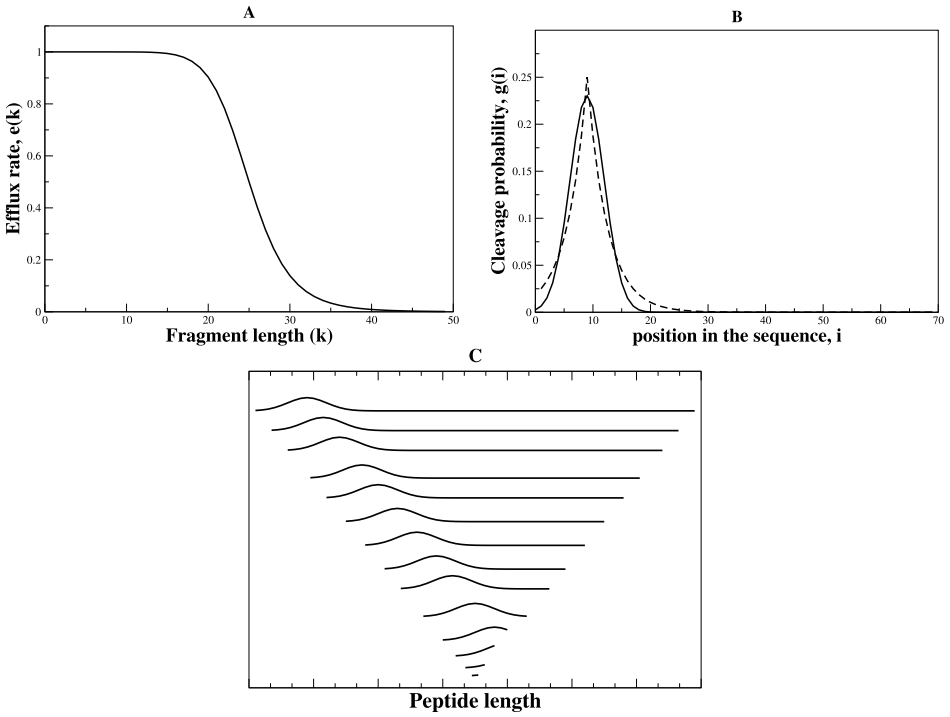

Figure 2.1: **A.** The efflux rate as given in Eq. (2.3). **B.** Binomial (dashed lines) and gaussian (solid lines) distributions for the cleavage probability. For the binomial distribution $p = 0.25, m = 9$ and for the gaussian distribution $\mu = 9, \sigma = 3$. **C.** Schematic representation of the phenomenological cleavage machinery given in Eq. (2.5) for different sequence lengths. The cleavage probability is peaked at $\mu = 9$ residues from one end of the substrate.

2002]. Our model also exhibits Michaelis-Menten kinetics (see Fig. 2.2). For various initial substrate concentrations, Fig. 2.2 depicts the depletion of the substrate ($L = 100$) in the solution (Panel A), and the corresponding filling of the proteasome (Panel B). There is a rapid initial phase during which the proteasome fills up by influx of the substrate. At the very early stage of degradation, due to the filling of the proteasome, the substrate loss is not linear. When the initial substrate concentration is low this initial phase accounts for a significant depletion of the substrate concentration N_L (see Fig. 2.2A). Otherwise, the substrate concentration remains high and the

filling of the proteasome approaches a quasi steady state corresponding to a maximum degradation rate.

To study the Michaelis-Menten kinetics, we fix the substrate concentration by fixing $N(t) = N(0)$ and let the model approach the corresponding steady state. At the steady state we measure the degradation rate as the number of substrate molecules in solution which are lost per unit time, and depict that as a function of the substrate concentration and the length of the substrate, L (see Fig. 2.2C). This reveals a family of Michaelis-Menten curves for the various lengths of the substrate. The longer the substrate, the smaller the maximum degradation rate, V_{max}, and the smaller the Michaelis-Menten constant, K_m. The degradation rate at low substrate concentrations is fairly independent on the length of the substrate (see Fig. 2.2C and Appendix). More formally, one can illustrate the Michaelis-Menten kinetics by an approximation employing the quasi steady state behavior observed with the model Eqs. (2.1, 2.2). In the Appendix, we develop a simplified model of three differential equations for the substrate concentration inside, $n(t)$, and outside $N(t)$, and for the total concentration of fragments inside, $p(t)$. By a quasi steady state assumption for the internal dynamics, i.e., $dn/dt = dp/dt = 0$, we arrive at the following equation

$$\frac{dN}{dt} = -\frac{V_{\max} N}{V_{\max}/\hat{a} + N} \quad \text{where} \quad V_{\max} = \frac{c\bar{e}}{vL(c+\bar{e})} \,, \tag{2.6}$$

and $\hat{a}$ is the influx rate of the substrate and $\bar{e}$ is an "average efflux rate" of the fragments (for details, see the Appendix). The latter should be taken as an average of the length dependent efflux of the full model (see Eq. (2.3) and the Appendix). The simplified model has a Michaelis-Menten constant $K_m = V_{\max}/\hat{a}$. This approximation is in good agreement with the kinetics of the full model for long substrates (see Fig. 2.2D). For small substrate concentrations, i.e., for $N \ll K_m$, $dN/dt \simeq \hat{a}N$, and the degradation rate is indeed independent of the length of the substrate. The line $\hat{a}N$ is depicted by the solid line in Fig. 2.2C and is in excellent agreement with the simulations of the full model. For the current parameter settings, V_{max} is approached rapidly, e.g., within 10 time units (results not shown). The plateau level in Fig. 2.2C depicted as dot-dashed line is the V_{max} value obtained from the simplified model for a substrate of length $L = 100$ and average efflux $\bar{e} = 0.2$ per time unit. In this model, $V_{\max}$ itself is a saturation function of the cleavage rate c and the efflux rate $\bar{e}$ (see Eq. (2.6)). This means that the efflux and the cleavage play a similar role in limiting the maximum rate of degradation. At high cleavage rates the degradation rate is limited by the efflux, and at high efflux rates it is limited by the cleavage.

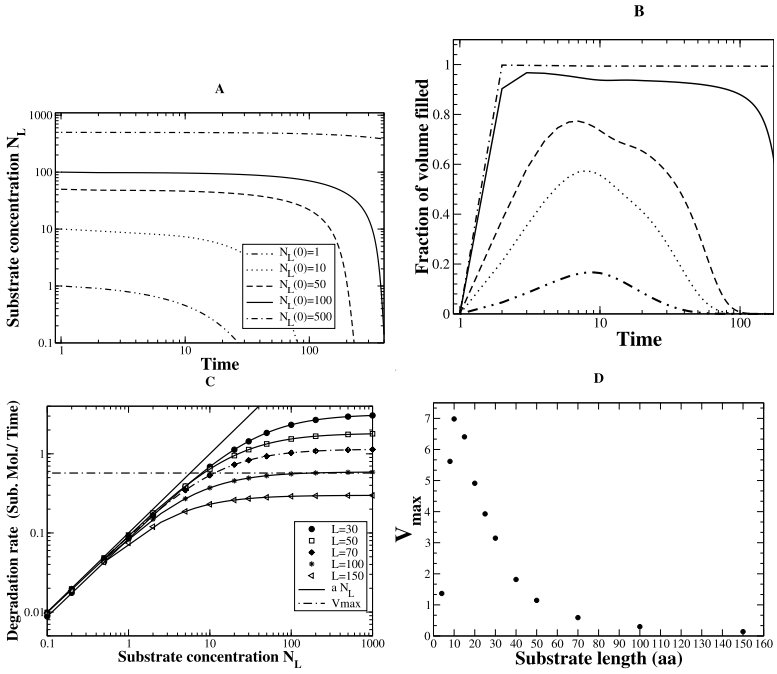

Figure 2.2: Michaelis-Menten Kinetics. **A.** Substrate consumption, each curve is the time course for a different initial concentration, $N_L(0)$. **B.** Filling of the proteasome core particle (in amino acids) for each curve shown in *A*. **C.** Michaelis-Menten log-log plot; each symbol-curve denotes a substrate of a different length (see legend) obtained from the model presented in Eqs. (2.1, 2.2) in conditions where the proteasome is in a bath of substrate in order to prevent substrate limiting effects. Solid lines are non-linear parameter fits with the Michaelis-Menten function. The solid line is given by the initial slope $\hat{a}N_L$ and the dashed-dot line is the V_{max}, both predicted with the simplified model (see Appendix) for the standard parameter values (see Table 2.1) and an average efflux $\bar{e} = 0.2$ (see Eq. (2.6)). **D.** V_{max} as a function of the substrate length. It increases for substrate shorter than 10 aa and decreases for longer substrates. The initial substrate concentration is $N_L(0) = 6000$ to ensure that for each length the proteasome digests at the saturation level.

Fig. 2.2D shows the maximum degradation rate V_{max}, calculated numerically from the full model Eqs. (2.1, 2.2), as a non-linear function of the substrate length. It increases for small substrates with a maximum at ca. 10 aa and decreases with the inverse of the length for longer substrates. Very small fragments are weakly degraded because of the low cleavage rate for fragments shorter than 9 aa. This explains why the degradation rate decreases for very short fragments. For longer fragments, V_{max} was found to decrease with the inverse of the length. This is due to the fact that the COP volume is finite and thus the influx decreases with the increase of the substrate length. Therefore, the degradation rate decreses accordingly. This compares well with experimental results ([Dolenc et al., 1998, Kisselev et al., 2000, Akopian et al., 1997, Kisselev et al., 1998, 1999]). Interestingly, the ratio of V_{max}/K_m increases with the increase of the substrate length [Dolenc et al., 1998] and saturates for long substrates reaching 50% of its maximum for substrate of 23 aa which indicating that both constants decrease with the length of the substrate in the same ratio.

2.3.2 Length distribution of the fragments

In vitro experiments generate cleavage products that range from 2 to 35 aa with an average length of $7-8$ aa [Nussbaum et al., 1998, Kisselev et al., 1998, Kohler et al., 2001, Kisselev et al., 1999, Cascio et al., 2001]. Using size exclusion chromatography and on-line fluorescence detection, Kohler et al. [2001] showed that the products generated by the wild type (WT) proteasome have a length distribution with three broad peaks corresponding to lengths of $2-3$, $8-10$, and $20-30$ aa, respectively. Other approaches, such as mass spectrometry, are not quantitative and fail to detect short peptides. We have searched the parameter space of our model to identify the regimes that result in similar fragment length distributions.

Parameter Sweep. In Fig. 2.3 we show how the fragment length distribution depends on the size of the gate, i.e., on the influx and efflux rates $\hat{a}$ and $\hat{e}$, as calculated with the model Eqs. (2.1, 2.2). In each panel, the distribution is depicted for the time point at which 20% of the substrate is degraded. The time at which this is achieved is indicated in each panel. For an intermediate efflux rate, we obtain three-peaked distributions similar to those observed in experiments [Kohler et al., 2001] for a wide range of influx rates. Note that the first peak has its maximum at 1 aa but we call this decreasing slope “peak" for simplicity. In our model, the three-peaked distributions are the result of the cleavage machinery, which tends to cut fragments of $8-10$ aa, and the efflux of products, which favors the short fragments. The distribution is insensitive to hundred fold variation of the

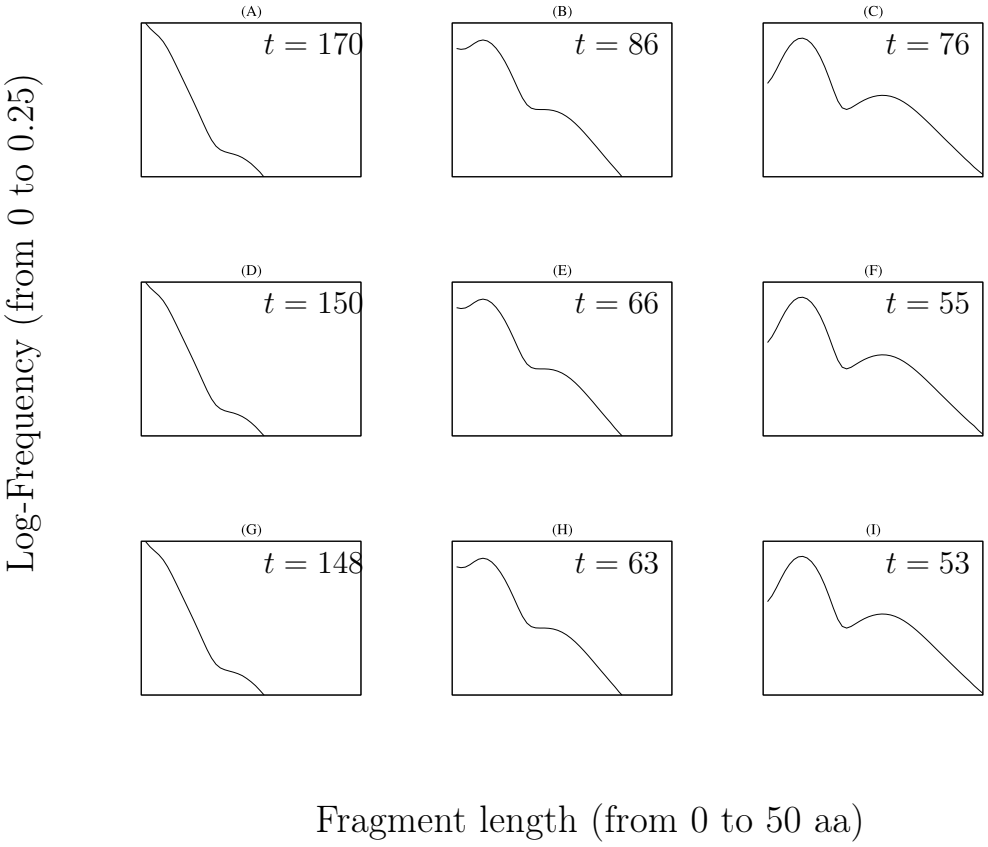

Figure 2.3: Parameter sweep for the influx and efflux rates: length distributions of the fragments outside the proteasome. From left to right the efflux rate $\hat{e}$ increases, from up to bottom the influx rate $\hat{a}$ increases. Each distribution has been taken at 20 % of substrate degraded. The time at which the 20 % of substrate degradation is reached is shown in each panel. Parameter's sweep: $\hat{a} = (0.01, 0.1, 1)$ and $\hat{e} = (0.1, 1, 10)$. Panel **E** and Panel **I** could represent the WT proteasome and an open-channel mutant respectively (see also Fig. 2.4). Note that the distributions are insensitive to the variation in the influx rate $\hat{a}$.

influx rate $\hat{a}$ (see Fig. 2.3). From Eq. (2.2) it is clear that the influx rate does not influence the distribution of produced fragments but only the rate at which the proteasome fills up. Due to the linearity of the efflux and of the cleavage rate with the density of internal fragments, the outside distribution is independent on the rate at which the proteasome fills up.

In the first column of Fig. 2.3, Panels A, D and G, the efflux is slow

compared to the cleavage ($c/\hat{e} = 10$). As a consequence, most substrate molecules are fragmented extensively before they are exported, and one observes short fragments in the solution. Increasing the efflux rate 10-fold (see the second column of Fig. 2.3, panels B, E and H) gives a similar time scale to the efflux and to the cleavage, and allows for a three-peak distribution (see below). Another 10-fold increase of the efflux rate (see Fig. 2.3, Panels C, F, and I) makes cleavage the limiting factor. The ratio of long to short fragments increases (which will later be interpreted as opening the gate, see below). Because the residence time of fragments in the COP is short, there is less fragmentation, and the first peak at 1-3 aa decreases.

Three-peaked distribution. When the efflux rate and the cleavage rate have a similar time scale we observe three peaks in the distribution of fragments (see Fig. 2.3 and the "WT" curves in Fig. 2.4). Similar to what is observed experimentally [Kohler et al., 2001], the third peak is much smaller than the other two, and the second peak is larger than the first peak. In our model, the first peak corresponding to the small fragments reflects an efficient cleavage mechanism where fragments are repeatedly cleaved before they are released from the COP. These "rest" products do not collapse to single amino acids because cleavage of very short fragments is improbable in our model (see Fig. 2.1B). The second peak corresponding to fragments with a length of $8 - 10$ aa, is the result of the preference to cut at $\mu = 9$ aa (see Section 2.2.1). Fragments are found in a broad peak around 9 aa, because of the variation in the cleavage (i.e., standard deviation of the Gaussian function). The third peak around 25 aa found in the WT distribution is due to the efflux function. It results from the high probability of a fraction of intermediate 25-35 aa fragments to exit the proteasome. As they would have been a source for fragments of length 15-25 aa, the production of fragments of this length drops. This intuitive explanation elucidates the presence of the third peak.

Gate Opening. Comparing WT eukaryotic proteasomes with open-channel mutants Kohler et al. [2001] showed that: i) mutants degrade substrates faster, ii) the median length of resulting fragments is 40% longer than when the same substrate is degraded with the WT proteasome, and iii) the main effect of opening the gate is to increase the amount of long fragments and to decrease the amount of short (2-3 aa long) fragments. In Fig. 2.4 we report the effect of the gate size by increasing the influx and efflux rate 3-fold from a WT with $\hat{a} = 0.1$ and $\hat{e} = 1$ to an "open-channel mutant" with $\hat{a} = 0.3$ and $\hat{e} = 3$. The fragment length distributions are compared at time points where 20% (Panel A) or 80% (Panel B) of the substrate is degraded. For these parameters the WT proteasome delivers the three-peaked distribution discussed above (see Fig. 2.4).

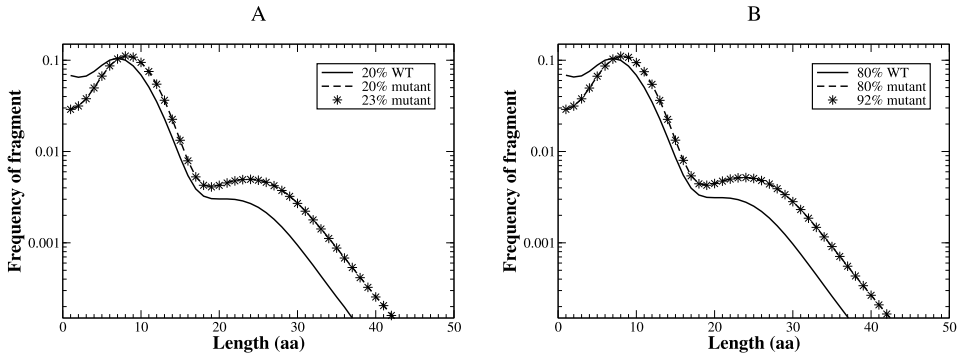

Figure 2.4: Fragment length distributions after opening the gate. Panel **A**: The solid line corresponds to the WT proteasome at time $t = 66$ and the dashed line to the open-channel mutant at time $t = 56$. At these time points 20% of substrate is degraded. The stars depict the distribution of the open-channel mutant at $t = 66$ (when 23% of substrate is degraded). This illustrates that the degradation rate is higher for the open-channel mutant. The average length of the products is 9.1 aa for the mutant and 7.3 aa for the WT proteasome. Panel **B**: Same as Panel **A** but at a time point when 80% of the substrate is degraded. The average length are the same as in Panel **A** and no evident shift of the peaks is observed. The stars depict the distribution of the open-channel mutant at $t = 279$, when 92% of substrate is degraded. Parameters: open-channel mutant $\hat{a} = 0.3, \hat{e} = 3$, and WT $\hat{a} = 0.1, \hat{e} = 1$.

In the "open-channel" mutant the flux of fragments through the axial channel is increased. As a consequence, the ratio of small over long fragments decreases (see Fig. 2.4A, dashed lines). In terms of the three-peaked distribution this results in a decrease in the first peak, and an increase in the second and the third peak. The average length of the outside fragments increases from 7.3 aa for the WT to 9.1 aa for the open-channel mutant. With the mutant, 20% substrate degradation is achieved at $t = 56$, and with WT this takes until $t = 66$. This corresponds to 18% increase in the degradation rate. Fragments are produced with the same frequency during the degradation process; the positions of the peaks remain similar between the distribution at 20% and 80% substrate degradation. In this case the average

fragment lengths are 7.3 and 9.1 respectively with an increase of 24.6% of the mutant with respect to the WT. The fraction of small fragments (1-5 aa) is 36.5% (22% mutant), of intermediates (6-11) is 51% (58% mutant) and of long fragments (> 11) is 12.5% (20% mutant) as reported experiemntally [Kohler et al., 2001]. The third peak is centered at 23 aa and at 27 aa for the WT and the mutant proteasome respectively.

2.3.3 Re-entry

In vivo the processed fragments of the proteasome degradation are exposed to amino peptidases and other proteases in the cytosol [Reits et al., 2004]. This strongly reduces the possibility that fragments can enter the proteasome and be further degraded. However, re-entry of fragments is possible *in vitro*, and this is a controversial point regarding the validity of *in vitro* experiments for the understanding of *in vivo* proteasomal activity. All results discussed above were obtained in the absence of re-entry because only the substrate had a non-zero influx rate $a(L) = \hat{a}$. To study the effect of re-entry of processed fragments we first give all fragments the same influx rate $a(k) = \hat{a}$ for $k = 1, 2, \ldots, L$. Fig. 2.5A and B show how re-entry affects the time course and the length distribution of fragments. Re-entry slightly reduces the degradation rate at late time points, e.g., after 50% of the substrate has been degraded, when the concentration of some fragments in the solution exceeds that of the substrate, see Fig. 2.5A. In open-channel mutants this late effect of re-entry is even weaker (not shown). The effect of re-entry increases when time proceeds, e.g., when the substrate is more than 80% degraded, because the products start to dominate in the solution, see Fig. 2.5A. Comparing the number of fragments of length $8 - 10$ aa illustrates that the effect of re-entry on the degradation process is small. The length distribution at 80% substrate degradation is shown in Fig. 2.5B. During the course of the degradation the position of the peaks shift to smaller fragments as a result of the reprocessing of products. The average fragment length shifts from 7.3 aa to 6 aa.

Re-entry becomes more important if we allow small fragments to have a faster influx than large fragments. For instance, this would be the case if the fragments are actively transported through the axial channel. One would then expect the transportation time to be proportional to the length of the substrate, and the influx rate would be inversely related to the substrate length, e.g. $a(k) = L\hat{a}/k$ for $k = 1, 2, \ldots, L$. Note that this function preserves the influx rate $\hat{a}$ for substrates of length L that was used above. With such a length dependent influx rate, the re-entry of products markedly slows down the degradation of the substrate (Fig. 2.5C). As a consequence of the re-

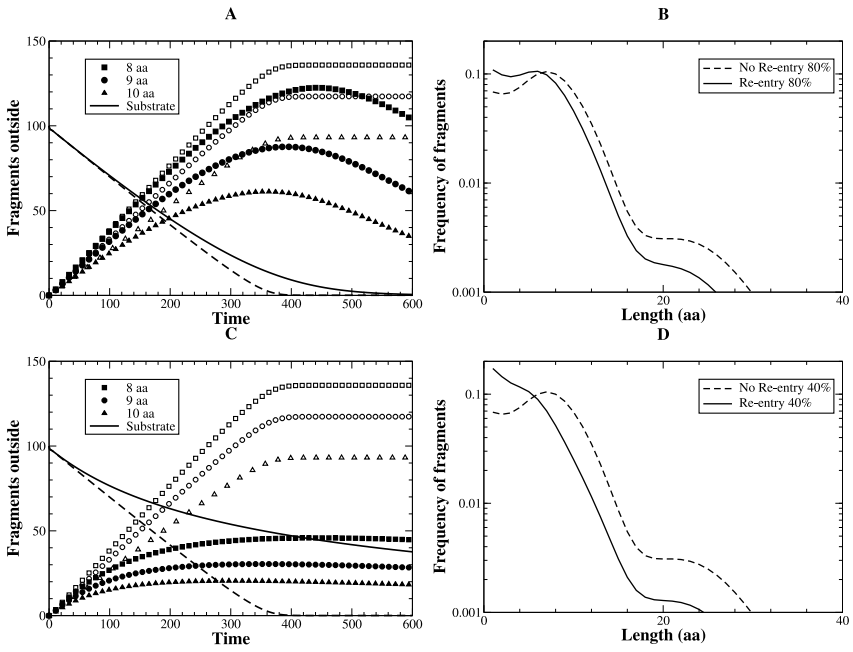

Figure 2.5: Effect of the re-entry of fragments. **A, B**: Comparison of the time course and fragment length distribution without re-entry and with re-entry employing a constant influx rate for all the fragments: $a(k) = \hat{a}$. Panel **A**: time course of the degradation process: the solid line is the substrate depletion with re-entry ($a(k) = \hat{a}$ for $k = 1, 2, \ldots, L$), and dashed line depicts the same without re-entry. The filled symbols depict the time courses of fragments with re-entry, the empty symbols those of the same fragment lengths without re-entry. **B**: length distribution of fragment with re-entry (solid line) and without re-entry (dashed line). **C, D**: same as panels **A, B** but with a length dependent influx rate $a(k) = L\hat{a}/k$ for $k = 1, 2, \ldots, L$. Because short fragments rapidly re-enter the COP, there are less fragments outside. **D**: The distribution shifts to the left increasing the first peak, $1 - 3$ aa, while the second ($8 - 10$ aa) and the third ($20 - 30$ aa) peak disappear.

entry, the peak at a length of $8-10$ residues vanishes, and more than 50% of fragments outside are smaller than 4 aa (see Fig. 2.5D). Allowing for re-entry, the average fragment length shifts from 7.3 to 4.7 aa. Summarizing, these results suggest that for *in vitro* experiments, re-entry could indeed be an issue: if the transport rate of substrates inside the COP is dependent on the length, the experiments should be terminated when less than 10% of the substrate is degraded to exclude the possibility of re-entry. At the moment many groups use 20% as the typical stopping criteria [Cascio et al., 2001, Kisselev et al., 1999]. An accurate analysis of the transport rates through the proteasome channel is required to resolve this issue further.

2.4 Discussion and Conclusion

This work provides insights on the effect of the size of the axial channel on proteasome degradation.

A realistic choice for the model parameters is hard to obtain. The model is phenomenological and is designed to qualitatively capture the main features of the kinetics of degradation. Furthermore, available experimental data are not yet adequate for a mechanistic and more realistic description of the gate functioning and the cleavage mechanism.

2.4.1 Length distribution

The main result of the model is that the residence time inside the COP, which depends on the gate size of the axial channel, drastically affects the fragment length distribution and the proteasome kinetics. We now understand how a three-peaked fragment length distribution that is observed in the experiments can be obtained. In the model the first peak is due to efficient fragmentation to the minimal length before the fragment is released from the proteasome.

The second peak is due to the preference of the cleavage mechanism (see Eq. (2.5)) to cut around position 9 from one terminus, delivering many fragments of approximately that length from a single substrate molecule. The third peak between 20 and 30 residues is the result of the size filter described by the efflux function Eq. (2.3). Very little is known about the effects of size, charge, and hydrophobicity on the transport of peptides through large aqueous pores. We therefore prefer our simple phenomenological function for the efflux (Eq. (2.3)) over complicated mechanistic functions. We simply assume that long fragments hardly leave the proteasome. An intuitive phenomenological reason may be that a partial re-folding or the bending of long fragments inside the COP (which are feasible for amino acid sequences

longer than 30 40 aa) may be responsible for the low rate of long fragments to exit from the narrow proteasome pores. Moreover, secondary binding sites that stabilize and increase the binding of long substrates are likely to exist [Bogyo et al., 1998].

In order to check the robustness of the model's results, we studied the length distribution of fragments when the efflux parameters are varied. Decreasing the value of the switching length θ, longer fragments have a very low exit rate. Therefore, they are hardly generated and the third peak is lost or becomes a shoulder of the second peak. The increase of θ results in an accumulation of long fragments outside without strongly affecting the position and height of the first two peaks. We obtain very similar results if the increase of the θ values is accompanied with a decrease of the efflux rate $\hat{e}$ (results not shown). This shows that the model is robust against perturbations of the parameter θ. The robustness of the resulting product length distribution was also checked against changes of substrate length. Intuition leads to the expectation that the proportion of fragments with a length around 8 aa is diminished with respect to the number of produced fragments of length around 23 to 27 aa, if the substrate length is shortened. This is due to the fact that a long fragment will lead to a higher production of fragments of lengths around 8 aa than a shorter one, before it can exit the COP with high probability. Indeed, model results show exactly this behavior concerning the frequencies of fragments, while retaining the three peaks: Shorter substrates yield a smaller second peak than longer ones (results not shown). With that, this model predicts that product length distribution changes with different substrate lengths. Indeed, Ferrington et al. [2001] observe that degradation of oxidized calmodulin by 20S proteasome produces a lower concentration of fragments of length around 8 aa than of fragments of length around 25 aa, for degradation of 10 % of substrate. Note that this substrate is almost three times smaller than the substrate used by Kohler et al. [2001], whose experimental data on length distribution is referred as comparison with our length distribution results. A more thorough experimental investigation of this effect could be used to confirm or falsify an efflux behavior like the one assumed here (Eq. (2.3)).

2.4.2 The cleavage

The cleavage mechanism in our model is also phenomenological and basically assumes that cleavage occurs, independently on the substrate orientation, at some preferred distance from one end (see Eq. (2.5)), and requires a minimal substrate length to efficiently cleave the sequence. This was inspired from crystallographic structure [Lowe et al., 1995, Seemuller et al., 1995, Groll and

Huber, 2003, Groll et al., 1997] describing a binding pocket nearby the active site where the substrate docks before the cut takes place and from enzymatic studies with inhibitors suggesting that a minimal length of 3-4 aa is required to dock to the internal walls and efficiently cleave the substrate [Lowe et al., 1995, Seemuller et al., 1995, Groll and Huber, 2003, Groll et al., 1997, Bogyo et al., 1998]. Additionally, it has been recently shown that both *in vitro* and *in vivo* initiation of proteolysis occurs close to the C-terminus of proteins [Zhang et al., 2004]. This result supports our hypothesis of high cleavage probability at the ends of the substrate although we do not address the question of the orientation of the substrate and thus the distinction of the C- from the N- terminus of the substrate. The low cleavage rate for fragments smaller than 9 aa (see Fig. 2.1 C) and the size filter effect are both responsible for the length dependent kinetics reported for the model. The rate characterizing the degradation of short fluorogenic peptides and decapeptide libraries [Kisselev et al., 2000] increases with length while, for long substrate, a decreasing slope for both V_{max} and K_m is found, as was found in this model. Random distributions for the cleavage probabilities have also been considered (data not shown). For instance, let the proteasome cut with probability p at a randomly chosen amino acid. The chance to cut a random amino acid will be uniformly distributed, namely $1/L$ where L is substrate length. This mechanism failed to generate a three-peaked distribution of the products unless specific "ad hoc" size filtering functions for the influx and/or the efflux were considered. Moreover, even though the kinetics of the degradation is not affected by this random mechanism, we would expect intuitively that the length distribution will not show the peak at 8-10 aa. Simulations have confirmed that the loss of the length scale introduced by the cleavage mechanism of Eq. (2.5) was responsible for the loss of the multi peaked distribution in a wide range of parameter values. We also investigated a different random cleavage in which each amino acid has equal probability to be cut, hence a constant cut probability for each position is assigned. As for the previous case, even if less short fragments are produced because long fragments have higher cleavage rate with respect to the short ones, the distribution is not a multi peaked curve. Other mechanisms have been also suggested in which the fragments are generated with a double cleavage performed sequentially on the same fragments [Wenzel et al., 1994, Holzhutter and Kloetzel, 2000]. We do not rule out this mechanism in our model since several consecutive single cuts from the end of intermediate fragments are very probable.

2.4.3 Kinetics of degradation

A major simplification of the model was to ignore the substrate specificity of the proteasome. This allowed us to find an expression for the relationship between the maximal degradation rate, V_{max}, and the length of the substrate (see Eq. (2.6)). Additionally, the Michaelis-Menten function, i.e., Eq. (2.6), showed that the degradation rate can be either efflux limited or cleavage limited. Kinetically, one can therefore distinguish between the "efflux limited case" where the cleavage is fast and the efflux is slow, and the "cleavage limited case" where the cleavage is slow and efflux is fast (see Fig. 2.3). When efflux is limiting the residence time is long, and long fragments are cleaved repeatedly into small products. When the cleavage is limiting long fragments will be produced. Since open-channel mutants have an increased degradation rate [Kohler et al., 2001], one can conclude that in the WT-proteasome the efflux was the limiting factor. On the other hand, experiments with mutant proteasomes, in which the catalytic site threonine was replaced with serine [Kisselev et al., 2000], showed that the V_{max} decreases strongly and longer fragments are produced when compared to the WT. This suggests that in this mutant proteasome cleavage is the rate limiting factor (see Eq. (2.6) and Section 2.3). It has been suggested that the regulatory 19S cap, which binds to the COP forming the 26S proteasome, increases the enzymatic activity [Hoffman and Rechsteiner, 1996], and facilitates the binding of the substrates. The 26S proteasome exhibits a fragment length distribution similar to 20S proteasome but the average length of the fragments is shorter [Kisselev et al., 1999, Emmerich et al., 2000]. These results are in agreement with our model which predicts that an increased efficiency in the cleavage activity limits the capacity of long fragments to go out, increasing the frequency of shorter products. The 26S can be therefore described as a proteasome with higher cleavage efficiency with respect to 20S and therefore releases less longer fragments.

Recently a new model addressing the length dependent aspects of antigen processing *in vivo* has been proposed [Kloetzel, 2004b]. Recent results suggest that the proteasome may be one of the several proteases involved in the production of peptides by a concerted multi-step mechanism. We do not address the question of the proteasome kinetics in vivo. Our results point on the proteasome digestion during *in vitro* experiment which might diverge from *in vivo* substrate processing emerging from a more complex machinery in which the fragment generated from a proteasome during one step could serve as substrate for other proteases.

2.4.4 Immunoproteasome

The relationship between proteasome activity and the IFN-γ induced subunit PA28 [Cascio et al., 2002, Sijts et al., 2000, Van Hall et al., 2000, Kloetzel, 2004b] remains controversial. Different forms of the IP, i.e., 20S+PA28, and 26S IP, cleave both short fluorogenic peptides and long substrates faster than the constitutive forms of the proteasome [Eleuteri et al., 1997, Glickman, 2000, Cardozo and Michaud, 2002, Tenzer et al., 2004], and generate longer products [Toes et al., 2001, Cascio et al., 2001, Dick et al., 1996, Kohler et al., 2001]. Nevertheless, some experiments have shown that the substrate turnover is very similar when compared between constitutive and immuno forms [Cascio et al., 2001, Toes et al., 2001, Peters et al., 2002]. Although experiments are still contradictory and the immunoproteasome not always results in a faster substrate turnover and increased production of long fragments, our model suggest that proteasomes equipped with the PA28, like the 20S IP +PA28, can be considered almost as being in an open gate configuration. Above we already discussed that the maximum degradation rate, V_{max}, saturates and can be limited by either the cleavage c or the efflux rate $\bar{e}$. In the cleavage limited case augmenting the efflux $\bar{e}$ of the products in Eq. (2.6) will hardly increase the degradation rate, and hence the average fragment length will remain the same.

2.4.5 Improving the quantification of the antigen processing pathways

Finally, our model can be used to achieve a more quantitative picture of the MHC class I antigen processing and presentation pathway. Based on estimates coming from the average turnover of proteins in a cell, Yewdell and colleagues argue that the efficiency of antigen processing is low, meaning that most of the potential MHC ligands are destroyed by the proteasome [Yewdell, 2001, Yewdell et al., 2003]. We also find that at least 50% of the fragments generated by the proteasome are shorter than eight amino acids (see Fig. 2.4) and therefore can not be used for antigen presentation.

Modeling the proteasome by an opened gate, as can be 20S+PA28 (constitutive and immuno), the average fragment length increases, and the steady state level of fragments from 8 to 35 aa is elevated (see Fig. 2.4). Thus, an open gate proteasome can markedly increase the amount of possible MHC ligands. With open gate the average fragment length is at least three amino acids longer and the steady state levels of fragments from 8 to 35 aa increases by at least 25% (see Fig. 2.4). Thus, the immunoproteasomes can increase the amount of possible MHC ligands by 25%. Adjusting the parameters of

the model to the values used by Yewdell et al. [2003], i.e., the degradation rate is 2.2 molecules degraded per time unit, $V_{max} = 11$ molecules per unit, $8 \cdot 10^5$ proteasomes per cell and an average substrate length of $L = 450$ aa [Yewdell et al., 2003], we estimate the amount of fragments of different lengths present in the cytosol during the steady state. Around 10% of fragments are octa-mers, 9% nona-mers and 7% deca-mers. The production rate α_k of fragments of length k can be found from the model simulations once the degradation rate is constant, e.g., $\alpha_9 = 6 \cdot 10^6$. Assuming that nona-mers have half life of 7 sec in the cytosol [Reits et al., 2003], the steady state concentration of nona-mers per cell becomes 10^6. This value is 16 times smaller than the rough estimations of Yewdell et al. [2003], and comes very close to the steady-state peptide concentrations measured in peptide competition experiments ($2 \cdot 10^5$, [Reits et al., 2003]). Similarly, summing over all k-mers longer than 8 produced by our degradation dynamics, we calculate the potential MHC ligands steady-state to be $7 \cdot 10^6$ circa.

Summary

It is evident that the proteasome degradation is a key-step in the processing of antigenic peptides, which serve for the IS to check the state of cells and to eventually recognize and destroy infected cells. This Chapter presents a simple model able to capture important aspects of the proteasome degradation. The model shows that the fragment length distribution depends on the substrate length and on the concentration with which proteins enter into the proteolytic chamber. The gate opening is the main regulator of the substrate degradation. Longer fragments, which have higher chance to reach the surface of cells and be presented to the T-cells, have increased abundance as far as an open gate proteasome is provided. It is worth to note that the size and the amount of peptides longer than 8 amino acids, which are generated by the proteasome, affect the antigen processing and therefore the IR. Longer peptides have higher chance to not be destroyed by several intracellular amino peptidases, which shorten the peptides during the transportation phase from the cytosol to the ER, where they become part of the MHCp complex. The open gate proteasome can be one of the factors which allow peptides to reach the ER. In fact, most of the peptides generated by the proteasome are totally destroyed or reduced to short length, losing immunological relevance. The model proposed suggests that some forms of proteasomes, which are replaced during an IR, have an open gate configuration. This allows a better degradation kinetics and longer fragments produced.

Part II

The antigen presentation and the clonal expansion

Chapter 3

Competition for resources and the shaping of the lymphocyte repertoire

Introduction

In this Chapter we shall review published models regarding competition phenomena for immunological resources between lymphocytes in the peripheral tissue. We shall define what immunological resources are, and describe how mathematical models are developed. In particular, we shall focus on competition phenomena related to biological space and to antigens through the description of three different mathematical approaches.

3.1 The concept of competition for resources

It has been accepted since decades that the IS is strongly regulated in size and functionality by resources which shape and keep functional the immune cells repertoire. We can define a “resource" for lymphocytes any antigen, MHC, poly-clonal activators, cytokines (interleukins), chemokines which can lead to increased cell survival or growth, at least in a certain availability range. In ecology, the total requirements of a species for all resources and physical conditions determine where it can live and how abundant it can be at any one place within its range. These requirements are termed abstractly the ecological niche. Lymphocytes can produce their own resources contributing to generation of their niche. Their heterogeneity allows for the co-existence of multiple niches. It is almost straightforward to imagine that these cells compete against each other for the for mentioned resources. Therefore, the

concept of competition between IS cells can be defined. We can take from textbooks the following definition of competition: an interaction between individuals brought about by a shared requirement for resources in limited supply leading to a reduction in the survivorship, growth, and/or reproduction rates of the individuals concerned [Tilman, 1982].

Immunologists focused on the importance of the competition since a long time [Mitchison, 1992, Rocha and Von Boehmer, 1991]. Several data point to competition between lymphocytes for three main classes of resources

1. antigenic epitopes and self-peptides, which both influence the homeostasis and the survival of lymphocytes.

2. cytokines, which are mediator of activation, proliferation, death, and survival signal pathways

3. the biological space

Criteria for the evidence of competition have been recently proposed by [Gaudin et al., 2004]:

1. The competition between cells should modify the equilibrium size of a population. It has been shown that the number of a certain clone depends on the presence of other clones which share common resources.

2. The competition between cells should alter the dynamics of a population. The half-life of lymphocytes is strongly dependent upon the presence of other cells competing for resources.

3. The manipulation of the available resources should modify the equilibrium dynamics of two competing populations.

B-cell and T-cell dynamics fulfill these three criteria of competition [Gaudin et al., 2004, Almeida et al., 2005]. Daily, our body generates a vast number of immune cells with new specificities. Although pre-selection mechanism (such as the thymus for T-cells) limits the influx of danger self-responding cells in the periphery, the appearance of self-reactive cells in the periphery is inescapable. Tolerance, therefore, must be determined not only at a single cell level but also by global properties of the system. Competition is believed to play a major role in shaping a diverse, as well as functional, cell repertoire.

3.1.1 Competition for space

Even though the mechanisms regulating the lymphocyte pools are very different, both T- and B-cells compete for space Fig. 3.1. Several examples

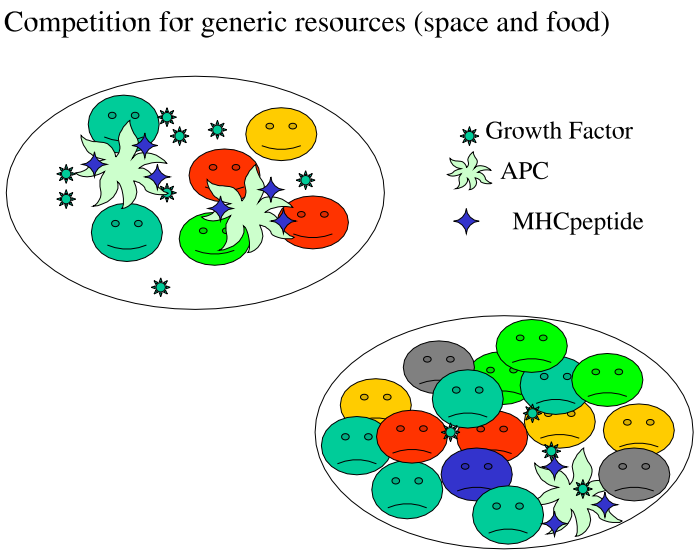

Figure 3.1: Competition for space. This cartoon represent the basic idea behind lymphocytes competition (B- and T-cells) for immunological space. Although a precise definition of what immunological space means is still a matter of debate, we can fairly imagine that during a proliferation phase, caused by some antigenic stimulus, cells may eventually fill the local environment. Unless a strong flux of cells makes again room, and cells occupy the entire space available, the proliferation phase will be suppressed. Experimental evidence suggests that a density dependent proliferation rate occurs during the proliferation of T- and B-cells, and that in extreme lymphopenic condition proliferation increases without antigenic stimuli in order to re-establish the homeostatic size of the repertoire.

taken from literature suggest this common element between these mechanisms. The death rate of lymphocytes depends on the cell density. Highly proliferating cells undergo higher apoptosis rate, while slowly proliferating or resting cells are characterized by a low death rate. As an indicative example we can cite the Fas-FasL mechanism. This is induced during the expansion of cytotoxic T-cells, which activate a programmed apoptosis leading to death. Typically, this mechanism has been observed during the contraction phase of a cellular immune response, where more than 90% of effector cells are eliminated [Wherry et al., 2003]. Fas-FasL interaction has been found also during the normal homeostatic maintenance of cells in the periphery (see also 5).

Experiments evidenced the importance of competition for the biological space [Almeida et al., 2005, Gaudin et al., 2004]. For instance, parabiosis

experiments, in which a series of mice are connected chirurgically to assess a common circulation of blood and immune lymphatic system, show that one mouse is able to fill the IS of a parabiotic system in which three mice are connected each others. This clearly shows that biological constraint are imposed on the pool of immune system cells, and that the pool size at the steady state is a function of the biological space as well. Moreover, aged individuals, despite the multiple antigenic experiences they underwent during life, show a slightly reduced IS size with respect to young individuals. It is worth to conclude that some general mechanisms must regulate the space occupied by the IS cells [Franceschi et al., 2000a].

3.1.2 Competition for antigens

The phenomenon of antigenic competition, in which immune responses to one determinant are inhibited by simultaneous exposure to another antigens on the same or different molecules, has been known since at least the turn of the century [Michaelis, 1902, 1904]. T-cell competition for antigen has been suggested. During an IR, the average affinity for MHC-peptides of the T-cell receptors on the responding T-cells increases [Busch and Pamer, 1999, Savage et al., 1999]. This occurs in the absence of somatic mutation, the phenomenon that drives the affinity maturation of B-cell responses. T-cell affinity selection appears to be caused by a preferential outgrowth of the higher affinity T-cells present within the pool of primary responders, suggesting that the higher affinity cells have a competitive advantage for responding to antigen. In case of chronic infections (HIV, mice LCMV) several response of cytotoxic T-cell clones against multiple epitopes presented on the antigen presenting cell (APC) are observed. This phenomenon can be considered as a competitive coexistence of multiple clones for different epitopes.

An accepted but still controversial phenomenon is the immunodominance, namely the selection of a restricted pool of epitopes from the wide spectrum of antigenic peptides showed during an infection. Only few of these peptides drive the clonal expansion. Mathematical models helped in the understanding of such a mechanism (see later on and [Yewdell and Del Val, 2004]). We also studied immunodominance and how this hierarchy can be changed or reduced during an immune response (see Chapter 4). Many earlier results on immunodominance have been attributed to differential processing of the peptide, which shapes the selection of T-cells. However, not all of epitope dominance can be explained in terms of peptide loading and affinity for MHC. There are data to suggest that T-cells responding to one antigen can actively interfer with T-cells responding to another [Wolpert et al., 1998, Kedl et al., 2003]. Moreover, experimental data demonstrated that some of

these epitopes do not appear to have significant differences in their levels of presentation [Chen et al., 2000]. Presumably, generation of a large number of T-cells specific for the subdominant epitope allows them to compete more effectively for access to APCs with cells specific for the traditionally more dominant epitope.

In recent years, many of the mysteries of B-cell competition have been elucidated and shown to be the consequence of somatic hypermutation and affinity maturation [Cyster, 1997]. B-cells undergo affinity maturation in the germinal center. They are the most well-characterized immune example of competition for niches. Germinal centers play a critical role in the maturation of the immune response by selecting B-cells with high avidity for antigen. Affinity maturation is present only in species capable of germinal center formation. Basically, a massive proliferation of few B-cells clones (on average three) driven by antigen held by follicular dendritic cells occurs. The B-cells expansion is accompanied by B-cell receptor hypermutation. Competition among proliferating B-cells, based on their ability to interact with antigen, leads to the preferential survival of the cells capable of high-affinity recognition and to the death by apoptosis of other cells.

T-cell competition and its effect are observed in several experimental model systems. The preponderance of data from diverse sources and models systems indicates that epitope dominance, T-cell competition and affinity maturation are part of a natural process of ongoing T-cell mediated immunity (see also Fig. 3.2).

We will focus now on a short review of published models regarding competition phenomena in B- and T-cell repertoire. Our main goal will be the understanding of general mechanisms behind competition for resources.

3.2 Models: an overview

For both T- and B- cells, mathematical models based on competition for resources have been proposed (e.g. for B-cells McLean et al. [1997], De Boer et al. [2001a] and for T-cells De Boer and Perelson [1994, 1997]). Most of them borrowed several concepts from theoretical ecology. Important concepts which found application in modeling the IS are

1. The principle of competitive exclusion: namely one species exclude another species with overlapped resources. Several examples are representative of this phenomenon from both ecological and immunological studies.

2. The principle of competitive coexistence: namely species coexist in the

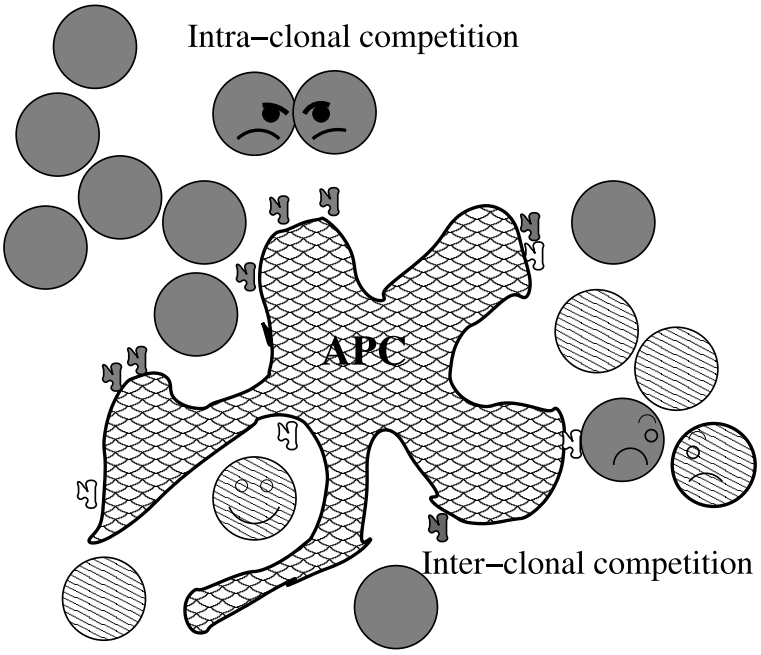

Figure 3.2: Sketch of the direct T-cell competition for antigen. Grey and black T-cells represent two different clones. Intra-clonal competition is the interaction between cells belonging to the same clone which compete for the same resource (MHC-peptide molecule). Inter-clonal competition refers to the impairment of some cells of a defined clone (light grey) to access resources which are blocked by some other cells belonging to a different clone (dark grey).

same environment even if they share resources. As an example, one can imagine a situation in which the competition prevails between individuals of the same species, and is less expressed between individuals belonging to different species.

At the equilibrium, an ecosystem characterized by N different resources can maximally sustain N species [Macarthur and Levins, 1964]. Sharing resources is an important feature for T-cell dynamics. In ecology the coexistence of multiple species is possible only if a minimum number of resources are available. T-cells are characterized by cross-reactivity, which allow different T-cells to recognize the same peptide. Coexistence and competitive exclusion are therefore useful concepts to describe the kinetics of immune cells.

Consider the following general representation of the standard predator-prey model

$$\frac{dX}{dt} = X(1-X) - \alpha F(X,Y) \tag{3.1}$$
$$\frac{dY}{dt} = \alpha\beta F(X,Y) - \delta Y \tag{3.2}$$

where X is the prey and Y is the predator. The function F represents mathematically the interaction between prey and predator and can assume different forms. By purpose the term β has been introduced to describe the proliferation of predators to the capture of the prey. In theoretical immunology the following expressions for the function F have been considered

$$F(X,Y) = XY \qquad F(X,Y) = \frac{XY}{K+X} \tag{3.3}$$

The first function corresponds to what we shall call the Nowak's model. This approach has been used to explain general interaction between immune cell clones competing against each other for resources (such as antigenic peptides) [Nowak et al., 1995a,b]. The second case (known in ecology as Holling type II function) leads to what we refer as the De Boer model. We discuss some example for both cases, and show how simple mathematical models account for competition mechanisms, and how strong is the effect of competition for resources on the cell dynamics.

3.3 Nowak's approach

We consider two application of the Nowak's model. The first deals with the immune response against multiple epitopes of the same virus, while the second describes the competition between humoral and cellular IR. The first example took inspiration from HIV infection [Nowak et al., 1995a,b]. This chronic disease is characterized by a strong initial cytotoxic immune response. Concomitantly to the AIDS development this IR vanishes, and rapid oscillating immune responses are observed. Longitudinal studies evidenced a fast change in epitopes presented on the APCs of infected individuals, which lead to a rapid incoming of new specific T-cell clones.

It has been proposed that antigenic variations, due to virus mutant, or dynamic change of the amount of epitopes presented on the APC, may underlie these unexpected changes. The model offers an interesting mechanism

to explain these phenomena, and suggests how competition between antiviral clones for epitopes can be the leading element for the explanation of this complicated dynamics.

The second example is based on competition between several predators for one prey. In this case, the predators are the different adaptive immune responses: the humoral (mediated by B-cells) and the cellular (mediated by T-cells) [Arnaout and Nowak, 2000]. The model clearly shows that the competitive dynamics between different cells shapes a better immune response. The coexistence of both responses may result in a better protection for the host against infections while, in case of competitive exclusion, the virus may persist at low concentration and re-expand later on, giving rise to danger reinfections. The authors highlight an interesting analogy with free-market economics: competition between companies results in a benefit for the consumer. The coexistence of both humoral and cellular immune response results in a benefit for the host, which can control much better the infection.

3.3.1 Immune responses against multiple epitopes

Suppose during an infection two different epitopes, say A and B, are presented on the surface of APCs. Each epitope can be represented by a sequence of 8-10 aa, which is the result of the degradation of viral proteins. T-cells recognize a spectrum of sequences with different affinity. Suppose several variants of the epitope A and B-are possible due to the viral mutation or simply to dynamic regulation of their abundance on the surface of APCs. Suppose also that a mutant of the epitope A appears. This leads to a new scenario for the antiviral response: the new IR can be very similar to the previous one, or change toward a new clones distribution with new dominant clones responding against the infections.

A simple way to show this is to write down the equations in the case of two clones, x and y, recognizing epitopes A and B. Moreover, n_1 possible amino acid sequences for epitope A, and n_2 possible amino acid sequences for epitope B-are considered. We can write down the equations for the clone x_i recognizing sequence i, and for the clone y_j specific for the sequence j of the epitope B

$$\frac{dv_{i,j}}{dt} = v_{i,j}(r - px_i - qy_j) \tag{3.4}$$

$$\frac{dx_i}{dt} = x_i(cv_{i,*} - b) \quad i = 1, .., n_1 \tag{3.5}$$

$$\frac{dy_j}{dt} = y_j(kv_{*,j} - b) \quad j = 1, .., n_2 \tag{3.6}$$

The parameters c, k are the immunogenicity of the sequence i of the epitope A and the immunogenicity of the sequence j of the epitope B-respectively. There are a total number of $n_1 \times n_2$ clones responding to the virus. Clones proliferate at rate proportional to the epitope immunogenicity and die at rate b. The virus is killed at rate p in case the sequence of epitope A is recognized, and at rate q in case sequence of epitope B. $v_{i,*}$ is the sum of all viruses which possess the sequence i. The same for $v_{*,j}$.

It is worth to note that the competition between clones x and y is governed by two factors: the immunogenicity of the epitope, namely the more immunogenic the better the IR, and the antigenic variability, which means the less variability the better the IR. Antigenic variability does not necessarily means that mutants of the virus arise over time. Oscillations between different immune responses can be observed also with a fixed number of epitopes present since the beginning. The immune response can reduce the viral peptide to very low level, and the number of clone cells diminishes. But later on, the epitope abundance can rise again leading to a new peak of the same clone. Competition between the IRs is decided by the ratios c/n_1 and c/n_2. Consider a steady state characterized by $\dot{x}_i = 0$. It is trivial to see that the solution is $v_{i,*} = b/c$, and the total virus abundance is $\bar{v} = bn_1/c$. On the other hand, suppose $\dot{y}_j = 0$. It follows that $\bar{v} = bn_2/k$. The competitive exclusion is evident: in general these two solutions for the total virus $\bar{v}$ cannot be simultaneously fulfilled (unless $n_1/c = n_2/k$). Trivially, (simple steady state analysis) one can show that a clone (x or y) will disappear and the other survive according to the magnitude of the ratios c/n_1 and k/n_2. If all the clones y_j vanish, we are left with the following equations

$$\frac{dv_{i,*}}{dt} = v_{i,j}(r - px_i) \tag{3.7}$$

$$\frac{dx_i}{dt} = x_i(cv_{i,*} - b) \tag{3.8}$$

The clones x_i oscillate, and the replication rate of the virus and the death rate of clones define the oscillation period. In fact, this is a system of n_1 uncoupled oscillators with an approximative period of $T \simeq \frac{2\pi}{\sqrt{rb}}$.

Let consider a more general situation in which each immune response face an epitope sequence with immunogenicity c_i and k_i.

We could than rise the question: which factors determine the immunodominance? This model suggests that the exclusion of the immune response against the epitope B, y_j is possible if the epitope A have immunogenicities such that $\sum_i \frac{1}{c_i} > \sum_j \frac{1}{k_j}$. The epitope A will then be the immuno-dominant. A same argument can be given for epitope B. If there is only a homoge-

neous virus population then the generic situation is that there is exactly one immuno-dominant epitope. But as we have already observed, immunodominance is a function both of the immunogenicity and of the diversity of the epitopes, and also of the replication rate of the various mutants. Antiviral clones can compete for epitopes because of their cross reactivity. The virus itself can replicate at different rates in dependence on the particular sequence. These conditions can indeed generate both x and y responses without competitive exclusion. We may expect coexistence of immune responses against several epitopes. Basically, if the various epitopes have comparable immunogenicity and eventually the virus mutants differ in their overall replication rates, we would aspect none of the immune response prevailing (at least for an arbitrary choice of the parameters). The model suggests that the virus heterogeneity will keep the resources diverse enough to stimulate a wide spectra of different clones.

For slowly replicating viruses with low heterogeneity a restrict repertoire of antiviral clones is expected and eventually a complete competitive exclusion may leads to a monoclonal response. In cases where the virus replicates fast and is very heterogeneously represented, than competitive coexistence of several immune responses is expected. Intuitively the clones x_i oscillate, and the replication rate of the virus and the death rate of clones define the oscillation period. In fact this is a system of n_1 uncoupled oscillators with an approximative period of $T \simeq \frac{2\pi}{\sqrt{rb}}$.

3.3.2 Competition between humoral and cellular response

The second model is based on similar assumptions [Arnaout and Nowak, 2000]. Consider the humoral (B), and the cellular, (T cytotoxic) responses. The former recognizes extracellular pathogens present in the body, while the latter is driven by intracellular infections. Therefore, the viral infection is modeled in terms of free virions v, which stimulate the humoral response, and of infected cells I which are responsible for the T-cell activation

$$\frac{dI}{dt} = \beta v - \alpha I - pTI \tag{3.9}$$

$$\frac{dv}{dt} = kI - uv - hvB \tag{3.10}$$

$$\frac{dT}{dt} = cIT - bT \tag{3.11}$$

$$\frac{dB}{dt} = fvB - gB \tag{3.12}$$

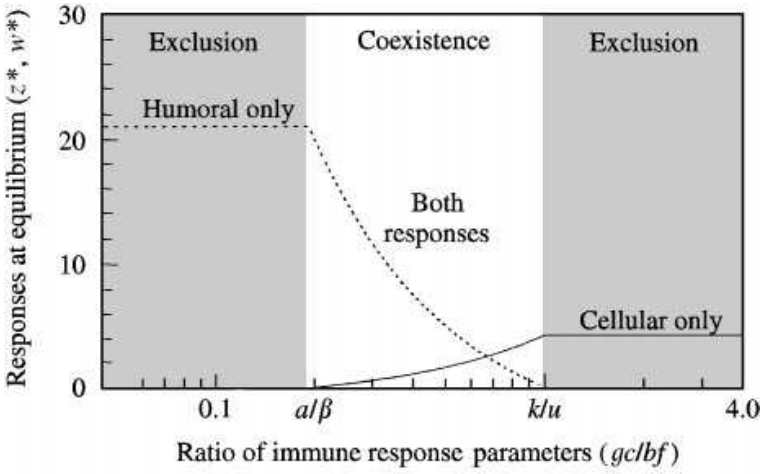

Figure 3.3: Competition between humoral and cellular immune response. This table is a summary of the steady states of the model presented in 3.3. On the x-axes the ratio gc/bf is reported. The values α/β and k/u represent the boundary values of the above defined ratio, which leads to the coexistence of both humoral and cellular immune response (see also Eq. (3.13)). The left and the right side of the figure represent the parameter region for which competitive exclusion for one of the IR is observed. This picture is taken from Arnaout and Nowak [2000]

Infected cells grow proportional to the virus at rate β, and die at rate α. Infected cells produce virions at rate k, u is the per virion decay rate of free virus. The cellular response limits the size of the infected cell pool by cell-mediated lysis (by perforin, Fas-Fas ligand interaction). This is captured in the pIT term, where p is the rate of killing. Similarly, the humoral response limits viral load by antibody-mediated neutralization, captured in the hvB term; h is the rate of antibody-mediated clearance. The constants c and f, respectively, denote cellular and humoral responsiveness, which are roughly measures of the quickness with which the host elaborates these responses. The constants b and g are the respective per capita natural decay rates of the cellular and humoral responses.

The system has four stable equilibria. It is possible to show that the following condition defines the steady state

$$\frac{k}{u} > \frac{cg}{bf} > \frac{\alpha}{\beta} \tag{3.13}$$

Three qualitatively outcomes are possible (see Fig. 3.3): viral clearance independent of the immune response (all of the above conditions do not

hold) persistence controlled by a single response (only one of the two side of the condition Eq. (3.13) hold: competitive exclusion) persistence controlled by both responses (Eq. (3.13) holds: coexistence). The Fig. 3.3 shows a schematic representation of the model outcome. Humoral and cellular immune responses can out-compete or coexist in dependence of the kinetics of the viral load and of the immune response. To better understand how the competitive exclusion and the coexistence between humoral and cellular immune response rises we consider two examples.

The competitive exclusion: suppose the virus is very cytopatic, namely $k/u \leq cg/bf$. In this case (see right side of Fig. 3.3 either the virion production rate k is too low (or its clearance u too high), or the humoral response has very low responsiveness f. This condition leads to a very high cellular immune response, which result in the clearance of the infected cells and to a very low viral load v. At equilibrium a strong impairment for the humoral immune response to persist is observed: the number of infected cells reaches very low level and viral load in not sufficient to keep a long term humoral immune response. On the other hand, if the infectivity or cellular responsiveness is reduced, the humoral response persists and keep the virus under control.

The competitive coexistence: suppose all the conditions in Eq. (3.13) hold. The two responses never out-compete (see Fig. 3.3). These relation results in a stable equilibrium for the system in which both humoral B and cellular T are non zero. Unless the virus is completely cleared it would be beneficial for the body to keep track of the virus from both humoral and cellular immune responses. Viruses present very different replication rates and present several degree of cytotoxicity. they can spread as free moving particle or intra-cellularly and most important these parameters can change during the course of the infection.

The message of this model is that competitive immune responses can control better the very diverse spectra of action that viruses possess.

3.4 De Boer's approach

The main feature of the model is the competition for binding of T- or B- cells to ligands expressed on MHC molecules. Cells recognizing these molecules according to some specificity rule are able to proliferate in the system. The model describes the homeostasis of the system, the total number of cells is kept almost constant with and is regulated by the cross-reactivity and th diversity of the repertoire as far as the peptides presented to the surface of APC are concerned. This approach will be used in the next Chapter as a

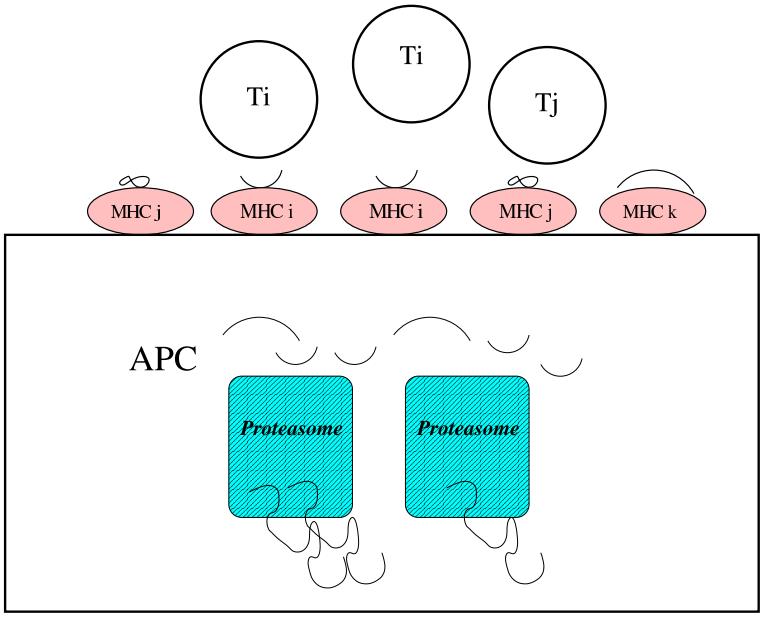

Figure 3.4: Protein sequences containing antigenic peptides are taken up and degraded by intracellular proteolytic pathways, such as the proteasome degradation. In the De Boer model a T-cell binds to the MHC-peptide molecule presented on the APC. Th binding is regulated by the affinity between T-cell receptor and the MHC-peptide complex. Each MHC molecule presents a peptide, and its abundance limits the size of the T-cell repertoire.

template for our model, and it has been widely used in T- as well as B-cells kinetics models [De Boer and Perelson, 1994, Borghans et al., 1999, De Boer et al., 2001a].

The model can be obtained by the following reaction scheme

$$T_i + F_j \rightleftharpoons C_{i,j} \rightarrow 2T_i + F_j \tag{3.14}$$

The cell T_i binds to a free MHC-peptide molecule F_j forming a complex C_{ij}. The binding affinity is given by the kinetics rates of the complex formation (see appendix B). Cells proliferate if the binding between the T-cell receptor and the MHC molecule on the APC is strong enough. With this scheme,

supposing a death rate δ for T-cells, one can write the following equations

$$\frac{dT_i}{dt} = \sum_{j=1}^{Pep} k^p{}_{ij} K_{ij} S_j T_i - \delta T_i \tag{3.15}$$

$$S_j = \frac{P_j}{1 + \sum_{i=1}^{N} K_{ij} T_j} \tag{3.16}$$

We consider N clones competing for M peptides (for more explicit calculations see Chapter 4 and De Boer and Perelson [1994, 1997]). S_j defines the number of free MHC-peptide complexes available on the APCs. Suppose the number of different clones is greater than the number of different peptides. For at least $N - M$ clones the equilibrium is given by $T_i = 0$. Therefore, only M clones, which correspond to the number of antigens, can survive. This result corresponds to the standard ecological concept known as principle of competitive exclusion. At the equilibrium

$$\sum_{j=1}^{Pep} k^p{}_{ij} K_{ij} S_j = \delta \tag{3.17}$$

For instance, suppose we have N clones and that the first $i = 1$ is the one that has maximum $\beta = \sum_{j=1}^{Pep} k^p{}_{ij} K_{ij} S_j$. At the equilibrium $\beta = \delta$ and $T_1 \neq 0$. This implies that all other clones $2, 3, ...N$ necessarily have to die ($\dot{T}_i < 0$).

Competitive exclusion is presented in the context of affinity selection: T-cells undergo a selection process during the clonal expansion without mutation of their receptor as commonly happens for B-cells. In this scenario, the principle of competitive exclusion state that given a peptide and the set of clones which has a defined affinity for it, the clone with the highest affinity will survive.

This model shows that the diversity of the T-cell repertoire is shaped by the diversity of self-peptides presented on the MHC molecules. The competitive coexistence of a diverse T-cell repertoire can be maintained by a sufficient diverse peptide repertoire. One should also keep in mind that in case the selection mechanism lasts for a very long timescale, such as the individual lifespan, the exclusion of some clones might never be observed. Studies on aged mice and cross-sectional human data evidence a reduced diversity in the naive T-cell pool. Probably competitive exclusion can be one of the mechanism influencing this phenomenon. Today we know that the affinity of an epitope specific immune response tends to increase with the duration of the antigen exposure, confirming the main result of this model [Busch and Pamer, 1999, Slifka and Whitton, 2001, Yewdell and Bennink, 1999].

3.4.1 T-cell competition for peptides presented on the same cell

A recent application of the De Boer's approach has been the competition between different T-cell clones when their specific epitopes are presented on the same antigen presenting cell [Scherer and Bonhoeffer, 2005]. Experimental data suggests another interesting way of competition between T-cells, and confirms the importance of competition mechanisms [Kedl et al., 2003].

T-cells compete for antigen at several levels. For instance, T-cells can directly inhibit the response of other clones by down regulating the epitope expression on the APC or inhibiting the contact between APC and other clones (Fig. 3.2). This is known as inter clonal competition. Intra clonal competition, namely competition between cells of the same specificity is also observed. T-cells can indirectly out-compete other cells by killing the APCs or by reducing general resources like cytokines, inducing proliferation and survival signaling.

The model proposed by Scherer et al. is based on the down-regulation of different epitopes presented on the same APC, and shows that T-cell competition occurs at the level of access to the limited number of antigen-bearing APCs.

$$\frac{dV}{dt} = rV(1-cV) - K_{kill}V(E_1+E_2) \tag{3.18}$$

$$\frac{dA_{1,1}}{dt} = \sigma V - \delta_A A_{1,1} \tag{3.19}$$

$$\frac{dE_1}{dt} = r_1 A_{1,1} F_1(E_1,E_2) - \delta_E E_1 \tag{3.20}$$

$$\frac{dE_2}{dt} = r_2 A_{1,1} F_2(E_1,E_2) - \delta_E E_2 \tag{3.21}$$

A population of virus infected cells, V grows with a maximal rate r in a density dependent manner, and has a carrying capacity of c. It is assumed that APCs present two epitopes on their surface. Virus infected cells are cleared with clearance rate K_{kill} by effector T-cells E_1 and E_2, that have respective avidities r_1 and r_2 for antigen presenting sites on APCs that express both epitopes. The influx of new epitope expressing APC sites is proportional to the number of infected cells with a proportionality constant σ. APCs and effector T-cells have death rate δ_A and δ_E respectively. The saturated proliferation functions $F_1(E_1,E_2) = E_1/(1/K + E_1 + E_2)$ and $F_2(E_1,E_2) = E_2/(1/K + E_1 + E_2)$ account for the competition between T-cells for the binding with the two epitopes on the same APC (see also Eq.

(3.3)). The main idea is that competition between the two effector cell clones responding to the epitopes exists. The number of APCs $A_{1,1}$, presenting both epitopes, decreases if there is epitope down-regulation. This pushes the system to differentiate and have more APCs which show independently the two epitopes. Namely we get $A_{1,0}$ and $A_{0,1}$. The equations for this APCs and the epitope down-regulation kinetics are not shown for the sake of simplicity (see Scherer and Bonhoeffer [2005] for a complete description). The inter-clonal competition decreases. Epitope down-regulation leads to differentiation of epitope presentation on antigen presenting sites. Different T-cell clones will not compete for their resources because they will be presented on different cells.

The conclusion is that APC differentiation promotes the coexistence of multiple epitope specific responses. The functional relevance of epitope down-modulation seems to enable the persistence of a broad immune response, despite competition for antigenic stimulation. We shall discuss a similar problem in the next Chapter. We consider the IR in the context of replacement of constitutive with immunoproteasome. The consequences on antigen presentation and the clonal selection of cytotoxic T-cells during the immune response will be discussed.

3.5 The fratricide mechanism

It is well accepted but still largely unknown that T-cells can kill each others. The reasons can be very disparate, going from space competition to overexpression of substances inducing death (perforin, or cytokines inducing apoptotic intracellular pathways). These phenomenon is generically named fratricide killing mechanism. In literature the concept of fratricide is not fully defined and the mechanisms behind are still largely unknown. Two possible mechanisms have been proposed. The first is an antigen dependent fratricide, where T-cell are recognized via their MHC class-I molecules by other T-cells, and committed to die (via perforin) [Su et al., 2004]. The second, is an antigen independent fratricide characterized by a generic competition for space. Highly proliferating T-cells fill fast the space available, and undergo a mechanism of apoptosis driven by Fas-FasL contact [Callard et al., 2003].

Antigen independent mechanisms are known to regulate T-cell proliferation and survival [Allan et al., 2004, Callard et al., 2003]. The next model introduces a nonlinear death term (fratricide) in the population of antigen activated cells, A, and memory, M, T-cells. Moreover, a certain amount of

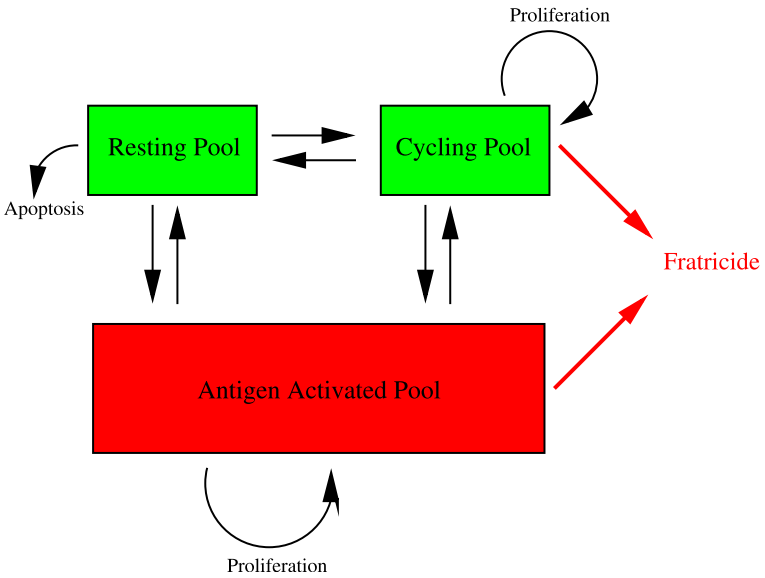

Figure 3.5: Scheme of the fratricide model. The fratricide killing mechanism acts only in the cycling and activated T-cell pools, which are capable to proliferate actively after antigenic stimuli. The resting pool has a very low apoptosis rate and is capable to stay in the system for a long period of time.

memory cells is supposed to cycle (self renewal process), C (see Fig. 3.5).

$$\frac{dM_i}{dt} = rC_i - (a+d+s)M_i + p(s)A_i \tag{3.22}$$

$$\frac{dC_i}{dt} = 2aM_i + cC_i - fC\sum_j C_j - (r+s)C_i \tag{3.23}$$

$$\frac{dA_i}{dt} = s(M_i + C_i * N) + cA_i - kA_i\sum_j A_j - p(s)A_i \tag{3.24}$$

Proliferation within compartments C and A occurs at a rate c. Fratricide is related to the proliferating pool: in the memory cells it occurs at rate f, and in the activated T-cell pool at rate k. During an infection, pre-existing memory cells of specificity i are recruited into the activated pool A at rate s. Recruitment also occurs from naive cells v. Activated cells are flowing back into memory pool at a constant per capita rate p, which is zero during the infection (proliferation happens only in the presence of the antigenic stimulus, $p(s=0)=0$). A flux of cells between the cycling and the resting pool is considered with the rates r and a. The quadratic terms have been introduced

by phenomenological considerations. Basically, if two different clones are proliferating, well mixed, and meet at random , the probability that their daughter cells will encounter and induce fratricide killing is proportional to the clone sizes. Because both clones are proliferating, we would expect a death rate proportional to the product of the proliferating cells numbers. Therefore, on a first approximation, fratricide should be a quadratic term of the clone size.

This model predicts that long-term clonal memory does not have to depend on antigen stimulation, but competition for space or for general resources could be crucially related to fratricide through Fas or Fas-like mechanisms of apoptosis. The size of the total repertoire is inversely proportional to the fratricide rate and independent on antigen (for more calculation see Yates and Callard [2001]).

A similar result is obtained with the De Boer's approach. The main difference is that in the fratricide model a separate cycling population of memory cells is considered. T-cell fratricide killing provides a T-cell density-dependent death mechanism, which defines the homeostatic level of the total T-cell repertoire and does not depend on antigen specific regulatory mechanisms.

3.6 Conclusion

This short review of mathematical models of T- and B-cell competition dynamics should help the reader to understand the importance of including such a phenomena in the quantification of the adaptive immune response. It is important to summarize the main differences between these models. Comparing the Nowak's approach with the De Boer's, we conclude that the competitive exclusion can be obtained from different hypotheses. The former is based on the fact that high affinity clones kill infectious agents very fast, and reduce the antigen to minimal concentration, that other cells can no longer be stimulated. This is what is usually called an indirect competition. The latter approach offers a more explicit mechanism of competition. Cells compete directly each other, even if the antigen is present at very low concentrations or is kept constant. The maintenance of the T-cells is due to the diversity of the MHC-peptide complexes, and not much dependent on antigen concentration. Regarding the model of T-cell fratricide, we conclude that competition for space during the proliferation phase is an interesting and general mechanism to control the immune repertoires in an antigen independent fashion. Chronic unspecific stimuli or fluctuating environment can affect the proliferation of clones. Fratricide via Fas-FasL interaction is a

possible mechanism which can cope such a perturbation and reestablish the homeostasis. In Chapter 5 we shall discuss how mechanism like Fas-FasL can set the equilibrium size of clones. Under specific hypotheses, a possible scenario for the maintenance and for the expansion of T-cell clones over long timescales is proposed. Moreover, a fluctuating environment disturbing the size of clones is described. The De Boer's approach suggests a mechanistic interpretation for the antigen recognition pathway, which is also missing in the fratricide model. One can therefore consider also a more detailed analysis of the peptide kinetics, and eventually a description of the intracellular pathways, which are responsible for the generation of MHC-peptide molecules. Recently, experimental data pointed on mechanisms of the antigen processing and on their quantification. The De Boer's approach offers a natural background where a more detailed theory of antigen presentation can seat and develop. In the next Chapter we shall face this problem.

In Chapter 4 the clonal expansion of T-cells in a competitive environment is considered. We show how competition for resources affects the homeostasis of the naive pool and the efficiency of the IR. The peptide distributions, which are the result of intracellular degradation, affect the clone size, the immunodominance, and the quality of the IR. Some experimental data are explained, and predictions regarding how vaccination strategy can be improved are proposed. For instance, we shall show that the clearance of a pathogen is improved when a re-shaping of the T-cell clones by the replacement of constitutive proteasomes with his immuno-forms is considered.

Summary

It is now accepted that the homeostasis and the functionality of lymphocytes are strongly affected by competition phenomena. The IS resources can be the cytokines, which are responsible for a high number of functions, the antigens, which constitute the main information source for the IS to get activated if infection factors come over, and finally the biological space, which somehow provides the physical conditions to allow proliferation and movement. We reviewed published mathematical models to describe the competition between T- and B-cells for resources. In the next Chapter we shall discuss a model based on some idea presented here.

Chapter 4

The clonal expansion of cytotoxic T-cells and the immunoproteasome

Introduction

How many naive T-cells in the peripheral repertoire belong to the same clone? Do large differences exist in the frequency of two distinct naive clones? Several factors may generate differences in the size of various pre-immune clones. Both the recombination machinery and thymic and peripheral selection processes can favor the accumulation of certain clonotypes. Alternatively, particular T-cell clones may have already undergone some rounds of cell division in the periphery, for example after cross-reaction with environmental or food antigens. Obviously, if large differences exist, the largest clones could dominate the immune repertoire by giving rise to a much more abundant progeny than that derived from a single precursor. In this chapter we propose a mathematical description of the peripheral T-cell repertoire and its dynamics. We show how low precursor frequency clones can efficiently kill intracellular pathogens with the help of a clever way to distribute resources.

4.1 The biology of the problem

As already explained in Chapter 1, the thymic selection is the first and fundamental selection phase that T-cell repertoire suffers. The repertoire selection is made by a positive and negative discrimination, which is based on the affinity between T cell receptor (TCR) and MHC- peptide complexes (MHCp). In the thymus, APCs present peptides generated with both the

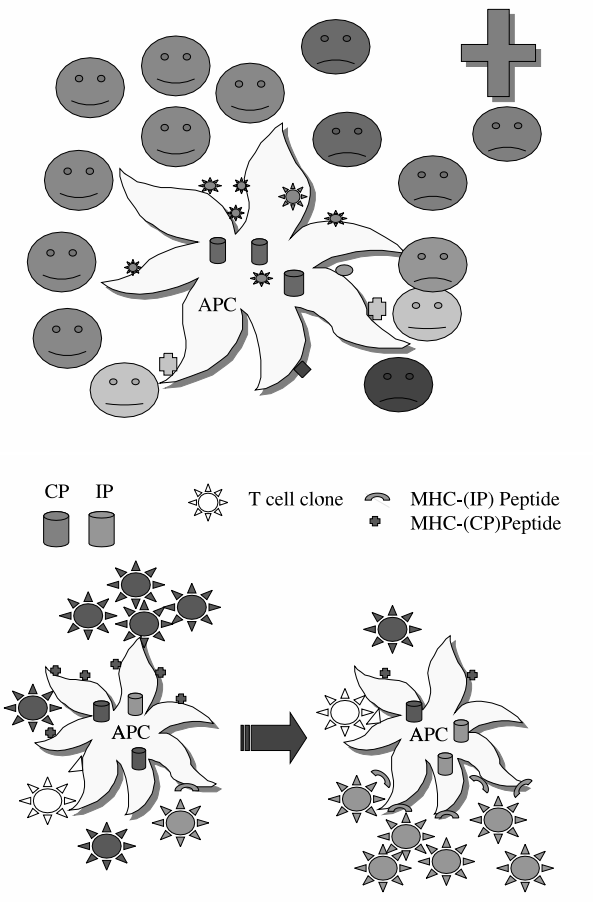

Figure 4.1: Upper panel: T-cells competing for peptides presented on the surface of APC. T-cell clones survive and keep their functionality in the peripheral tissues requiring contact with MHC molecules presenting self-peptides. Moreover, the peptide abundance is a major factor in shaping the T-cell clone abundance. Bottom panel: intracellular processing of peptides. The replacement of CP (light grey cylinder) with the IP (dark grey cylinder) induces a new peptide distribution on the surface of the APC. This is the base for a re-shaping of the T-cell repertoire.

constitutive (CP) and immunoproteasome (IP). IP and CP shape the peptide repertoire which selects the candidate T-cells for the emigration through peripheral tissues. During our lifespan the thymus reduces in activity, but still an efficient repertoire of peripheral T-cells is maintained. How can this happen? It has been shown that peripheral mechanisms maintain an efficient immune repertoire. Efficient means diverse enough to fight challenges, and

tolerant at the right point to not destroy non dangerous factors that immune cells meet during the continuous rendezvous with parts of our body.

In order to understand these selection mechanisms, it is very important to know the diversity and the abundance of the peptide distribution presented on the MHC molecules. In the periphery, T-cell homeostasis depends upon MHCp T-cell receptor contact (for a review see Almeida et al. [2005]). Several experiments highlight the importance for the peripheral mature T-cell pool to recognize self-peptides with low or medium affinity [Holler and Kranz, 2004, Jameson, 2005]. Before an IR starts, there is a very heterogeneous distribution of clone sizes, and very often small clones are capable to outcompete huge clones.

Quantification of T-cell and MHCs diversity suggests that the clone distribution responding to a given antigen is heterogeneous and time dependent [Zhong and Reinherz, 2004]. It has been estimated that up to thousand different clones can be stimulated with a given antigen [Naumov et al., 2003, Pewe et al., 2004]. The majority of these cells belongs to few big clones, while the other part make up a very large repertoire of small clones, and all with a potential capability to rise an IR. Several statistical models have been applied to fit these data. Basically, the distribution of clone frequencies looks like a power law distribution or like a log-normal distribution [Naumov et al., 2003, Pewe et al., 2004]. These functions are characterized by a long-tail in which few clones represent the majority of cells, and a very high number of low-frequency clones defines an evident and non-excludable tail which play a major role for shaping the diversity of the responding T-cell repertoire.

During an IR some of the APCs, the most important being dendritic cells, become professional, and show on the surface a fairly different MHCp repertoire. Within these cells, the IP content is increased and the CP abundance reduced. Professional APCs initiate the differentiation program, and during an IR naive T-cells are activated by the APC and differentiate to experienced T-cells which are capable to fight pathogens. Only few of the activated T-cells will respond to the antigenic peptide, and the selection is performed during the expansion phase [Blattman et al., 2000]. T-cells are characterized by cross-reactivity, namely are sensitive to a diverse ensemble of MHCp.

The timescale of an IR is of the order of weeks for acute infections, and can last for years in case of chronic infections (HIV, Hepatitis C, Coriomeningitis, etc.).

During an infection, many different viral peptides are presented on the surface of APCs, but only some will elicit an IR. It is a matter of debate why only few of these peptides drive the immune repertoire and a hierarchical distributions of IRs are observed. This phenomenon is commonly called

peptide immunodominance [Yewdell and Del Val, 2004]. Several factors are involved in shaping the immunodominance. The intracellular viral kinetics and the antigen processing machinery are the most known and important factors. Notably, the IP affects the immunodominance. Mice deficient in IP (such as IFN-γ and immunoproteasome-subunit deficient mice) present alterations in the immunodominance hierarchy of peptides presented on their APCs.

We investigate the hypothesis that the IS has a clever way to allow few cells to become the best weapon against pathogenic challenges.

4.2 Purpose of the model

We investigate how competition for peptides shapes the cytotoxic T-cell repertoire during an IR. The model is based on the assumption that the amount of CP and of IP in the APC influences the peptide distribution presented on the MHC molecules, and with that influences the T-cell repertoire. Our goal is to show a possible role of the production of IP during an IR.

We investigate the IP-effect, namely the effect of a change of the MHCp distribution presented by APCs, induced by an increased intracellular IP content. In Fig. 4.1 a cartoon which present this idea is shown. We show how the clearance of the pathogen can be improved without any change of the parameter values, besides a change in the IP concentration in APCs.

The model is based on De Boer's approach (see Chapter 3 and De Boer and Perelson [1994]). Due to the very high diversity and size of the T-cell clone repertoire, a caricature model which takes into consideration only families of clones is proposed. Clones are grouped according to their pattern recognition of MHCp (see Tab. 4.3). The model first describes the steady state condition in a given peripheral tissue, namely the homeostasis of the T-cell repertoire without the pathogenic insult. It takes into account the thymic output, and competition between T-cells for MHCp. Starting from this steady state condition, we describe the following IR against pathogenic peptides for two cases. First, no MHCp redistribution, second we suppose an MHCp redistribution due to IP induction in APCs at the onset of the IR.

4.3 The model

This model describes the dynamics of naive N and the experienced E cytotoxic T-cell pools (see also Fig. 4.2 and Chapter 3 for a review of the the general approach). Our ansatz is that both naive and experienced T-cell

pools require MHCp-TCR contact to maintain their homeostatic size (see Fig. 4.1). Naive cells are activated and proliferate. Some of them become antigen experienced cells and move towards the infection sites and kill the infected cells which present the antigenic peptides. The following scheme is proposed:

$$N_i + F_j \quad \underset{k^d}{\overset{k^a}{\rightleftharpoons}} \; {C^N}_{ij} \overset{{k_p}^N}{\rightarrow} {T^*}_i + F_j \tag{4.1}$$

$$E_i + F_j \quad \underset{k^d}{\overset{k^a}{\rightleftharpoons}} \; {C^E}_{ij} \overset{{k_p}^E}{\rightarrow} 2E_i + F_j \tag{4.2}$$

$$T^* \quad \overset{k^*}{\rightarrow} 2\phi N_i + 2(1-\phi)E_i \tag{4.3}$$

This reactions describe the proliferation and differentiation rates for both T-cell pools considered. The indexes i, j denote T-cell clone i, $i = 1 \cdots N_{clone}$ and MHCp of specificity j, $j = 1 \cdots N_{pep}$, respectively. F_j is the amount of free MHCp sites on the APCs with specificity j. ${C^N}_{ij}$ and ${C^E}_{ij}$ are the complexes formed between TCR and MHCp of the naive and experienced pool respectively. The kinetics of complex formation are described by the classical enzyme reaction kinetics with association and dissociation constant k^a and k^d respectively. For the sake of simplicity, we consider the same complex formation kinetics for both the naive and the experienced pool. Naive cells are activated after MHCp contact with rate ${k_p}^N$. They become T^*. These cells proliferate with rate k^*, and stay in the naive pool with probability $0 \leq \phi \leq 1$, or differentiate to experienced cell with probability $1 - \phi$. The probability ϕ can be considered a function of the APC state (professional or non-professional APC), and/or of the γ-chain cytokines amount (IL-7, IL-15 and IL-2). If the APC presents co-stimulatory signals, a naive cell tends to differentiate, while in case the APC is non professional, naive undergoes a self-renewal process. Experienced cells E_i are characterized by a proliferation rate ${k_p}^E$ and constant death rate δ_E. We suppose that the experienced cells proliferate faster than naive cells, namely ${k_p}^E > {k_p}^N$. During the presence of foreign pathogenic peptides, both the naive and experienced cells may proliferate. The latter can kill infected cells reducing concomitantly the expression of foreign peptides on the surface of infected cells. The phase characterized by the establishment of memory T-cells is not considered in the model. We consider the thymic output, H_i, per clone defined as a constant number of cells coming from the thymus for each specificity i. Moreover, a death rate for naive, δ_N, and for experienced cells, δ_E, has been considered.

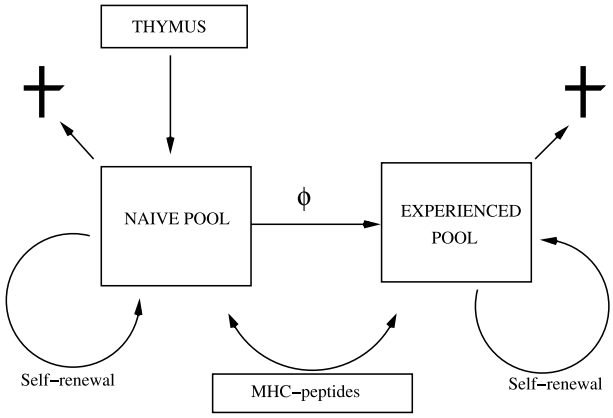

Figure 4.2: Scheme of the model presented in Eqs. (4.1 - 4.3). Thymic output is considered as a constant flux which uniformly fills the naive compartment. Naive cells share resources with the pool of experienced cells. They compete for MHCp. Naive cells can be activated and proliferate. Once activated they can differentiate into the pool of experienced cells or stay in the naive pool according to the rate ϕ. Death is considered for both pools. Experienced cells proliferate and die faster than naive.

We define the following constants

$$K^N{}_{ij} = \frac{k_{aij}}{k_p{}^N + k_{dij}} \qquad K^E{}_{ij} = \frac{k_{aij}}{k_p{}^E + k_{dij}} \tag{4.4}$$

The equations for the complete dynamics are

$$\frac{dN_i}{dt} = H_i + (2\phi - 1)\, k_p{}^N \sum_{j=1}^{N_{pep}} K^N{}_{ij}\, F_j N_i - \delta_N N_i \tag{4.5}$$

$$\frac{dE_i}{dt} = 2(1-\phi)\, k_p{}^N \sum_{j=1}^{N_{pep}} K^N{}_{ij}\, F_j N_i + \sum_{j=1}^{N_{pep}} k_p{}^E\, K^E{}_{ij}\, F_j E_i - \delta_E E_i \tag{4.6}$$

The equations are obtained under a quasi-steady state approximation (QSS) on the kinetics of T-cell clones. Basically, we supposed that T-cell differentiation after complex formation is supposed to happen with a rate much faster than the rates characterizing complex formation and T-cell proliferation. This allows us to consider an instantaneous reaction (Eq. (4.3)). Moreover, we suppose that the dynamics of the complexes $C^N{}_{ij}$ and $C^E{}_{ij}$ are at the steady state, namely $\frac{dC^N}{dt} = \frac{dC^E}{dt} = 0$ (we skip the index for simplicity).

In order to model the MHCp concentration available on the surface of APC we have followed De Boer and Perelson [1995]. In this paper the peptide concentration is at the equilibrium, and is limited by the MHC availability , which is defined by the maximum abundance M_T, and by the T-cell, which binds to MHCp. In Appendix B the explicit calculations are shown. Peptides are generated intra-cellularly by the proteasome degradation of cells (see also the cartoons in Fig. 4.1 and Fig. 4.2). Given the following scheme

$$P_i + E \underset{k_-}{\overset{k_+}{\rightleftharpoons}} S_i \tag{4.7}$$

$$Z = M_T - \sum_{j=1}^{N_{pep}} S_j \tag{4.8}$$

with $k = \frac{k^-}{k^+}$, where Z is total amount of MHC molecules available intracellularly. Peptides of specificity P_j meet a free MHC molecule forming a MHCp named S_j. Peptides are mounted on the MHC molecule at faster kinetics with respect of T-cell - MHCp contact.

Writing the explicit equations for P_j, and considering the steady state approximation $dS_j/dt = 0$ we get an explicit formula for F_j

$$F_j = \frac{S_j}{1 + \sum_{l=1}^{N_{clone}} (K^N{}_{ij} N_l + K^E{}_{ij} E_l)} \tag{4.9}$$

Clearly, increasing the total T-cell pool, the number of free complexes diminishes. Competition for MHCp, which are considered resources for survival i.e. free sites (see Chapter 3), limits the clonal size [De Boer and Perelson, 1997]. It should be emphasized that a normalized distribution of peptides on the surface of APC is considered

$$\sum_{l=1}^{N_{pep}} P_l = 1 \tag{4.10}$$

In this way it is possible to consider only the frequency of each peptide.

The pathogen dynamics and the definition of a foreign peptide

Suppose that a pathogen infects cells. Foreign peptides will be processed and presented on the surface of infected cells. For instance, a virus like Lymphocyte Coriomeningitis virus (LCMV) infects mice intracellularly. APCs, which

Parameter	Description	Dimension	Default value
δ_N	death rate naive	day^{-1}	0.005
δ_E	death rate effector	day^{-1}	0.4
ϕ	naive renewal		0.99
K_{ij}	affinity T-cell-MHCp	day^{-1} $\text{site}^{-}1$	$[10^{-7}\text{-}10^{-2}]$
k_i	affinity MHCp	day^{-1} $\text{site}^{-}1$	1
ρ_E	prol. rate per complex	day^{-1}	100
ρ_N	prol. rate per complex	day^{-1}	10
H_i	thymic output	$\text{day}^{-1}\text{clone}^{-1}$	1
M_T	MHC complexes		10^5
θ	sensitivity of pathogen presentation		1
P_0	max. foreign peptide frequency		0.07
r	pathogen replication	day^{-1}	10
c	pathogen capacity	cell^{-1}	10^{-7}
Δ_I	Clearance of infected cells	day^{-1} cell^{-1}	$1.2 \cdot 10^{-4}$

Table 4.1: Parameter values chosen for the model Eq. (4.5) and Eq. (4.6). If not specified, simulations are made according to these values. The value of δ_E is from De Boer et al. [2003], while δ_N and H_i are taken from Chao et al. [2004]. ρ_N has been chosen in order to have a proliferation rate similar to the experimental data of Veiga-Fernandes et al. [2000]. The infection parameters, r, Δ_I, c have been chosen ad hoc to simulate an infection which is comparable to the time scales found in experiments with mouse LCMV or LM infections (see also De Boer and Perelson [1995]). The peptide kinetics parameters K_{ij}, k_i, and M_T are also chosen to simulate kinetics fairly similar to experimental data.

take up infected proteins, home into secondary lymphoid tissues, activating naive T-cells which recognize the viral peptides together with other self peptides presented. A distribution of different foreign peptides derived from viral proteins are presented on the surface of APCs (see also Section 4.5.2). In the first model, for simplicity, we suppose that there is only one foreign peptide which we call P_v. Antigen experienced cells which show specific affinity with this peptide are able to kill infected cells. The dynamics of the infected cells I is described with a standard model [De Boer and Perelson, 1995, Scherer and Bonhoeffer, 2005]. The amount of foreign peptide P_v is supposed to be a non linear function of the number of infected cells. This assumption has been made in order to have a linear dependency with the amount of infected cells and a saturation for high values of I, which is based on experimental

Peptide Class	Definition
P_1, CP-self	Self-peptides mainly generated by CP
P_2, IP-self	Self-peptides mainly generated by IP
P_3	Foreign peptide during an IR

Table 4.2: Peptide classes

data showing a saturation threshold in the amount of peptide presented on the surface of APCs. The equations for I and for P_v are

$$\frac{dI}{dt} = r(1-cI)I - \Delta_I(\sum_{i=1}^{N_{clone}} {K^E}_{iv}E_i)I \tag{4.11}$$

$$P_v(t) = \frac{P_0}{1+\frac{\theta}{I(t)}} \tag{4.12}$$

Infected cells replicate with maximum rate r, which is controlled by a maximum capacity of the system to contain infected cells. This is accounted with the parameter c. $1/c$ is the maximum number of infected cells in the organism. Infected cells die proportionally to the amount of antigen specific T-cells which are stimulated during the IR. This is accounted with the second term in the equation given for I. The Eq. (4.12) represents the amount of foreign peptide P_v. The parameter θ describes the sensitivity of the antigen presentation. It is the amount of infected cells needed to mount 50% of the maximum viral peptide, $P_0 \leq 1$, presented on the surface. The peptide concentration increases with the increase of the number of infected cells, and saturates when P_0 is reached. The homing mechanism of APC from the site of the infection to the secondary lymphoid tissue, where typically the contact with T-cells occurs, is considered to evolve fast and therefore we consider only a single type of APC, which presents all peptides. The parameter values used in this chapter are summarized in Table 4.1.

4.4 Caricature of the cytotoxic T-cell repertoire

We assess the following questions: does the dynamics of the IR change when the relative frequency of presented peptides varies at the onset of the IR? If this is the case, how? As already explained in the introduction of this Chapter, we assume that the expression of IP during an IR elicits a change

Clone Class	Definition	Pept. Class	Thymic output
N_1, E_1	Recognizes CP-self	P_1	H_1=1000
N_2, E_2	Recognizes IP-self	P_2	H_2=1000
N_3, E_3	Recognizes CP-self and foreign pep.	P_1, P_3	H_3=1
N_4, E_4	Recognizes IP-self and foreign pep.	P_2, P_3	H_4=1

Table 4.3: T-cell clone classes

in the peptide frequencies. We shall call IP-effect the redistribution of MHCp on the surface of APCs during an IR. The high diversity and enormous size of the cytotoxic T-cell repertoire make the quantitative description of the dynamics of the IR very difficult. Therefore, in order to capture the main feature of the problem, we have chosen a simple caricature representation of the T-cell repertoire.

We divide clones, as well as peptides and affinities, in few classes. Basically we classify peptides according to their proteolytic origin (see Table 4.2). We define CP-self as the set of self-peptides which are mostly generated by intracellular degradation performed with the CP. Similarly, IP-self is the set of self-peptides which are mostly generated by intracellular degradation performed with IP. Before the IR starts, we suppose that CP-self class is characterized by high frequency, while the IP-self has a low value. We also consider the class of foreign peptides, which is zero before the infection. We named peptide classes as in the general model with P_1, P_2, $P_3 = P_v$ (see Table 4.2). Each of this peptide classes give rise to the corresponding MHCp class. T-cell clones are classified by the affinity between TCR and MHCp class, and by the thymic input (see Table 4.3). We define the class of T-cell clones recognizing CP-self, and the class recognizing IP-self. We further consider other two classes of T-cell clones: the first recognizing, together with self-peptides, the foreign pathogenic peptide, namely the clone recognizing P_1 and P_3, and the second class recognizing the peptide classes P_2 and P_3. Finally, we define the thymic input for the T-cell classes recognizing self-CP and self-IP as $H_1 = H_2 = 1000$, while for the clone classes recognizing specific foreign peptide we chose $H_3 = H_4 = 1$. These values represent a situation in which the majority of clones does not recognize foreign peptides and therefore, for the first two classes of our caricature repertoire, a high value for the thymic input H has been defined. In contrast, few clones with respect to the whole repertoire will recognize with high affinity a foreign peptide. For these classes the thymic input of 1 cell per day per clone has been chosen according to published data (for a review see [Almeida et al., 2005].

Further, we will refer to a change in the proteasome content by a change

Phase	Definition	P_1/P_2	P_3
I	Before IR starts	10	0
II-a	IR, low IP	10	P_v
II-b	IR, high IP (IP-effect)	0.1	P_v

Table 4.4: Relative peptide distributions used. In phase I there is no foreign peptide P_3 (no infection), and the peptide resources are rich in CP peptide, namely $P_1/P_2 = 10$. Phase II is the infection phase. This phase can be II-a (no IP rich peptide), or II-b (IP rich peptide). Phase II-b is characterized by the IP-effect.

in the peptide ratio P_1/P_2. We used $P_1/P_2 = 10$, which has been extrapolated from Skoberne and Geginat [2002]. Table 4.4 represents the peptide distribution that we used in the simulations to describe different phases of the T-cell dynamics. Phase I is the condition without pathogen in which only self peptides are presented. Phase II is the IR which can be of two types: the first with low content of IP, and the second with high production of IP. In the next sections we will refer to IP-effect or to phase II-b indistinctly.

We suppose that T-cells bind to MHCp either with low, k_s, or with high, k_h, affinity. We choose the following values for the affinities: $k_s = 5 \cdot 10^{-2}$ day^{-1} site^{-1} and $k_h = 5 \cdot 10^{-5}$ day^{-1} site^{-1}. The affinity matrix will then read (see Eq. (4.5) and Eq. (4.6))

$$K^E = K^N = \begin{pmatrix} k_s & 0 & 0 \\ 0 & k_s & 0 \\ k_s & 0 & k_h \\ 0 & k_s & k_h \end{pmatrix}$$

4.5 Results

With the proposed mathematical model we test several hypothesis. Based on experimental evidence we suppose that during an IR the MHCp abundance increases, the IP also rises and, consequently, the IP-self epitopes are more expressed as well. We investigate the role of these phenomena during an infection mediated by cellular IR. We recall that we define IP-effect as the change in the relative abundance of CP- and IP-self peptides when a foreign peptide is shown (see Phase II-b in Table 4.4 and Section 4.4). The measure of this effect will be the ratio P_1/P_2.

4.5.1 Simulations

We perform simulations of the caricature of the T-cell repertoire with the equations given in Eq. (4.5) and Eq. (4.6). The parameter values used are given in Table 4.1, while we refer to Table 4.4 for the values of the peptide frequency distributions used to simulate the IR dynamics.

The system is considered at $t = 0$ at the steady state of phase I, in which foreign peptide is absent. The introduction of the foreign peptide P_v perturbs the system, which evolves towards a new steady state. In the simulation the number of infected cells I can assume non integer numbers. Therefore, we introduce a cut off: I was set to zero for $I < 1$. Infection results in the expression of the foreign peptide (P_v), causing the activation of highly specific T-cell clones (E_3 and E_4). Both clones, E_3 and E_4 proliferate proportionally to the peptide amount, but with different rates. This is due to the different self-peptide repertoire they recognize (CP-self and IP-self, i.e. P_1 and P_2). Therefore, during the proliferation phase the amount of proliferating T-cells depends on the overall peptide distribution. In the model we envisage two possible scenarios: the experienced pool is already present in the pre-immune system and does not expand because of the low affinity for self peptides. This condition corresponds to $\phi < 1$. The second scenario regards the experienced pool present only if the viral peptide is introduced. In this case the differentiation from naive to experienced is present only with the antigenic load. This condition corresponds to $\phi < 1$ only when $I \neq 0$. We show simulations for the first scenario, although we did not observe strong differences when results coming form both cases are compared.

In Fig. 4.3 the dynamics for the naive and the experienced pool, and for the infected cells are shown. Panel A shows the time course of the IR, namely $E_3 + E_4$, and of the number of infected cells, I, for both phases II-a and II-b (see Table 4.4), which correspond to the IR with low and high IP content respectively. In both cases a 2-fold increase in the value of M_T during the time course of the infection has been chosen. Infected cells (dashed lines) are deleted only in case of high IP content (IP-effect, Phase II-b). The peak of the IR for the phase II-b is at day 8 as suggested from experimental data of in vivo mice infections (see also the next section). The IP-effect results in the viral clearance because of a higher proliferation rate of the E_4 clone (see Fig. 4.3B), which takes advantage of the increased resources given by the increased IP content, and of the presence of foreign peptide. In the case II-a, both specific clone classes E_3 and E_4 proliferate with the same rate. The proliferation rate returns to the steady state value as soon as the infection vanishes, namely $I = 0$ and M_T is set to the original value. The phase II-a is characterized by a chronic presence of infected cells. We also found that the

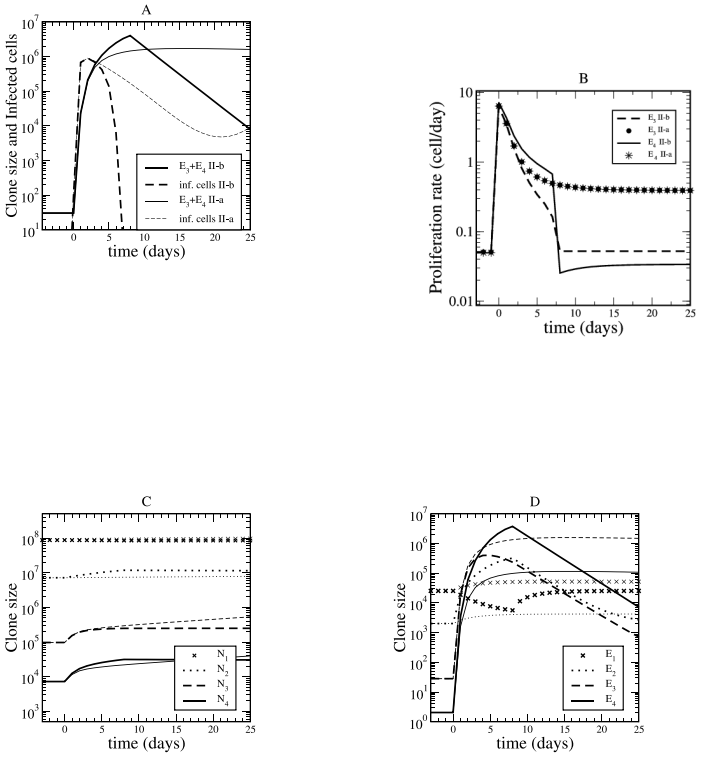

Figure 4.3: Comparison of the dynamics of the IR with (phase II-b) and without (phase II-a) the IP-effect. The parameters of the model are the same for both cases (see Tables 4.1 and 4.4). In all panels, heavy lines represent the IR with the IP-effect. Panel A: the sum of the clone classes E_3 and E_4, and the number of infected cells, I are shown. Panel B: the proliferation rate for E_3 and E_4 are shown for both cases. A fast proliferation phase is observed soon after the onset of the IR. This phase terminates with the deletion of infected cells (see also the text). Panel C: the time course of the naive clone classes. This pool is not strongly affected by the infection dynamics due to their slower proliferation and death rate with respect to the experienced pool. Panel D: the time course of the experienced clone classes.

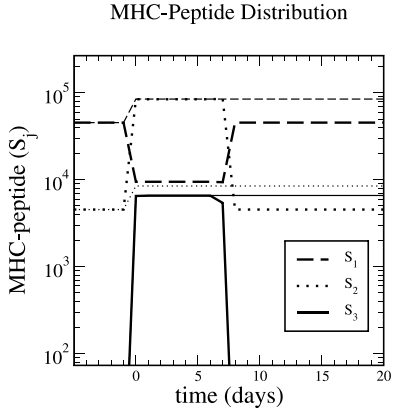

Figure 4.4: MHC-peptide abundance on the antigen presenting cells during the IR. The parameters of the model are the same as in Fig. 4.3. The difference between the two cases (light line phase II-a, heavy line phase II-b) shown is the different ratio of peptides produced by constitutive vs. immunoproteasome (see also Table 4.4). During the IR, the total amount of MHCp increases 2-fold. For the IP-effect case, the infected cells are deleted and therefore the number of MHCp returns to the steady state value. In the other case (phase II-a) the infection persist in the system and therefore the number of MHCp remains at high values (see light curves).

size and the diversity of the naive pool is not strongly influenced during the IR (see Fig. 4.3 C). This is due to the slow proliferation and death rate characterizing naive cells with respect to antigen activated cells. As can be seen in Fig. 4.3D, the IP-effect, together with the injection of foreign challenge, influences the proliferation phase and the size of experienced cells responding to the pathogen. The E_4 clone recognizing IP-self peptides undergoes a fast expansion ranging from 10 to 10^7 cells circa. The size of self-CP specific clone E_1 is reduced during the IP-effect as result of the MHCp redistribution. The proliferation rate, the clone abundance at the peak of the IR, and the size of clones shown are in accordance with the experimental values [De Boer et al., 2003, Murali-Krishna et al., 1998, Badovinac et al., 2000]. If the infection is

cleared the foreign peptide reduces, and the clones stop the expansion and return to a steady state situation. In Fig. 4.4 the time course of the MHCp, S_1, S_2, S_3, corresponding to each peptide class are shown. The figure corresponds to the same parameter values of Fig. 4.3. As expected, the MHCp mounting the foreign peptide, S_3, for the phase II-b lasts in the system for $t = 7 - 8$ days, which is the time at which infected cells are present in the system. The IP-effect is responsible for the increase in the abundance of S_2 with respect of S_1 during the course of the IR (see the dashed S_1, and the point-lines, S_2, in Fig. 4.4). After infection, the total amount of MHCp, M_T, reduces. In the no IP-effect phase, II-a, the foreign peptide stays at high level, as well as the total amount of resources.

We tested if the increase of the total amount of resources, M_T, during the IR might be sufficient to mount an IR resulting in the deletion of infected cells. In Fig. 4.6 we show that the IR efficiently eliminates the pathogen only if a 4-fold increase in the MHC molecules abundance is considered. A 2-fold increase will not lead to the deletion of infections. On the contrary, the IP-effect, together with a moderate increase in the total number of MHCp (2-fold), eliminates infected cells as good as the no-IP case in which a more pronounced increase of resources is considered. The IP-effect can be a clever and less expensive way (from an energetic point of view) to defeat the pathogen.

In order to better understand the IP-effect we consider a simpler scenario. The dynamics of infected cells is not taken into account. Instead, constant peptide distributions were considered. This allows us to compare steady states before and during the IR.

Phase I (Table 4.4), where $P_1/P_2 = 10$ and no foreign peptide is present, represents the healthy state. The steady state of Eq. (4.5) and Eq. (4.6), in this case, is denoted by I in the phase space projections shown in Fig. 4.5. In phase II-a, $P_1/P_2 = 10$ still holds and the foreign peptide is introduced with $P_v = P_0 = 0.07$. This phase represents a chronic diseased state. Phase II-b represents a diseased state as well, but the frequencies of P_1 and P_2 are interchanged. In Fig. 4.5 the steady states of these two phases are denoted by a and b. These two steady states are identical but for the interchange of the indices 1 and 2 respectively 3 and 4. Therefore, they are symmetric with respect to the bisectrix. The sums of the foreign peptide specific T-cells, $E_3 + E_4$ and $N_3 + N_4$, are the same in both cases. The IP-effect, hence, does not influence the effectiveness of the IR at the steady state.

The fact that the IP-effect results in the pathogen clearance, as shown in Fig. 4.3A, thus has to stem from transient behavior. We simulated the trajectories into the steady state of both phases II-a and II-b. The initial condition was given by the steady state of phase I. These trajectories, shown

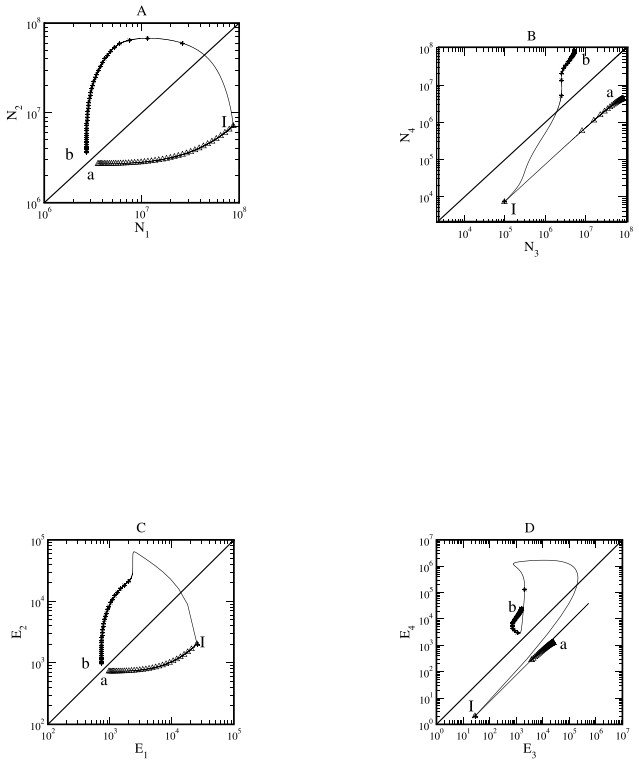

Figure 4.5: Trajectories in the phase space projections. Peptide distributions are considered to be constant. Trajectories relax into the steady states of the infected phases, II-a and II-b (see Table 4.4. Other parameters from Table 4.1 with $P_3 = 0.07$), denoted by a and b respectively. The initial condition, denoted by I, corresponds to the steady state values with peptide distributions of phase I.

in Fig. 4.5, represent the transition from the healthy to the chronic diseased state.

When approaching the new steady states, a and b, the trajectories are symmetric with respect to the bisectrix. But soon after the introduction of the foreign peptide, the IP-effect (phase II-b) leads to a more efficient IR, as

can be clearly seen in Fig. 4.5D. Simulations performed for a vast parameter set never evidenced the IP-effect to be less effective than the case in which the self peptide distribution does not change. Thus, this phenomenon seems to be robust although further investigations have to be performed.

Intuitively, it is reasonable to imagine that a small perturbation, such as a small increase in the foreign peptide frequency, does not lead to a new steady state which is very distant from the initial state. Therefore, we would not expect a big change in the proliferation rates. In this model proliferation rates are small close to the steady state, since they only outbalance the death rates. On the other hand, a strong re-shaping of the peptide distribution, such as the IP-effect or a significant increase in the total amount of resources M_T, may push the system far away from the actual steady state. This requires a transitory fast proliferation rate for at least some clones.

In this model, the changing in performance due to the IP-effect is a feature of the onset of the IR. It suggests that during a chronic disease, in which the foreign peptide never disappears, the IP-effect does not influence the performance of the IS.

4.5.2 Comparison with experimental data

In this section we compare our simulations with some experimental results. We focus on two experimental data sets: mice infected with Lymphocytes Coriomeningitis virus (LCMV) and mice infected with a bacteria, Listeria Monocytogenes (LM). Depending on the viral strain, LCMV can affect acutely or chronically the organism, resulting in a clearance or in a chronic pathogenic state respectively. LCMV infection is characterized by a peak of the IR at day 8 in wilde type, and at day 12 in IFN-γ deficient mice (GKO mice). IP is strongly regulated by IFN-γ. IFN-γ is produced by T-cells and NK-cells, and it enhances the antigen presentation by up-regulating MHC expression as well as TAP. IFN-γ induces the synthesis of the proteasome immuno subunits and PA28, which are then responsible for changing the cleavage activity of the proteasome. IP deficient mice (LMP2-/-, LMP7-/-, MECL-/-) and IFN-γ deficient mice possess an altered T-cell repertoire, which emphasize the crucial role of IP for T-cell selection [Toes et al., 2001, Chen et al., 2001b, Basler et al., 2004]. We therefore are interested in the GKO mice model because of their impaired capability to form IP. They can be a reliable experimental evidence for the importance of the IP-effect during an IR. This gives the opportunity to compare the IR in both cases, as has been done in the simulations. It should be emphasized that IFN-γ deficiency has also other effects, such as an impaired apoptosis phase and a different homeostatic level of cytotoxic T-cells [Harty and Badovinac, 2002]. Khan

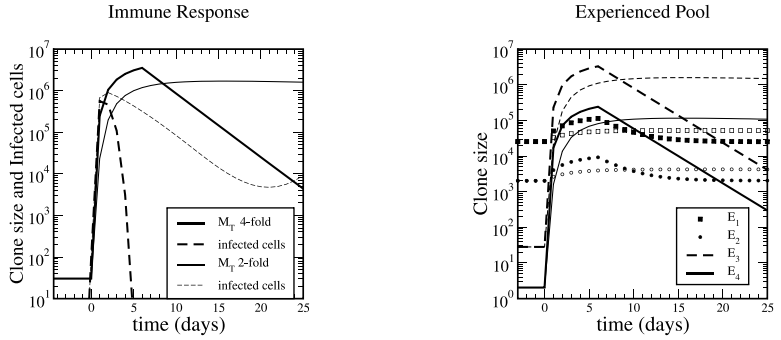

Figure 4.6: Increase in the total amount of resources, M_T, also results in a better IR. Left-side panel: same as in Panel A in Fig. 4.3. The comparison between the immune responses correspondent to a different increase in the amount of MHC-peptide molecules M_T are shown. In the absence of the IP-effect, phase II-a, the pathogen can also be cleared, but with an increase of resources, M_T. Right-side panel: comparison between the clonal expansion of all clone classes (same condition as the left-side panel). Symbols represent self-specific clone classes: squares E_1, circles E_2. Pathogen specific clone classes, E_3 and E_4 (dashed and solid lines), expand faster than the clones recognizing only the self-peptides (see Table 4.3). Parameter values are as given in Table 4.1, the variation in the MHCp abundance is 4-fold (heavy lines), and 2-fold (light lines)

et al. [2001] have shown a total replacement within 7 days of CP with IP in wilde type mice infected with LCMV or LM. This suggests that IP deficiency plays a role in shaping the antigenic peptide repertoire presented on the surface of APCs. Moreover, GKO mice do not always clear the virus and in case they succeed, the peak in the number of cytotoxic T-cells is shifted by few days (from day 8 to day 10 after immunization with LCMV) and the number of infected cells in the organism is increased. Interestingly, a change in immunodominance hierarchy of antigenic epitopes is observed in GKO mice in both infections [Badovinac et al., 2000, Bartholdy et al., 2000].

LM infected GKO mice show a higher peak in the number of cytotoxic

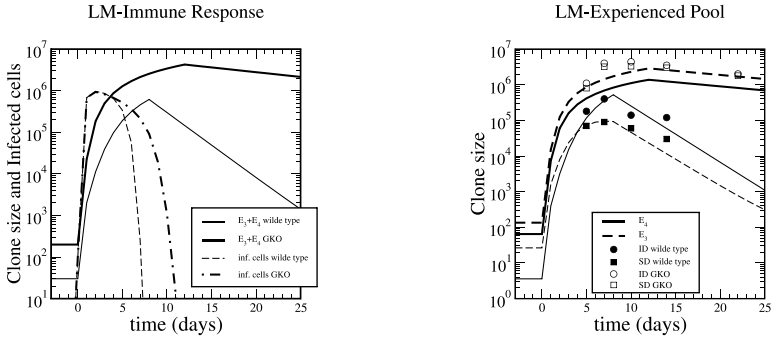

Figure 4.7: LM infection in IFN-γ deficient mice. Immune response against LM with and without IP-effect, and with different apoptosis rates. Left panel: The immune response, $E_3 + E_4$ (solid curves), and the number of infected cells, I (dashed curves), are shown. Heavy lines represent the case of GKO mice, while light lines represent the wilde type case. Right panel: Antigen specific clone classes, E_3 (dashed lines), and E_4 (solid lines), are shown for both GKO and wilde type. Experimental data of cytotoxic T-cells specific for one immuno-dominant (wilde type filled circles, GKO empty circles) and one subdominant (wilde type filled squares, GKO empty squares) peptides for LM infection are shown. The IP-effect in the wild-type mice is shown (comparison between light and heavy lines). Parameters: the same as in table 4.1 but $\delta_E = 0.1$, $\Delta_I = 0.8 \cdot 10^{-4}$ for the GKO mice, and $P_0 = 0.03$, $\Delta_I = 0.8 \cdot 10^{-3}$ for the wilde type mice. The ratio P_1/P_2 is 2 for the GKO and 6 for the wilde type mice.

T-cells with respect to wilde type. The peak is shifted from day 7 to day 10. Moreover, in LM infected mice the experimental ratio between two dominant peptides is found to be 5:1 in wilde type and 1:2 in IFN-γ deficient mice [Skoberne and Geginat, 2002], suggesting that IP affects the hierarchy of immunodominant peptides. It is interesting to note that, in contrast to the LCMV infection case, GKO mice infected with LM show a higher peak in the total amount of antigen experienced cytotoxic T-cells when compared to wilde type response.

Clone Class	Definition	Peptide Class
N_1, E_1	Recognizes CP-self	P_1
N_2, E_2	Recognizes IP-self	P_2
N_3, E_3	Recognizes CP-self and CP-foreign peptide	P_1, P_3
N_4, E_4	Recognizes IP-self and IP-foreign peptide	P_2, P_4
N_5, E_5	Recognizes CP-self and IP-foreign peptide	P_1, P_4
N_6, E_6	Recognizes IP-self and CP-foreign peptide	P_2, P_3

Table 4.5: T-cell clone classes for the extended caricature representation of cytotoxic T-cell clones with two foreign peptides.

We try to explain these experimental data according to the IP-effect. We identify the wilde type IR as the IR with IP-effect (phase II-b), and the GKO mice as the no IP-effect case (phase II-a, see also Table 4.4).

The Listeria Monocytogenes infection in mice In Fig. 4.7 the case of LM infection is considered. Again, simulations for the wilde type show a clearance of the infection with a peak of the IR at day 8, while the simulations for GKO mice (no IP-effect) show a peak at day 11. We were not able to fit the data only with the IP-effect. In order to compare our simulations with experiments a lower apoptosis rate for the experienced pool ($\delta_E = 0.1$) and a lower killing efficiency, δ_I, was introduced for the GKO mice (see Fig. 4.7). These changes in the parameter values have also been suggested by the authors of the experimental work, Badovinac et al. [2000]. They suggested that IFN-γ deficient mice suffer a reduced capacity to undergo apoptosis. They observed a delay of the peak of the IR and an increased number of antigen specific T-cells against the dominant epitopes. It has to be noted that the role of IFN-γ during an IR is still controversial [Wodarz and Thomsen, 2005], and the IP-effect may clarify some aspects of this complex scenario.

The LCMV infection in mice In Fig. 4.8 a semi-quantitative fit of LCMV infection data is shown. For this purpose we chose a modified caricature model in which we consider four peptide classes and six clone classes (see Table 4.5). This has been made because experimental data show at least two main dominant peptides shaping the IR, which are hierarchically organized and differentially produced by CP and IP. We describe therefore two foreign peptides: the first as CP-dependent and the second as IP-dependent peptide; their abundance is proportional to the concentration of CP and IP respectively. This leads to six different T-cell clone classes: two classes recognizing only self-peptide, and four classes recognizing self-peptide and one

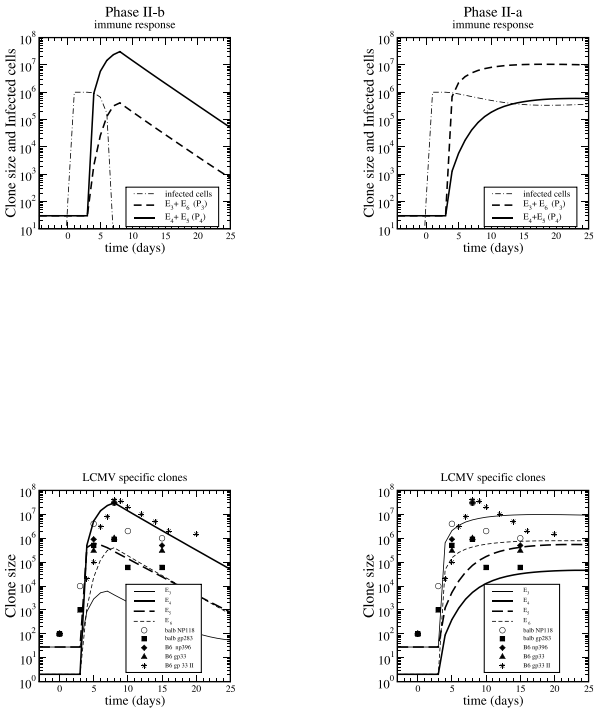

Figure 4.8: Comparison between LCMV infection and the numerical results of Eq.4.5 and 4.6 with the caricature of the cytotoxic T-cell clones extended to six classes (see also Table 4.5). Upper panels: Sum of the clone class $E_3 + E_6$, correspondent to P_3 specific clones, and $E_4 + E_5$, correspondent to P_4 specific clones, and the number of infected cells, I are shown. Left side with IP-effect (wilde type), and right side without IP-effect (GKO). Bottom panels: Dynamics of the LCMV specific T-cell clones. The IP-effect (left panels) characterized by a different peptide distribution (see text), changes the immunodominance hierarchy and allows a faster and more effective clonal expansion. Symbols represent experimental data of LCMV specific T-cell clones. Dominant epitopes for BALB/C and C57BL6 mice infected with the same amount of LCMV infection are shown (data from Murali-Krishna et al. [1998], De Boer et al. [2003]). Parameter values: as in Table 4.1 except for $\Delta T = 2.7$ days, $P_0 = 0.06$, $r = 50$ and $\Delta_I = 3 \cdot 10^{-6}$. In both cases the total amount of MHCp, M_T, is increased of 7-fold.

of the two viral peptides (see Table 4.5). On the top of that, in order to show a more clear fit of the experimental data, a delay in the activation of the experienced pool with respect to the time at which the infection starts has been introduced. We choose a delay $\Delta T = 2.7$, as suggested from a published model in which a precise quantitative fit of LCMV infection has been performed [De Boer et al., 2001b]. The IP-effect is now defined as a change in the proteasome content which affects all four peptide classes. The ratio P_1/P_2 and P_3/P_4 are both influenced by the IP-effect, and have been taken equal, $P_1/P_2 = P_3/P_4 = 10$ as given in Table 4.4 for the previous caricature repertoire.

Simulations were performed with an increase of 7-fold of the total amount of MHCp, M_T, during phase II. Our simulations show a peak of the IR at day 8 for wilde type, and a chronic infection (infected cells are not deleted) for GKO mice (see upper panels in Fig. 4.8). For a small change in the parameter values of the infection variable (killing efficiency of T-cell Δ_I and pathogen capacity c), the model accounts also for viral strains which do not cause chronic disease but only a delay in the peak of the IR. This has been also observed experimentally with weakened viral strains [Bartholdy et al., 2000, Harty and Badovinac, 2002]. As expected, a reverse order of the hierarchy of pathogen specific clone sizes, E_3, E_4, E_5, E_6, is found when the IP-effect (bottom panels, left side) and the NO-IP-effect (bottom panels, right side) are compared. We show that the increase of IP, and therefore the augment of the IP viral epitope, results in a change of the hierarchy of clones responding to viral epitopes.

Our results confirm that the absence of IFN-γ results in a delay of the clearance, or in a chronic infection. We explain the change in immunodominance with the IP-effect, which is responsible for the change of the clonal size of T-cell clones. In support of our results, experiments showed a suppression of clones specific for epitopes which were produced at lower rates as effect of IFN-γ treatment [Basler et al., 2004]. IP-deficient mice presented an opposite scenario: T-cell clones recognizing IP-dependent peptides were drastically reduced in size or disappeared. In this model, an increase in the IP content would result in a higher peak of the IP-dependent clone classes and a reduction of the size of CP-dependent clones.

4.6 Discussion

We investigate how the immune system can take advantage of the double population of proteasomes, the CP and IP, and with it to select the appropriate cytotoxic T-cell pool responding against a foreign epitope which is

presented on the APCs. Competition between T-cells for MHCp influences the immune response. The idea behind this model is that the same pathogen can potentially activate a very different T-cell specific repertoire. Its diversity and size are shaped by the particular distribution of MHCp. We show how the simple change of self-peptide abundance on the surface of APC can have a remarkable effect on the T-cell selection.

One problem the immune system faces is how to use a finite TCR repertoire, distributed on a finite number of T-cells, to deal with a very large number of epitopes. It is essential for immune defense that sufficient numbers of cells are deployed to combat infection. Simultaneously, specificity of recognition must be high enough for the repertoire to respond to foreign, but not to self, peptides. Our model in fact suggest that, during an IR, the reshaping of the MHCp distribution on the surface of APC might be a smart way to adjust the immune cell repertoire to combat pathogens. When the fight is over the re-establishment of the steady state distribution will guarantee the normal conditions without that the IR would strongly influence the homeostasis of the system. Nevertheless, this re-shaping of the antigen presentation could be detrimental in case undesired peptides are over-expressed for a short time period. This would lead to a clonal expansion of self-responding clones.

The relative abundance of peptides and not their diversity seems to be influenced by the IP induction. Nevertheless, significant differences in the amount of some epitopes with the immunoproteasome induction resulted in a different selection of the T-cell repertoire during an immune response [Basler et al., 2004] It has been recently shown (Groettrup M., personal communication) that intra-cerebral LCMV infected mice get ill. The brain presents a significant reduction of IP content, and probably the antigen presentation can be impaired. Also, LCMV intra-venal infected mice ,which normally respond and kill the virus, have a reduced clonal expansion in the brain. These data, even if still controversial, suggest a role of IP in the immune response of LCMV infected mice.

This model offers an answer to some questions which are waiting to be answered:

1. How is the diversity of T-cells restored and maintained after the IR? The model suggests that the clone size re-distribution due to the IP-effect lasts in the system for a short period. The IP has a higher turnover with respect to the CP [Heink et al., 2005]. This suggests that the functionality of the IP is required only for a short timescale.

2. Can the self-repertoire be involved in the activation of an IR? The model suggests a positive answer. The-self repertoire may improve the IR by favoring the proliferation of clones which were kept at lower sizes

during the steady state. A more vigorous proliferation of the wanted clone can be achieved if the self repertoire favoring the responding clone is provided.

One can argue that this dependence of the IR on the distribution of the entire repertoire involved in the IR can be detrimental, especially if the reshaping of the distribution of peptides is a random process. For instance, a different proteasome composition in the thymus might be dangerous because it will influence the selection of the peripheral T-cell pool. Suppose that a different initial condition is given, like an opposite situation in which more IP than CP is present. The model predicts that increasing more the IP content will not result in a better IR. On the contrary, we would expect a deletion of the infection only if more CP is introduced. Basically our results suggest that what is important is not how much CP and IP are present, but the change in the peptide distribution arising from a gradient in the proteasome concentration. This has also been suggested from experimental data [Kuckelkorn et al., 2002].

What happens after the sixth decade of human life, when the thymic output is compromised [Haynes et al., 2000, Nikolich-Zugich, 2005]? Future investigation of T-cell dynamics over longer time scales is required. According to general evidence, we would expect that the IR would be driven by very few big clones. The IP can still play a role but probably there would be a more undefined differentiation between high and low affinity clones. To investigate such a problem, a more complex model which takes into consideration a more variate clone distribution and higher number of clones is required. There is evidence that the distribution of clones activated after a viral infection is very heterogeneous, constituted by few big clones and a huge amount of low frequency clones [Pewe et al., 2004]. According to our model, we expect that this distribution changes over the course of the infection, selecting only some clones which are able to take advantage of the peptide distribution presented on the APC. A possible problem to face can be the level of cross-reactivity characterizing the responding clones. We performed simulations to investigate how cross-reactivity can influence the IP effect. As a trivial result we found that the IP-effect is not efficient in defeating the infection for high values of cross-reactivity. In fact, suppose that each clone has a finite probability to recognize each peptide presented on the surface of APCs. This would lead to a situation in which each clone compete against each other for the same resources and no specific clone would be able to prevail over the others. These results are very dependent on the characteristic of the affinity matrix, which defines the cross-reactivity. A possible future direction can be to define a random distribution of low affinity values for the T-cell MHCp

interaction as well as of peptide amounts.

We conclude suggesting that it is not only the peptide amount, or its affinity towards MHC binding grooves, or the clonal size of T-cells recognizing the peptides that defines the immunodominance hierarchy. The peptide distribution, as a whole, is responsible as well in shaping the pathogen specific T-cell clone repertoire. A subdominant epitope can be so not because it is expressed in less amount. As we have shown, its rank in the dominance hierarchy during an IR depends on the dynamics of the clonal expansion.

These considerations are extremely important in designing vaccination strategies. This model suggests that two clones recognizing the same peptide with the same affinity can behave very differently. Thus, screening a naive T-cell repertoire against MHC molecules mounting foreign epitopes, as can be done with high throughput in vitro analysis of T-cell binding to MHC-peptide complexes, might be misleading.

At the beginning of this new millennium, pathogens and cancer remain one of the leading causes of death world-wide. The development of vaccines to prevent diseases for which no vaccine currently exists, such as AIDS or malaria, or to treat chronic infections or cancers, as well as the improvement of efficacy and safety of existing vaccines, remains a high priority. In most cases, the development of such vaccines requires strategies capable of stimulating cytotoxic T lymphocytes and thus, to deliver antigen to MHC class I molecules.

Summary

Competition for resources, such as MHCp, biological space and cytokines are known to play an outstanding role in the dynamics of T-cell clone at the steady state as well as during a pathogen challenge. We have proposed a possible role for the IP in shaping the T-cell repertoire during an IR. We showed how the capability to fight a pathogen can be improved by reshaping the self peptide distribution for a short time period. The same pathogenic condition, which may lead to chronic infection, can be defeated by a reshaping of the MHC-self peptide distribution driven by the change in the intracellular immunoproteasome composition.

Chapter 5

Clonal expansion and chronic stimulation

Introduction

The clonal expansion is the result of a complex dynamical process in which the main actors are the acute and the chronic antigenic stimuli, and the local environment in peripheral tissues. The latter is characterized by the presence of several resource-competing T-cell clones, and the cytokinic network [Jameson, 2005, Almeida et al., 2005, Freitas et al., 1996, Gaudin et al., 2004] (see also Chapter 3 for a review of competition phenomena in T-cells dynamics). The IS is obsessed with very large T-cell clones, which are oligoclonally dominating the memory repertoire. There are some open questions:

- Why do these clones survive so long even if most of them are nonfunctional?
- Why are they not sensitive to apoptosis?
- Which are the sources for these clones?

In this chapter we introduce a stochastic model to approach these issues over long timescales, and under chronic antigenic stimuli. A possible scenario based on phenomenological assumptions is proposed.

In the proposed scenario two main driving forces define the dynamics of T-cell clones. The first is the acute antigenic stimulus (acute infection) which impinges upon the T-cell clone via the T-cell recognition of antigenic stimulus (via TCR), which causes the activation and then proliferation of cytotoxic T-cells. The second is the chronic immune stress (CIS), consisting of endogenous stimuli (self-antigens) and exogenous stimuli (non-self antigens), which in turn affects the dynamics of the AE T-cell clone in two distinct ways: the

T-cell receptor cross-reactivity and the inflammatory cytokine response. We therefore define the CIS as the effects of the ceaseless and lifelong stimulation of the IS due to the continuous challenge with antigenic stimuli.

The secretion of inflammatory cytokines is the hallmark of the natural immunity, whose main actors are macrophages and natural killer cells, when they are aspecifically challenged by every sort of antigenic stimuli. Inasmuch, the constitutive cytokine production plays as the principal factor in the homeostasis (proliferation, survival) of antigen experienced (AE) T-cells. The bursts of cytokine secretion is due to specific (antigen specific T-cells) and aspecific (macrophage and natural killer cells) immune response. Such cytokines contribute to generate a fluctuating "cytokine noise", which is expected to affect the long timescale dynamics of AE T-cell clones [Tough et al., 1996].

Many authors suggested that the dynamics of AE T-cells can be affected by i) MHC-mediated [Jameson, 2002, Kaech and Ahmed, 2001, Veiga-Fernandes et al., 2000, Butcher and Picker, 1996, Tanchot et al., 1997] ii) MHC non-mediated mechanisms [Murali-Krishna et al., 1999, Tough et al., 2000, Ku et al., 2001, 2000, Tough et al., 1996, Jameson, 2005]. Concerning the MHC mediated stimuli, it should be pointed out that the dynamic expansion of a AE T-cell clones is affected not only by specific peptides causing high affinity TCR-MHC peptide binding, but also by cross-reactive antigens that repeatedly stimulate the previously generated AE T-cell clone. On top of that it has recently been shown that AE T-cell clones may not only expand but also contract in response to a new antigen. This phenomenon, known as attrition caused by "heterologous immunity", has relevant consequences for our model [Chen et al., 2001a, Selin et al., 1999]. Regarding the MHC non-mediated stimuli we recall the effect on T-cells of inflammatory cytokines (such as IL-15 and its cognate network INFa,b,g, IL-12,IL-18) produced during most immune challenges. These molecules can elicit "bystander effect", i.e. stimulation of T-cell proliferation in the absence of a specific antigenic stimulus [Jameson, 2002].

5.1 A model proposal

The model refers to a single AE T-cell clone located in an inflamed tissue whose size (number of cells) is denoted by $c(t)$. We introduce the variable $x(t) = \log_{10} c(t)$ and its time variation, we denote by $v(t)$.

The body of the model is a description of the homeostatic process as a mechanism of relaxation to a given equilibrium size after the action of an external antigenic stimulation. Changes of the clone size are due to both the

acute antigenic stimulus, represented by an impulsive function, and the CIS described as a stochastic process.

$$\frac{dx}{dt} = v \tag{5.1}$$

$$\frac{dv}{dt} = F(t) + f_0 + \gamma\xi(t) - \beta v - \frac{dV(x)}{dx} \tag{5.2}$$

The acute antigenic challenge is represented by the impulsive function $F(t)$, and acts for a time interval T, with constant mean load of intensity $F_0\omega^2$

$$F(t) = \begin{cases} F_0\omega^2 & \text{for} \quad 0 \le t \le T \\ 0 & \text{for} \quad t > T \end{cases} \tag{5.3}$$

ω^{-1} is a constant with the dimension of a time, T is the duration of the acute antigenic insult. The CIS is composed by a constant mean intensity f_0, and a fluctuating term $\gamma\xi(t)$, where $\xi(t)$ is a white noise. The CIS is responsible for the long timescale expansion or contraction (attrition) of the clone.

The last two terms of the equation Eq. (5.2) describe the interactions between the clone and the local environment which are supposed to influence the rate at which the clone size evolves. Experimentally it has been shown that the homeostasis of T-cell clone is a tissue dependent mechanism [Ku et al., 2000, 2001, Harris et al., 2002, Tough et al., 2000, Kaech and Ahmed, 2001]. The clone size grows or shrinks depending on a "bidirectional cross-talk" between the T-cell clone and the immunological microenvironment [Butcher and Picker, 1996].

The size-landscape function $V(x)$ defines a collection of metastable states for T-cells size, while $-\beta v$ modulates the variation of the T-cell number by reducing the very rapid changes in the rate of clonal expansion. The parameter β fixes the timescale to restore the clone equilibrium size. In our model its value has been fixed as $\beta = .02$ days^{-1}, which correspond to a timescale of 50 days. This is the typical timescale found during experiments on T-cell expansion and down regulation in mice after secondary influenza challenge[Marshall et al., 2001]

The values we choose in our numerical simulations without CIS are $T = 24$ days, $F = 2$ and $\beta = \omega = 0.1$ days^{-1}, which correspond to an oscillation period of about 40 days and a decay period $2/\beta$ of 20 days as suggested by experiment [Marshall et al., 2001]. For the general case, in which the CIS is present, slightly different values have been chosen: $T = 9$ days, $\beta = .02$ days^{-1} whereas we still have $\omega = .1$. The small oscillations period is approximately $2\sqrt{2}/\omega \sim 30$ days. According to the hypothesis that the "immunological space" (total number of T lymphocytes in the whole body) is

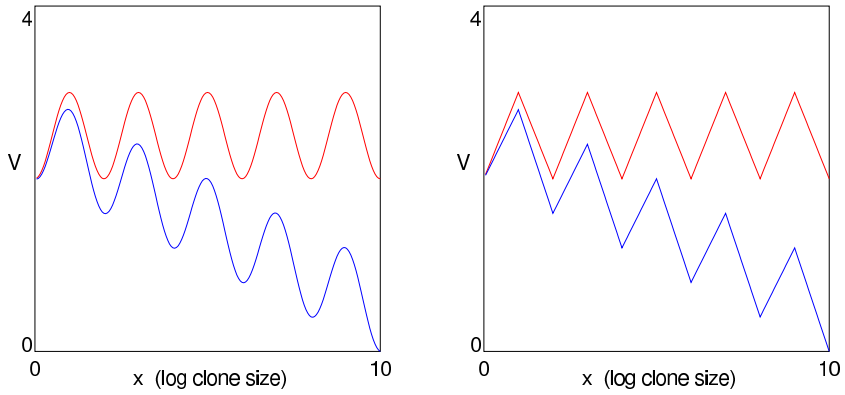

Figure 5.1: Sinusoidal (left panel) and saw-tooth (right panel) size-landscapes (upper curves) and effective landscape (lower curves). The effective landscape function $V_{\text{eff}}(x) = V(x) - f_0 x$ includes the contribution of the mean antigenic stress, which binds the plot of the size-landscape function.

finite, and that the total T-cell pool in a single organ cannot exceed a fraction of the total mass of the organ itself, we introduce a size limit of the clone L by using an infinite barrier in the size-landscape function corresponding to that size. The estimate of the number of T-cell repertoire and of the tissue mass can be used to guess this limit size.

The role of the size-landscape function

The function V can be seen as a sort of mean field approximation of local interaction of the clone with other cells present in the periphery. For the sake of simplicity we assume the function $V(x)$ to be periodic and symmetric with period $2\pi/\omega$, with an excursion between the minima and maxima equal to ω^2. The shape of the function is not relevant once the period is fixed. We have examined explicitly two different cases, the saw-tooth and the sinusoidal function, as shown in Fig. 5.1.

$$V(x) = \begin{cases} \omega^2 \left| (x+1) \bmod 2 - 1 \right| & 0 < x < L \quad \text{saw-tooth} \\ \omega^2 \dfrac{1 - \cos(\pi x)}{2} & 0 < x < L \quad \text{cosine} \\ +\infty & x < 0 \quad x > L \end{cases} \tag{5.4}$$

In order to describe the homeostasis we only require the size-landscape function $V(x)$ to have a sequence of minima, and the term $-\beta v$. The equilibrium size of x follows the linear law $x = n$ which implies an exponential increase

in the clone size c, as suggested by experimental results [Marshall et al., 2001]. The way $x(t)$ rises during an acute antigenic impulse depends on the shape of the size-landscape function, but the average growth is linear in t (exponential with the size of the clone), as suggested by experimental results. Different shapes of the size-landscape-function would correspond to different peripheral tissues.

A biological mechanism for the damping term

The term $-\beta v$ prevents uncontrolled proliferation as well as the extreme rapid depletion of cytotoxic T-cells during the oscillatory phase around the steady state (see Fig. 5.2 and Fig. 5.3). A possible biological mechanism which can cause such a phenomenon is the Fas-FasL mechanism. This is an important peripheral mechanism for the regulation of apoptosis of activated T-cells [Arnold et al., 1999, Pinkoski et al., 2002, Krammer, 2000] (see also Chapter 3. We hypothesized that fluctuations in the CIS induce a gradient in the concentration of Fas-FasL, and consequently a modification of the Fas-Ligand expression in the peripheral microenvironment. For instance, If the rate of the pro-inflammatory cytokines increases, the expression of Fas-Ligand on the epithelial cells also increases and those T-cells expressing Fas are more prone to apoptosis. On the other hand, in case of a temporary reduction of the antigenic chronic stimulus, a reduction of Fas-L-inducing cytokines may result in a reduced expression of Fas-Ligand on the epithelial cells, giving rise to a moderate re-expansion of the T-cell number.

5.2 Results

Analytical solutions

The system of equations Eq. (5.1) and Eq. (5.2) can be analytically solved in the strong damping approximation, namely high value of β (see also appendix C). This means that the IS strongly counteracts any acute stimulus $F(t)$, which changes the homeostatic metastable equilibrium of the clone. With the condition $\beta \gg \omega$ the term dv/dt is negligible, and the equation reduces to

$$\beta \frac{dx}{dt} = -V'(x) + F(t) \tag{5.5}$$

If $V(x)$ is zero, the clone expands linearly and its size $c(t)$ grows exponentially. When the acute stimulus is over the clone reaches the constant value $x(T) = F_0 T/\beta$, basically the clone grows proportionally to the antigenic impulse $F_0 T$.

Landscape	T_1	T_2	T_3	T_4
cosine	64	143	223	302
saw-tooth	52	116	180	244
approx Eq. (5.7)	50	116.6	183.3	250

Table 5.1: Comparison of the duration of the impulse, T_n, which allows to jump after the maximum $x = 2n - 1$, for the cosine and the saw-tooth size-landscapes. Parameters: $\omega = 0.1,\ \beta = 0.5, F_0 = 2$ so that $\beta_* = \sqrt{2}\,\pi\omega = 0.44$

The case of the saw-tooth function can be analytically solved, the condition for a jump to the interval $[2n - 1,\ 2n + 1]$ between two subsequent maxima is given by

$$1 + (n-1)(1 + \frac{F_0 - 1}{F_0 + 1}) \leq\ T\ \frac{\omega^2}{\beta}\,(F_0 - 1) < 1 + n\,(1 + \frac{F_0 - 1}{F_0 + 1}) \qquad (5.6)$$

and the time needed to reach the maximum $x = 2n - 1$ at rest is

$$T_n = \frac{\beta}{\omega^2}\frac{n}{F_0 - 1} + \frac{n-1}{F_0 + 1}\left(\frac{n}{F_0 - 1} + \frac{n-1}{F_0 + 1}\right) \qquad (5.7)$$

The duration T of the impulse which allows the clone size to overcome the maximum $x = 2n - 1$ without overcoming the next one $x = 2n + 1$ is $T_{2n-1} < T < T_{2n+1}$. In this case the clone remains trapped in the corresponding interval, and evolves asymptotically to the value $x = 2n$. We have checked that the above conditions are approximately verified also for a cosine function. In this case the critical damping value above which no oscillations occur is $\beta_* = \sqrt{2}\,\pi\omega$. In Table 5.1 we compare the jump time T_n evaluated by accurate numerical integration of the exact equation with the corresponding estimate Eq. (5.7). A comparison between the strong damping approximation and the weak damping approximation ($\beta \ll \omega$) is shown in Fig. 5.2 (see appendix C). The rise of $x(t)$ during the acute stimulus is monotonic and can be approximated by a linear function after an averaging process. As one would expect, this corresponds to an exponential growth of the clonal size $c(t)$. In the strong damping case the rise is piecewise linear and close to linear when $T\omega^2 F_0/\beta \gg 1$.

Effect of the local environment

It is plausible that the parameters of the function V (timescale and equilibrium sizes) might vary in different organs. Keeping the height of the

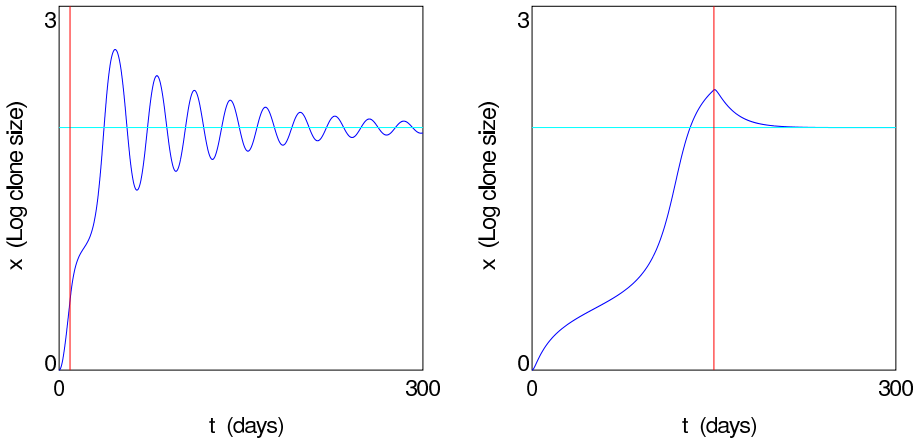

Figure 5.2: Left panel: weak damping case ($\omega = 0.1, \beta = 0.02,\ F_0 = 2\omega^2$, $T = 9$) T-cell clonal expansion in the case of a sinusoidal size-landscape function $V(x)$. Right panel: over damping case ($\omega = 0.1, \beta = 0.8$, $F_0 = 2\omega^2$, $T = 150$). The jump to the first minimum occurs for $T \simeq 100$ days, whereas for the saw-tooth size-landscape the jump threshold is $T = \beta/(\,F_0 - \omega^2) \sim 80$ days.

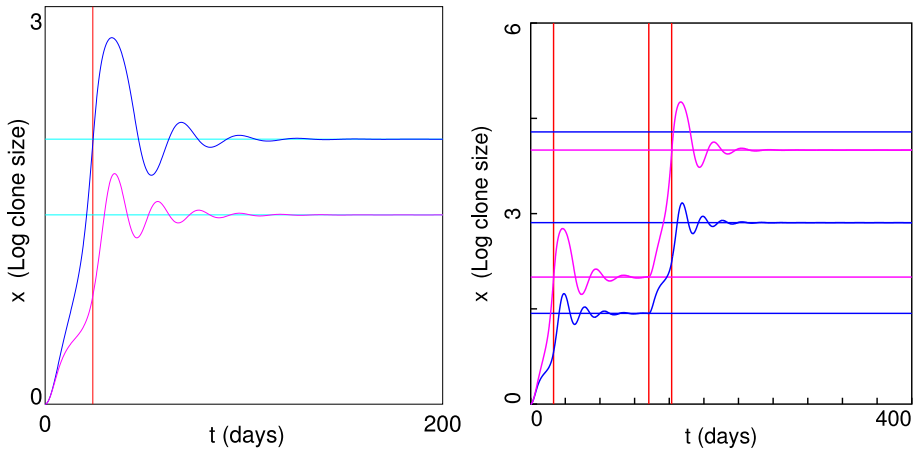

Figure 5.3: Left panel: comparison of the clonal expansion for two different sinusoidal size-landscape functions defined by $V = \frac{1}{2}\,\omega^2\,[1 - \cos\pi\,(1-\epsilon)\,x]$. Parameter values are $\omega = 0.1$, $\beta = 0.1$, $F_0 = 2$, $T = 24$ and $\epsilon = 0$ for the first landscape (grey curve) and $\epsilon = 0.4$ for the second landscape (black curve). Right panel: same comparison as in the left panel for a clone undergoing two antigenic impulses of the same duration and with a time delay of 100 days.

maxima unchanged, we vary the periodicity from 2 to $2/(1+\epsilon)$, namely $V = \frac{1}{2}\,\omega^2\,[1-\cos\pi\,(1+\epsilon)\,x]$. In Fig. 5.3 (right panel) we show the effect of the antigenic insult with two different values of the parameters (ω, ϵ), which can be associated to two different organs where the infection takes place. These curves are qualitatively similar to experimental data [Marshall et al., 2001].

Chronic stress

The analysis of the chronic stochastic stimulus, $f_0 + \gamma\xi(t)$, has been made on the basis of the analytical treatment of stochastic dynamical systems. The probability density $\rho(x, v, t)$ to obtain a certain solution $x(t)$ of the clone size at time t and rate of change $v(t)$ satisfies the Fokker-Planck equation

$$\frac{\partial\rho}{\partial t} + \frac{\partial(v\rho)}{\partial x} - \frac{\partial}{\partial v}\left[(\beta v + V_{\text{eff}}\,)\,\rho\,\right] = \frac{\gamma^2}{2}\frac{\partial^2\rho}{\partial v^2} \tag{5.8}$$

The equilibrium configuration, reached as $t \to \infty$, is

$$\rho_{\text{eq}}\,(s, v) = \frac{1}{Z} e^{(\frac{-v^2}{2k_B T})} e^{(\frac{-V_{\text{eff}}}{k_B T})} \tag{5.9}$$

where Z is a normalization constant (see calculations in appendix C) and $k_{_B}T = \frac{\gamma^2}{2\beta}$. To reach this configuration the system undergoes a relaxation process. A diffusion with respect to the deterministic trajectory occurs with a the diffusion coefficient $D = \frac{1}{2}\gamma^2 = \beta k_{_B}\,T$. There is a finite probability for the expansion of the T-cell clone to an equilibrium size $x = 2, 4, \ldots, 2N$ by the action of a weak chronic stimulus. As a consequence, we can state that the number of T-cells depends not only on the acute antigenic challenge but also on the CIS impinging upon the IS continuously. The transition time necessary to move among the equilibrium states can be estimated by evaluating the time needed to complete this transition, which is given by the Kramer's formula [Risken, 1989]

$$\tau = C \exp \frac{V_{\text{eff}}\,(x_2) - V_{\text{eff}}\,(x_1)}{k_{_B}T} = C \exp \frac{2\beta(\omega^2 - f_0)}{\gamma^2} \tag{5.10}$$

where

$$C = \frac{\omega_{2n}}{2\pi\omega_{2n+1}}\left[-\frac{\beta}{2} + \sqrt{\frac{\beta}{2}^2 + \omega_{2n+1}^2}\right] \tag{5.11}$$

$\omega_{2n} = V''(x_{2n})$ and $\omega_{2n+1} = V''(x_{2n+1})$.

We define an effective size-landscape function by rewriting the function V including the average chronic stress f_0, $V_{\text{eff}}\,V - f_0\,x$. This function simply

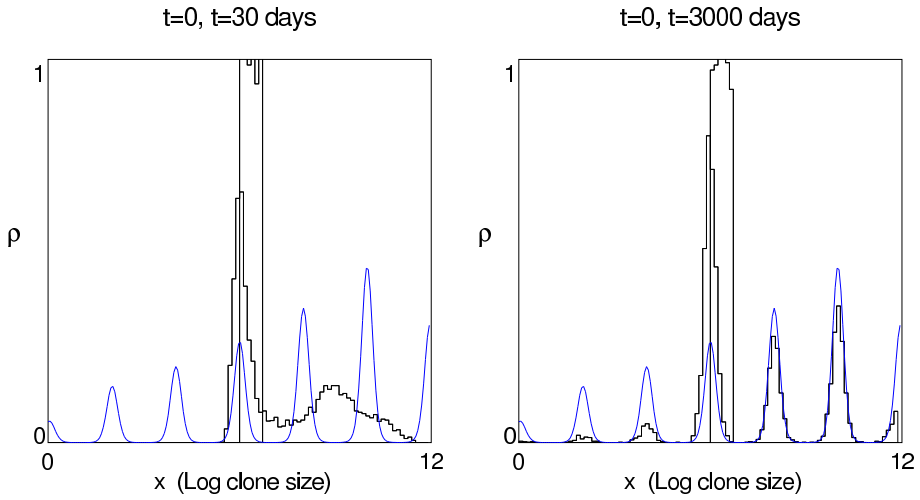

Figure 5.4: Clonal expansion due to an acute antigenic load of intensity $F_0 = 2$, and duration $T = 9$ days, and chronic stress with average value $f_0 = 0.02$ and fluctuation amplitude $\gamma = 0.0075$. The remaining parameters are $\omega = 0.1, \beta = .02$. The pictures represent the probability density function ρ, at a given time t, of having a clone size $c = 10^x$. Initially, the clone size is uniformly distributed around the value $x_0 = 6$ with a spread $\Delta x = 0.35$. With the stochastic stimuli the probability distribution of the clone size evolves, and asymptotically peaks around the equilibrium values. The histogram represents the simulation, whereas the continuous curve is the analytical curve of the asymptotic solution of the Fokker-Planck equation. There is a small but finite probability that the clone size decreases with respect to the initial value. The histogram in the left panel refers to the distribution at time $t = 30$ days, whereas the histogram in the right panel corresponds to time $t = 3000$ days. The central rectangle in both panels represents the initial distribution and is the same for both panels.

tells that the average effect of the stochastic term is to bend the curve correspondent to the function V (see Fig. 5.1). This enhances the probability of having large clones by reducing the activation threshold. The fluctuating part of the CIS is responsible for jumps in the size-landscape function. This stochastic effect leads to an asymptotic stationary state, where the probability of having a clone of size $c = 10^x$ is peaked in at the minima of $V_{\text{eff}}\, x$). The height of the peaks increases with f_0. In figure Fig. 5.4 the situation in which both the acute stimulus and the CIS are present is shown. In the absence of CIS the clone would reach a new equilibrium size after the acute stimulus, and performs damped oscillations around it (see Fig. 5.3). If the

stochastic term is considered, as shown in Fig. 5.4 (left panel), short after an acute stimulus (of duration $T = 9$ days) the probability density of the clone size is spread out. A first peak is found at the initial value ($x = 6$), and a second broader peak between the next two equilibrium sizes. After a long time ($t = 3$ years) the asymptotic stationary distribution is approached, as shown by the comparison of the simulation with the analytical solution Eq. (5.9) (Fig. 5.4 right panel). A longer time or a smaller damping ($\beta = 0.01$) are required to reach more closely the equilibrium distribution. We can indeed estimate the relaxation time being proportional to β/ω^2 according to a strong damping estimate (see appendix C). Smaller clone sizes with respect to its initial value $x(0) = 6$ are observed (see Fig. 5.4). This is due to the CIS effect, which has a finite probability to be negative on a short time interval ($f_0\Delta t + \gamma\xi\sqrt{\Delta t}$ where ξ is here a random number uniformly distributed in [-1,1] with variance 1). From a biological view point this negative contribution causing a temporary reduction of the clone size, is acceptable since it has been experimentally observed that under heterologous stimulations the clone size can decrease (attrition) [Selin et al., 1999, Chen et al., 2001a]. From a probabilistic point of view this mechanisms would imply that during the homeostasis of a peripheral T-cell clone, the size does not grows monotonically but, due to further different environmental conditions, can even reduce, in order to make possible the expansion of other specific T-cell clone. Clones with a size several times the initial configuration value are observed within a long time period. This phenomenon is enhanced by increasing the amplitude of the chronic fluctuations. In Fig. 5.5 we analyze the effect of a change in the average value of the chronic term f_0. The right panel shows the results of the probability density of the clone size for a value of f_0 ten times bigger with respect to the left panel. With larger value of f_0 the probability of having clones smaller than the initial value is practically zero, which means that the attrition phenomenon is negligible. On the contrary, for the smaller value of f_0 the effect of the attrition is visible.

5.3 Discussion and conclusion

In this work we proposed a model to test the hypothesis that the maintenance over long timescales of AE T-cell clones in the peripheral infected tissues can be strongly affected by CIS. The CIS can also play a relevant role in the reduction of the clone size caused by the attrition mechanism [Chen et al., 2001a, Selin et al., 1999]. In this minimal model we have introduced the size-landscape function in order to describe the interactions between competing cells in infected organs during the proliferation and maintenance of AE T-

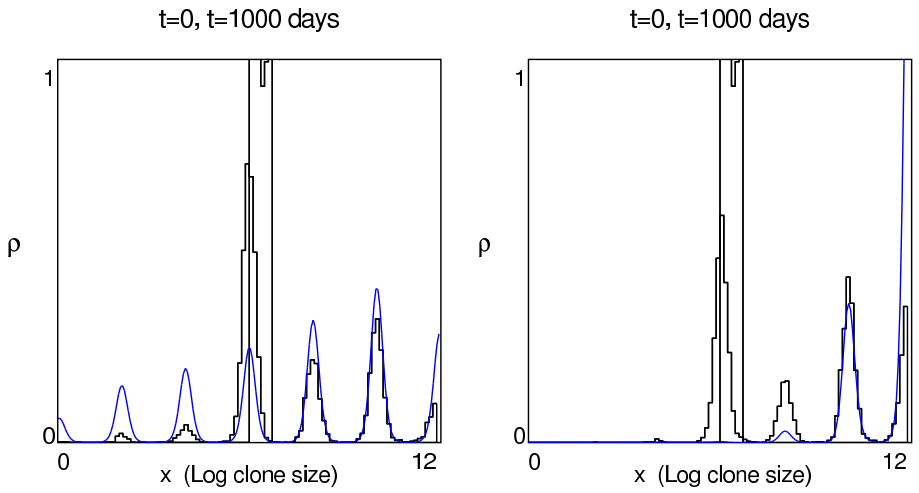

Figure 5.5: Clonal expansion due to an acute antigenic stimulus with the same parameters as in Fig. 5.4. Left panel: probability density ρ of the clone size at time $t = 1000$ days for an average value of the chronic stress $f_0 = 0.02$ and a fluctuation amplitude $\gamma = 0.008$. Right panel: probability density of the clone size at time $t = 1000$ days for an average value of the chronic stress $f_0 = 0.2$ and a fluctuation amplitude $\gamma = 0.008$. This figure shows that by increasing the average value of the chronic stress the expansion probability is strongly enhanced and the probability of reducing the clone size becomes very small.

cell pool. Although a mechanistic explanation for this function is unknown, we can recall that AE T-cells recruited to the site of the antigenic exposure undergo a dynamic regulation which is dependent on the particular microenvironment that T-cell meet [Butcher and Picker, 1996, Harris et al., 2002]. The main idea is that the joint action of the function V and of the damping term $-\beta v$ works as a spring-dash pot system which describes, at least in a first approximation, the complicated homeostatic process underlying the T-cell clone dynamics over long timescale.

We found that Cytotoxic T-cell clones can differ in their expansion rates even if the same antigenic insult is given. The housekeeping message we propose is that chronic fluctuations of a generic stimulus can modify the dynamics of the clonal expansion in a non-trivial and non-predictable fashion. The model is adequate to describe the sensitivity and the differences of the clone homeostasis with respect of the local environment as suggested by recent experiments [Marshall et al., 2001]. Moreover, the recruitment and the maintenance of T-cells in the periphery is not only due to acute

challenges, but also to chronic non specific stimulations, which can strongly modify the T-cell repertoire. This model confirms that cytokines can be envisaged as a major unspecific response of the IS to a chronic stimuli. This, over tenth other function of cytokines, can be fundamental to keep the IS alarmed. We therefore support the hypothesis that the antigenic specificity is not the only important determinant of the long term survival of AE T-cells clones [Jameson, 2005, Veiga-Fernandes et al., 2000, Tough et al., 2000, 1996]; Memory T-cells may follow a different rule with respect to the naive pool. Their function to prevent dispendious energy activity of the IS against previously encountered pathogens would probably be done more efficiently without strong specificity. Together with the results presented in Chapter 4, we conclude that the maintenance of AE T-cells can be a function of both antigen specificity and generic environmental stimuli. The first gives a precise signal regarding what T-cells should combat, while the second shapes the local environment, which influences the timing and the size of the IR. If one speculates on the consequences that the clonal expansion may have on ageing it could be pretty natural to envisage a detrimental effect. The loss of diversity is the direct effect of a huge expansion of specific cells in a system where the total amount of cells is kept almost constant. It is known that clonal expansion is a major feature of immunosenescence. Some mathematical models [De Boer and Perelson, 1994] highlight the role of cross-reactivity, being the safe-site of the clonal expansion of memory cells. Despite the cross-reactivity as a positive sign of the clonal expansion, we suggest that the CIS is one of the predominant forces driving immunosenescence [Franceschi and Bonafe, 2003, Franceschi et al., 2000a]. We have shown that a specific AE T-cell clone shrinks (with a low probability), as a consequence of the CIS and subsequent attrition. This would suggest that during vaccine recalls the size of the long lived AE T-cell pool could not change at all, or worst, could even decrease in some individuals, with a negative effect on the maintenance of the clone.

We are currently working on a 2-dimensional multi-agent system with the aim to investigate mechanistically the clonal expansion of T-cells during an infection. The result of this new approach should be to bridge the mean field approximation, such as the model here proposed, and a more mechanistic description based on cell-cell interaction. Recent data on the kinetics of T-cell interaction with the APC may help in such an attempt. Competition for epitopes, timing of the TCR-MHCp binding kinetics and the availability of APCs can be modeled in a 2-D multi agent simulation. These approach evidence new features which a mean field approach cannot easily detect.

Summary

Although the IR against acute stimuli has been largely addressed, and simple mathematical models provided quantitative results, the question of the T-cell clone dynamics under chronic infections is still a matter of debate. Based on phenomenological facts, we suggested a stochastic mathematical model for the investigation of the T-cell dynamics over a long timescale. Moreover, the role of chronic stimuli have been discussed.

Part III

The immune system over long timescale

Chapter 6

Ageing and survival probability

Introduction

The focus of this chapter is ageing and the effect that T-cell dynamics during chronic stimuli has on it. In previous investigations [Luciani et al., 2001b] we hypothesized that lifelong, chronic immune stress (CIS) is the major driving force of immunosenescence. CIS impacts on human lifespan by reducing the number of naive antigen-non experienced (ANE) T-cells, and filling the immunological space with expanded clones of antigen-experienced (AE) T-cells. A model has been proposed to relate CIS with the conversion rate from ANE to AE $CD8^+$ T-cells [Luciani et al., 2001b, Mariani et al., 2003]. In order to account for individual variations of immunosenescence and lifespan, a noise term has been introduced for the description of the individual fluctuations of CIS. This model was able to follow with a reasonable approximation the age-related decrease of ANE $CD8^+$ T-cells, as well as human survival curves. The quality of the fit of historical demographic data improves as we approach recent the last decades of this century. Indeed, the almost linearity in the increase of lifespan and in the decrease of the noise fluctuation amplitude within this historical period data suggests that the improvement of life conditions has steadily lowered the intensity of CIS and restricted its variability. As a whole, this approach allows to appreciate when and how immunosenescence has started to impact on survivorship and predicts its crucial role in explaining human mortality in hygienized/economically-developed societies.

6.1 Ageing and immunosenescence

There are some hints suggesting that ageing is, at least in part, a consequence of IS activity. We still don't know much about it and therefore most of the

models regarding ageing has been limited to demographical studies. We attempt here to make a sort of bridge between demographic study and the knowledge of the IS dynamics.

Physiological ageing is characterized by the decline in physiological capacity of the body. This decline can be approximated by a linear function. Ageing is very heterogeneous. There is a remarkable difference in the individual patterns of physiological ageing and in the individual chance of survival. Ageing is also characterized by elevated variance: genetically identical individuals in the same environment can have different patterns of physiological ageing and different lifespans [Franceschi et al., 1999, 2000b,a]. In the last 50 years old-age mortality rates in the developed countries have steadily been declining and life expectancy have been increasing. A general theory of ageing which accounts for all these aspects is still missing.

The immunosenescence

The IS exhibits profound age-related changes, which define the immunosenescence [Franceschi et al., 1995]. The most visible of these changes is the decline in protective immunity, which results from a complex interaction of primary immune defects and compensatory homeostatic mechanisms. Many processes that normally ensure optimal immune function are gradually compromised. Immunosenescence manifests itself at several scales, from the organism to the individual cells. Morbidity and mortality is increased in elderly humans and old animals. These characteristics are associated to viral infections, such as influenza, Varicella, Herpes simplex virus-1 pox viruses and to bacterial diseases like pneumococci, E. coli, and Salmonella [Miller, 1996, Wick et al., 2000]. Dysregulation of immunity plays a big and critic role in this processes. Responsiveness to vaccination in the elderly is also diminished [Cohen, 2005]. Experimental data suggests that persisting pathogens are very important in modulating the homeostasis and functions of T-cells as they results in an ever increasing fraction of T-cells that are continuously stimulated [Pawelec et al., 2004]. Antigen presentation has been reported to be diminished during ageing [Pamer, 1999]. In principle, there is either a limit to the number of divisions that each cell can undergo, or the stochastic accumulation of mutations after n divisions (with n being highly variable even within the cells of the same clone) simply produces replicative incompetent cells. In humans, the age of 65 is usually taken as the beginning of senescence, as this is when the incidence of severe infection diseases becomes elevated. Indeed, there is a log linear decrease of in thymic output during middle age (20-60yr), and in the seventh decade a rapid shrinkage of naive $CD4^+$ and $CD8^+$ T-cell pool is observed. In the following sections we will first introduce the classical

mathematical approach for the description of biological variables describing biological ageing processes. Successively, we will present a new model in which the T-cell dynamics will be introduced.

6.2 Gompertz: the first law

The first important work regarding demographic curves arising from the analysis of some quantity describing the state of the population has been proposed by Gompertz in the nineteenth century [Gompertz, 1825]. Before comprehensive measurements and sophisticated experiments became possible, Gompertz understood the importance of establishing consistency between physiological and demographic theories of ageing. He proposed that there is an hypothetic physiological index, called vitality, which some how reflects the state of the population and its capacity to stay alive. This quantity decreases with time according to an exponential law and correlates with the mortality of the system. Today we know that physiological concepts like heterogeneity, homeostasis and stochasticity are to be taken into account to describe and explain the observed mortality data. The interesting fact is that this simple model describes intriguingly well the human mortality curves in the range of 35-85 years old. Gompertz's model supposes an exponential growth for the mortality of the population, R and a survival probability, S which decreases according to an exponential law [Gompertz, 1825]

$$R = R_0\, e^{t/\tau} \tag{6.1}$$
$$dS/dt = -R(t)\, S \tag{6.2}$$

The solution is

$$S(t) = e^{\,-C(e^{t/\tau}-1)\,\left(\,-C(e^{t/\tau}-1)\,\right)}, \qquad C = R_0\,\tau \tag{6.3}$$

6.3 Bio-markers of ageing: a model

We generalize this approach considering an ensemble of biological markers which are governed by deterministic laws whose parameters can fluctuate due to genetic mutations, and to the presence of external fields. We refer to these quantity as bio-markers. Some of them may be correlated to the mortality of the population. Basically, bio-markers tell us the state of the evolving system.

Waiting for the rationale of ageing to be clarified, the research of immunological bio-markers has been undertaken [Piantanelli et al., 2001, Yashin et al., 2000, Luciani et al., 2001b, Weitz and Fraser, 2001]. The shortening of telomers at the genetic level, the decrease of cytotoxic naive T-cells and the reduction of the memory clones repertoire in the immune system have proved to be correlated to ageing [Akbar et al., 2004]. An increase of heterogeneity at the level of DNA and of the organs has also been observed and more generally, a spread of most biological variables around their mean value. These processes are partly triggered and certainly enhanced by the fluctuations (of physical conditions, antigenic load and stress) of the external environment [Franceschi et al., 1999, 2000b, Luciani, 2000, Mariani, 2001]. The accumulation of small random fluctuations on a long timescale can lead to important changes in the organism. A generalization of the model for the vitality equation given by Gompertz can be given assuming a linear response of the system to the external and internal fields. We neglect the fluctuations of the parameters describing the interactions among the bio-markers. The system of stochastic differential equations with additive noise read

$$\frac{dx_k}{dt} = F_k(x_1, \cdots, x_n, \alpha_1, \alpha_p) + \sum_{j=1}^{n} C_{k,j} \left(f_j(t) + \epsilon_j \xi_j(t) \right) \qquad (6.4)$$

Here, x_k is a general biological marker, F_k are generic operators representing the deterministic effect of external stimuli on the bio-markers. The parameters α_k are representative of the interaction between the n bio-markers. Finally, the last term of the equation is the stochastic stimulus which has an average f_j and a fluctuation amplitude ϵ_j. If the functions F_k are linear, $F = A\,x$, and the dependence on the parameters α_k and the average fields f_k can be neglected, the above system can be analytically solved (see next section). The matrix A must have eigenvalues with negative real part to ensure asymptotic stability. In this case, the variance of the bio-markers x_k is also asymptotically bounded. The formulation of this type of models is significant if there are in vivo experiments which allow to monitor the time evolution of the bio-markers. However, this type of experiments over a long timescale are onerous and time consuming. Having selected a significant sample of bio-markers, we now define the function $v = v(x_1, \cdots, x_n)$ as the *vitality* function, which is commonly used in demographic models [Yashin et al., 2000]. A sharp threshold is assumed, chosen conventionally to be zero, which marks the transition from life to death. Since our markers are stochastic variables, the vitality is a random variable as well.

Starting with a cohort of genetically identical individuals living in the same environment, it is natural to associate to each of them a vitality cor-

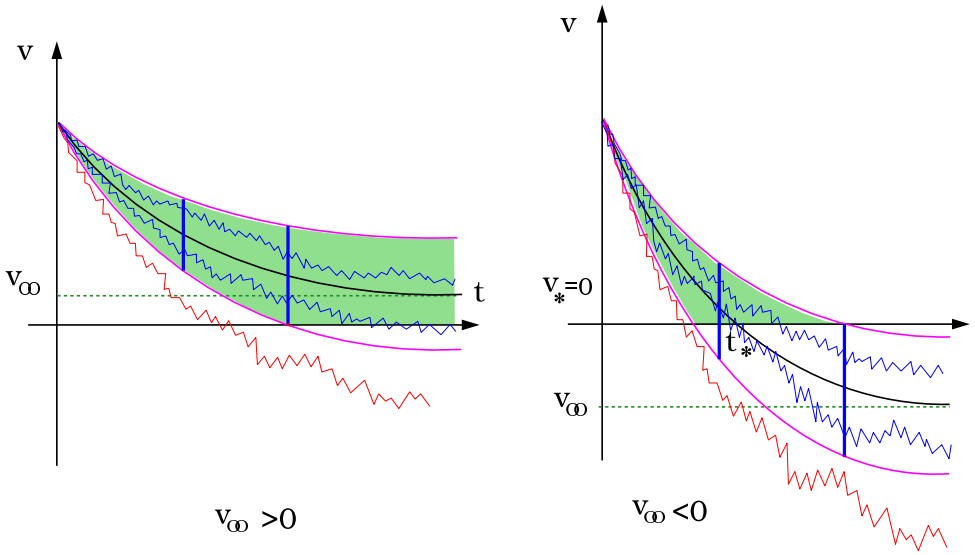

Figure 6.1: Sketch of the trajectories of the concentration of the naive T-cells as an example of bio-marker of mortality (Taken from Luciani et al., 2001b).

responding to a realization of a stochastic process. This means that every trajectory-realization of the stochastic process in the space of the bio-markers $\mathbb{R}n$, corresponds to a trajectory for the vitality, which is represented by the graph of $v(t)$ (see for example Fig. 6.1). The survival probability $S(t)$ can be obtained starting from the distribution function $\rho(v,t)$ of the stochastic variable v according to

$$S(t) = \int_0^\infty \rho(v,t)\, dv = \int_{-\langle v(t)\rangle/\sigma(t)} \rho\big(\, \langle v(t)\rangle + u\sigma(t),\, t\,\big)\, du \qquad (6.5)$$

where we denote with $\langle v(t)\rangle$ and $\sigma(t)$ the mean value and the variance of the process.

The linear model

In order to have a better insight into the equations satisfied by $v(t)$, it is convenient to introduce an invertible map of $\mathbb{R}n$ defined by the set $(v_1, v_2, \ldots, v_n)$ of functions of $x = (x_1, \ldots, x_n)$ where $v_1 \equiv v$. The system of equations Eq. (6.4) in the new variables reads

$$\frac{dv_i}{dt} = \Phi_i(v_1, \cdots, v_n) + \sum_{k=1}^{n} \Gamma_{ik}\,(v_1, \cdots, v_n)\,\big(\, f_k(t) + \,\epsilon_k\,\xi_k(t)\,\big) \qquad (6.6)$$

The Fokker-Planck equation for the distribution function $\rho_n(v_1, \cdots, v_n, t)$ for the above variables can be written according to the standard procedure (see Risken [1989]) and the function $\rho(v,t)$ is then the corresponding marginal distribution

$$\rho(v,t) = \int_{\mathbb{R}n-1} \rho(v, v_2, \ldots, v_n,\, t)\, dv_2 \cdots dv_n \tag{6.7}$$

A drastic simplification occurs if the functions F_k (see Eq. (6.4)) defining the interactions among the bio-markers are linear. The vitality is in turn a linear function of them, $v = w \cdot x$, where w is a constant vector of unit norm. Letting $W = (w_1, \cdots, w_n)$ be an orthogonal matrix whose first column is $w_1 \equiv w$ it is straight forward to verify that the stochastic system given by Eq. (6.6), satisfied by the variables v_i, are

$$\frac{dv_i}{dt} = \sum_{j=1}^{n} B_{ij}\, v_j + \sum_{k=1}^{n} D_{ik} \left(f_k(t) + \epsilon_k\, \xi_k(t) \right), \qquad B = \tilde{W}\, A\, W,\; D = \tilde{W}\, C \tag{6.8}$$

In this case we write a Fokker-Planck equation whose solutions are Gaussian distributions. They are specified by the mean values $\langle v_i(t) \rangle$ and the covariance matrix $\sigma_{ij}^2 = \langle\, (v_i - \langle\, v_i \,\rangle)\, (v_j - \langle\, v_j \,\rangle)\, \rangle$. The marginal distribution for $v \equiv v_i$ is given by

$$\rho(v,t) = \frac{1}{\sqrt{2\pi\sigma^2(t)}}\, e^{-\frac{(v - \langle\, v(t)\,\rangle)^2}{2\,\sigma^2(t)} \left(-\frac{(v - \langle\, v(t)\,\rangle)^2}{2\,\sigma^2(t)} \right)} \tag{6.9}$$

the survival probability takes a very simple form

$$S(t) = \frac{1}{\sqrt{2\pi}} \int_{-\langle v(t) \rangle / \sigma(t)}^{\infty} e^{-\frac{u^2}{2}}\, du \equiv \frac{1}{2}\, \mathrm{Erfc}\, - \frac{1}{\sqrt{2}} \frac{\langle v(t) \rangle}{\sigma(t)} \left(-\frac{1}{\sqrt{2}} \frac{\langle v(t) \rangle}{\sigma(t)} \right) \tag{6.10}$$

A bio-marker of mortality: cells in a random environment

Consider a population of interacting cells $(x_1, \ldots, x_n) \equiv x$ in a random environment. We assume that the deterministic equation is linear and the noise is additive. From Eq. (6.4) we can write

$$\frac{dx}{dt} = -A(t)\, x + f(t) + \epsilon \frac{d\eta}{dt} \tag{6.11}$$

$$\frac{d\eta}{dt} = -\beta \eta + \xi(t) \tag{6.12}$$

where A is a positive semi-definite matrix and $\xi(t)$ is a white noise. The system experiences a colored noise of Ornstein-Uhlembeck type η. The first term $A\,f$ describes the exchanges among cells x due to mutual interactions, the second term $f(t)$ is the sum of two vector fields associated to the signaling or control processes of the organism and to the average environmental stress. The noise describes the rapid random fluctuations of the previous fields. In the simplest case where A and f are time independent and in the absence of noise, the system reaches an homeostatic equilibrium $x_* = A^{-1}\,f$. If f varies periodically with respect to a constant value, the populations $x(t)$ undergo periodic oscillations with the same frequency, provided that the equilibrium reached when $f = 0$ is stable. For instance, this can be observed in periodic viral attacks over the lifespan (such as Herpes virus infection) [Crough et al., 2005, Dunn et al., 2002]. Let $v = w \cdot x$ be the bio-markers of interest, where w is a constant unit vector. Following the general approach proposed (see 6.3 and Eq. (6.8)), we change Eq. (6.13) into a new set of equations by introducing an orthogonal matrix $W = (w, w_2, \cdots, w_n)$. whose first column is the vector w. The new vector $v = \tilde{W}\,x$, whose first element is the vitality v, satisfies the equation

$$\frac{dv}{dt} = -B\,v + g(t) + \epsilon\,b\,\xi(t) \qquad\qquad B = \tilde{W}\,A\,W \tag{6.13}$$

where $g = \tilde{W} f$ and $b = \tilde{W} a$. Assuming for simplicity that A is time independent and the noise to be white $\beta = 0$, the probability density function (p.d.f.) $\rho(v,t)$, solution of the Fokker-Planck equation corresponding to the Langevin equation Eq. (6.13), is a Gaussian whose parameters $\langle\, v_i \,\rangle$ and $\langle\, (v_i - \langle\, v_i \,\rangle)^2 \,\rangle$ can be explicitly determined. The marginal distribution $\rho(v,t)$, obtained by integration over $(v_2, \ldots, v_m)$ is

$$\rho(v,t) = \frac{1}{\sqrt{2\pi\sigma^2(t)}}\, e^{-\frac{(v-\langle\, v\,\rangle)^2}{2\sigma^2(t)}\left(-\frac{(v-\langle\, v\,\rangle)^2}{2\sigma^2(t)}\right)} \tag{6.14}$$

Let us suppose that v has a critical threshold v_c strongly correlated to the death of the organism. For the sake of simplicity by a simple translation we can shift the threshold to 0 without affecting the results. As a consequence, we assume that our bio-marker of mortality is positive and that the organism death corresponds to $v = 0$ (see Fig. 6.1). In the absence of noise, a population of identical organisms in an identical environment has the same lifespan T defined by $v(T) = 0$. The presence of fluctuations allows to personalize the individual histories because every organism experiences its unique sequence of random events which are responsible for changes during lifespan. It should be noted that this is again a reasonable but strong approximation. It has

been observed that individuals modified to have very similar genetic background, and living in a very similar environment show significant changes in their lifespan [Brooks et al., 1994]. We define by T the average lifespan $\langle\, v(T)\,\rangle = 0$. For each organism death occurs at time t, when v first vanishes. At subsequent time v might also be negative, but this mathematically defined solution becomes meaningless from the biological viewpoint. In the language of stochastic process we are facing a first passage problem, whose p.d.f. can be obtained only by a numerical procedure. If we consider the probability distribution function defined by Eq. (6.14) for a fixed t and $0 < v < c$, integrating it on $[0, c]$, we do not obtain the percent of our identical organisms born at time $t = 0$ whose bio-marker at time t are in the interval $[0, c]$. Therefore, we do not obtain the percentage of organisms still alive at time t. In this case we are overestimating the real number, since we count as alive also those organisms whose bio-marker has previously become negative, recovering a positive value at time t. This upper bound can be computed analytically, and proves to be very close to the exact value for small values of the fluctuation amplitude. The upper bound $S(t)$ to the exact survival probability $S_{\,\mathrm{ex}}\,(t)$ is given by

$$S(t) = \frac{1}{\sqrt{2\pi}} \int_{x(t)}^{+\infty} e^{\frac{-u^2}{2}} du \equiv \frac{1}{2} \mathrm{Erfc} \frac{x(t)}{\sqrt{2}} \tag{6.15}$$

where

$$x(t) = -\frac{\langle\, v\,\rangle(t)}{\sigma(t)} \tag{6.16}$$

We recall that the mortality is related to the survival probability $S(t)$ by

$$R(t) = -\frac{1}{S(t)} \frac{dS}{dt} \tag{6.17}$$

6.4 Vitality: stochastic equation

We shall compare three cases of the generic model described above (See Sec. 6.3);

- the Wiener process, suitable to explain the anomalous survival queues observed in simple organisms [Weitz and Fraser, 2001]
- the Ornstein-Uhlenbeck process, proposed for the naive $CD8^+$ cytotoxic T-cells [Luciani et al., 2001b]
- a stochastic process whose survival curve is very close to Gompertz law, which describes most of the demographic data for different organisms.

In order to simplify the analysis, we consider the general model given in Eq. (6.6) in the case $m = 1$. The Langevin equation for the bio-marker v is

$$\frac{dv}{dt} = -a\,v - f_0 - f_1 t + \epsilon \frac{d\eta}{dt} \tag{6.18}$$

$$\frac{d\eta}{dt} = -b\eta + \xi(t) \tag{6.19}$$

where η is is the noise term.
f $b = 0$ the equation for the stochastic variable is known as Wiener process. The general solution for the average of the stochastic process $v(t)$ is given by

$$\langle\, v(t)\,\rangle = v_0 e^{-at} + \frac{f_1}{a} - f_0\left(\frac{f_1}{a} - f_0\right)\frac{1 - e^{-at}}{a} - \frac{f_1}{a}\,t \tag{6.20}$$

Moreover, in the following special cases,

$$\langle\, v(t)\,\rangle = \begin{cases} v_0 e^{-at} - a^{-1}\, f_0(1 - e^{-at}) & \text{case a)} \quad f_1 = 0 \\ v_0 e^{-at} + a^{-2}(1 - at - e^{-at}) & \text{case b)} \quad f_0 = 0 \\ v_0 - f_0 t - \frac{1}{2} f_1 t^2 & \text{case c)} \quad a = 0 \end{cases} \tag{6.21}$$

the function $\langle\, v(t)\,\rangle$ decreases monotonically in all cases if the parameters a, f_0, f_1 are positive. The curve is convex in case a), concave in case c), and in case b) convex if $a^2 v_0 < f_1$, and concave if $a^2 v_0 > f_1$. The noise term is given by

$$\eta(t) = \int_0^t e^{-b(t-s)}\,\xi(s)\,ds \tag{6.22}$$

and it is not difficult to check that the mean square deviation σ is given by

$$\sigma^2(t) = \langle\,(v(t) - \langle\, v(t)\,\rangle)2\,\rangle \tag{6.23}$$

$$= \frac{1}{(b-a)^2}\Big[\frac{b}{2}(1 - e^{-2bt}) + \frac{a}{2}(1 - e^{-2at}) - \frac{2ab}{a+b}\,(1 - e^{-(a+b)t})\Big] \tag{6.24}$$

For $b = 0$ and $a = b$ the variance becomes

$$\sigma^2(t) = \frac{1 - e^{-2at}}{2a} \quad (b = 0) \tag{6.25}$$

$$\sigma^2(t) = \frac{1}{4a}\left[1 - e^{-2at}(1 - at + a^2 t^2)\right] \quad (b = a) \tag{6.26}$$

We now consider three distinct relevant cases, characterized with only two parameters, the mean lifetime T, and the noise amplitudes ϵ.

1. Gompertz-like model (GM). The model is defined by $a = f_0 = 0$ and $f_1 = 2/T^2$, $b = 3/T$.

$$\frac{dv}{dt} = -\frac{2t}{T^2} + \epsilon \frac{d\eta}{dt} \tag{6.27}$$

$$\frac{d\eta}{dt} = -\frac{3\eta}{T} + \xi(t) \tag{6.28}$$

   Next we will show that the survival curve obtained from this model presents very similar features of the standard Gompertz curve. Furthermore, it will be shown that the rate of mortality increases as a power law, $R(t) \propto t^k$ for $t \to \infty$ (see Fig. 6.6)

2. The Wiener model (WM). The following model has been recently proposed to describe mortality plateau in species where individuals could reach a lifespan up to ten times the average[Weitz and Fraser, 2001]. This model is defined by $f_0 = -1/T$ and $f_1 = a = b = 0$

$$\frac{dv}{dt} = -\frac{1}{T} + \epsilon\, \xi(t) \tag{6.29}$$

   In this case the solution becomes

$$\langle\, v(t) \,\rangle = v_0 - f_0 t \qquad\qquad \sigma(t) = \epsilon\sqrt{t} \tag{6.30}$$

   and, as it will be shown later on, the survival curve exhibits a long tail and the mortality rate has a slow asymptotic increase. The rate of mortality, therefore, can present an asymptotically constant plateau, $R(t) \propto 1$ for $t \to \infty$.

3. The Immuno-Model (IM) [Fagnoni et al., 2000, Mariani et al., 2003, Luciani et al., 2001b]: defined by $f_1 = b = 0$ and $T = 1/a$. With the further constraint $f_0 = T^{-1}\,(e-1)^{-1}$ we have

$$\frac{dv}{dt} = -\frac{v}{T} - \frac{1}{T}\,(e-1) + \epsilon\xi(t) \tag{6.31}$$

   The rate of mortality has an exponential asymptotic decrease $R(t) \propto e^{-t/T}$ for $t \to \infty$.

6.5 The immuno-model

This model is based on the hypothesis that the loss of some of the immune system functions are responsible for the reduced functioning of the body

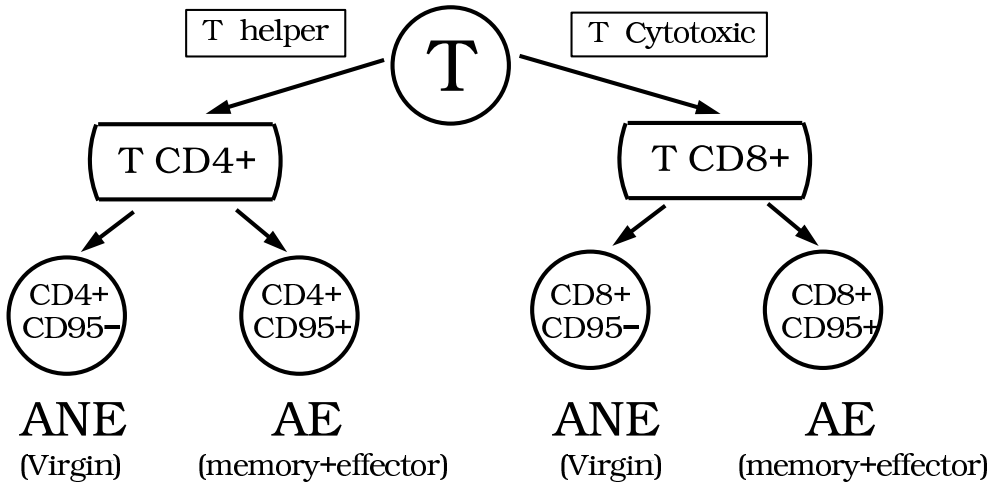

Figure 6.2: Markers of Naive, $CD95^-$, and Memory-Effector, $CD95^+$, T lymphocytes for both the $CD4^+$ (Helper) and the $CD8^+$ (cytotoxic) pool. This sketch has been derived from experimental results [Fagnoni et al., 2000].

during ageing. The vitality function has been identified with the Naive T-cell concentration $v = V/(V + M)$. Several data showed that defects in the IS functions arise from the T-cell senescence. In particular human ageing is characterized by a strong reduction of naive T-cell repertoire [Fagnoni et al., 2000, Nikolich-Zugich, 2005]. A shrinkage of the total T-cell clone repertoire has been reported [Franceschi et al., 1995, 2000a]

We recall that T lymphocytes split into two groups: the cytotoxic and helper T-cells. The former attacks and destroys intracellular infected cells, while the latter contributes to extracellular antigenic response and to regulate the immune response. They are labeled by $CD8^+$ (cytotoxic) and $CD4^+$ (helper) respectively, according to the surface markers used to identify them. We are interested in the dynamics of two populations, the antigen non-experienced (ANE) naive T-cells, and the antigen experienced (AE) T-cells, which are identified by the $CD95^-$ and $CD95^+$ surface markers respectively [Fagnoni et al., 2000] (see Fig. 6.2). The deterministic part of the model describes the decrease of the ANE $CD8^+$ T-cells concentration, in agreement with experimental data[Fagnoni et al., 2000, 1996]. The stochastic forcing, describing the chronic stress [Franceschi et al., 2000b,a], allows to obtain individual histories. The model here described is intended to introduce some improvements of a previous model [Luciani et al., 2001b], by taking into account the remodeling of the immune system during the lifespan. The model shows a further improvement, especially for the early stage, were the simpli-

fied model was not adequate. The model is defined by

$$\frac{dV}{dt} = -\alpha V - \beta M + \mu\ e^{-\lambda t} + \epsilon \cos^2(\theta)\ \xi(t) \tag{6.32}$$

$$\frac{dM}{dt} = \frac{\alpha V + \beta M}{1 + \gamma M_+} + \epsilon \sin^2(\theta)\, \xi(t) \tag{6.33}$$

V denotes the number of ANE (Naive) $CD8^+$ T-cells and M the number of AE $CD8^+$ T-cells, $M_+ = M$ if $M > 0$ and $M_+ = 0$ if $M < 0$. The parameter α gives the conversion rate of ANE cells due to primary antigenic insults, whereas β is the reactivation rate of AE cells due to secondary antigenic stimulus. AE cells re-expand and occupy a larger quota of the space available. On the other hand, the total T-cell repertoire remains almost constant. Therefore, an inhibitory effect on the ANE cells caused by the reactivation of AE clone during a secondary antigenic stimulus has been considered. Indeed, it has been shown that during ageing the T-cell pool undergoes a small but well defined shrinkage [Franceschi et al., 2000a]. In order to account for this phenomenon, an inhibition effect with the term $-\beta M$ has been introduced. This reduces the size of ANE cells as the number of AE clones rises. Finally, we supposed the conversion and reconversion terms of AE pool, α and β, to be proportional to $(1 + \gamma M_+)^{-1}$, in order to account for the shrinkage of the T-cell repertoire. The term $\mu\, e^{-\lambda t}$ describes the production by the thymus, which is assumed to decay exponentially [Nikolich-Zugich, 2005]. Finally, the stochastic term

$$\langle \xi(t) \rangle = 0 \qquad \langle \xi(t)\, \xi(t') \rangle = \delta(t - t') \tag{6.34}$$

represents the stochastic fluctuations to the conversion rates. The mixing angle θ weights this term among the ANE and AE compartments. The results are compared with experimental data (see Fig. 6.3 and Fig. 6.4). The stochastic term generates a family of immunological histories. Their spread is measured by the variance. In Fig. 6.3 the effect of the mixing angle is shown. When θ grows, the root mean square (rms) spread $\sigma_{_V}$ decreases, whereas the rms spread $\sigma_{_M}$ of M increases. In Fig. 6.4 the effect of thymus and of the shrinkage are shown. The graph of $\langle\, V(t)\,\rangle$ exhibits a peak at $t = (\log\lambda - \log\alpha)/(\lambda - \alpha)$ if $V(0) = 0$. The peak disappears when the thymus contribution vanishes. Experimental evidences suggest that newborns undergo a rapid proliferation in the T-cell poll, followed by a slower rate which define the homeostatic level [Grossman et al., 2004]. The shrinkage reduces considerably the increase of $\langle\, M(t)\,\rangle$, whereas it does not affect $\langle\, V(t)\,\rangle$. Fixing the parameters in a range of values compatible with the experimental

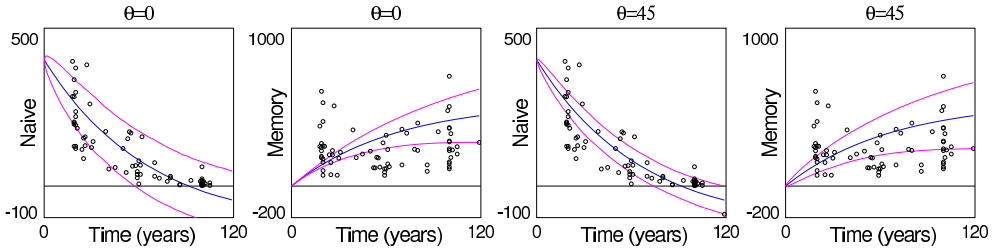

Figure 6.3: Comparison with CD95 data [Turchetti et al., 2002, Luciani, 2000] of naive (ANE) and memory plus effector (AE) populations for the model without shrinkage and thymus for two different mixing angles. The parameters are $\alpha = 0.02,\ \beta = 0.005,\ \epsilon = 10,\ V(0) = 400$ and $\theta = 0$ (left figures) and $\theta = 45^o$ (right figures). The curves are $\langle\, V(t)\,\rangle + k\sigma_{_V}(t)$ and $\langle\, M(t)\,\rangle + k\sigma_{_M}(t)$ with $k = -2, 0, 2$.

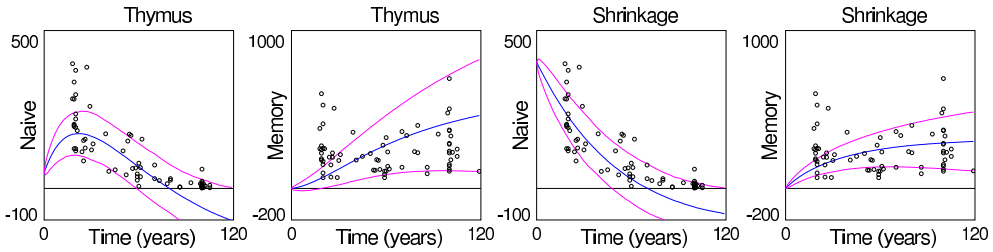

Figure 6.4: Comparison with CD95 data [Luciani et al., 2001b, Mariani, 2001] of naive (ANE) and memory plus effector (AE) populations for the model with shrinkage and thymus. The parameters are $\alpha = 0.025,\ \beta = 0.01,\ \epsilon = 15,\ \theta = 35^o$. On the left side we consider the contribution of thymus with $\lambda = 0.05,\ \mu = 15,\ \gamma = 0$ and $V(0) = 50$. On the right side the contribution of shrinkage is shown for $\gamma = 0.004,\ \mu = 0$ and $V(0) = 400$. The curves are $\langle\, V(t)\,\rangle + k\sigma_{_V}(t)$ and $\langle\, M(t)\,\rangle + k\sigma_{_M}(t)$ with $k = -2, 0, 2$.

data [Fagnoni et al., 2000, Luciani et al., 2001b], we find that the leading statistical properties of $v(t)$ (average and variance) can be described with a more simple model for the concentration of AE cells

$$\frac{dv}{dt} = -(\alpha - \beta)v - \beta + \epsilon\xi(t) \tag{6.35}$$

This corresponds to our general model (Eq. (6.20)) with $f_0 = \beta,\ a = \alpha - \beta, f_1 = b = 0$. In the next section the survival curves and mortality rates obtained from these three models for the vitality equation will be discussed. A very important difference is found with respect to the classical Gompertz survival law [Gompertz, 1825]: the rate of mortality vanishes initially and asymptotically, whereas it increases exponentially in the Gompertz

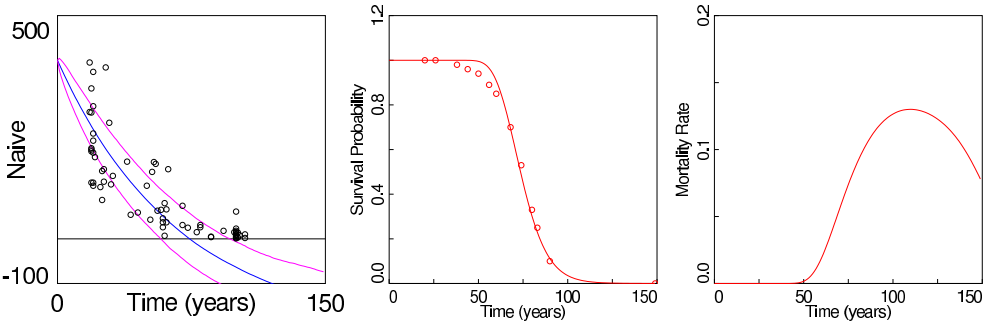

Figure 6.5: Naive cells population $\langle V(t) \rangle \pm 2\sigma_V(t)$ with $v_\infty = -0.5$, $T = 67$ and $\hat{\epsilon} = 0.016$ (left). Corresponding survival curve (center) and mortality rate (right). These values correspond to $\alpha = 0.022$, $\beta = 0.0075$, $\epsilon = 6.5$ $\gamma = \mu = 0$ and $V(0) = 400$

law. This explains the presence of very long lived individuals (centenarians), and supports the biological hypothesis of a depletion in the ANE T-cells pool [Franceschi et al., 2000a, 1995, 2000b].

6.5.1 The survival probability

In the theory of stochastic processes, the simplified model for the concentration of T-cell clones given by equation Eq. (6.35) is known as the Ornstein-Uhlembeck process. The probability density function satisfies the Fokker-Planck equation, and has an explicit solution (see appendix C)

$$\langle v \rangle(t) = v_\infty + (1 - v_\infty)e^{-t/T} \tag{6.36}$$

$$\rho(v,t) = \frac{1}{\sqrt{2\pi\sigma^2(t)}}\, e^{\left[-\frac{(v-\langle v \rangle(t))^2}{2\sigma^2(t)}\right]} \tag{6.37}$$

where

$$\begin{aligned} T &= (\alpha - \beta)^{-1}, \\ v_\infty &= -\beta T \\ \sigma^2(t) &= \frac{1}{2}\,\hat{\epsilon}^2\, T\,(1 - e^{-2t/T}) \end{aligned} \tag{6.38}$$

The survival probability $S(t)$ (see Eq. (6.15)) has been applied to demographic data [Mariani et al., 2003, Turchetti et al., 2003]. The lower integration end-point $x(t)$ can be written as

$$x(t) = C\frac{1 - e^{\frac{t_* - t}{T}}}{\sqrt{1 - e^{-2t/T}}} \tag{6.39}$$

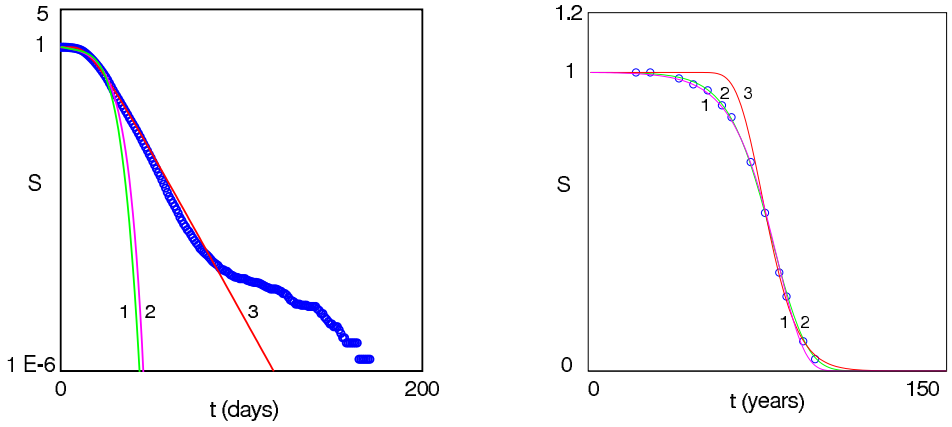

Figure 6.6: Left frame: plot of the survival curves in a semilogarithmic scale for a cohort of mad-flies (circles).We compare the best-fits with Gompertz law (purple curve 2), with the Gompertz-like model i (green curve 1) where $T = 20, \epsilon = 0.55$ and with the Wiener model ii (red curve 3) where $T = 19.3,\ \epsilon = 0.1$. Right frame: plot of the demographic data for a cohort of Danish (circles). We compare the best-fits with a Gompertz law (purple curve 1), with the Gompertz-like model i (green curve 2) where $T = 75, \epsilon = 0.1$ and with the immunological model iii (red curve 3) where $T = 75, \epsilon = 0.015$.

where

$$C = \frac{1}{\hat{\epsilon}} \left(\frac{2}{T}\right)^{1/2} (v_* - v_\infty) \tag{6.40}$$

In this formalism t_* is the age at which death occurs $\langle\, v(t_*)\,\rangle = v_*$, namely $e^{-t_*/T} = (v_* - v_\infty)/(1 - v_\infty)$. We notice that $S(t)$ is a three parameters function. In Fig. 6.5 the fit of the demographic data of human males using Eq. (6.15) has been performed. The parameters values have been chosen very similar to the values obtained from the fit of the $CD8^+$ T-cells concentrations [Fagnoni et al., 2000]. The mortality rate is not monotonically increasing, as in the Gompertz model, but decreases after reaching a maximum (see Fig. 6.5).

6.6 Analysis of demographic data

The proposed models have been applied to different sets of data: a population of mad-flies, [Carey et al., 1992, Turchetti et al., 2002], and a cohort of Danish, born at the beginning of last century [Vaupel and Jeune, 1996]. The GM and WM models have been compared for the first data set, and the GM model with the IM model for the second data set. For the GM model, the

function $x(t)$, which defines the survival curve, is given by

$$x(t) \;=\; -\,A\,\frac{1-(\frac{t}{T})^2}{(1-e^{-6t/T})^{1/2}} \qquad\qquad A=\epsilon^{-1}\,(\frac{6}{T}^{1/2}) \tag{6.41}$$

and the mortality rate grows like t^3. For the WM model, a constant mortality rate is obtained for $t \to \infty$. According to asymptotic studies (see appendix D) the following approximation for the mortality rate can be written:

$$R(t) \simeq -\frac{\dot{S}}{S} = \frac{\epsilon v_0}{2\sqrt{2\pi}}\,\frac{e^{\frac{-v_0}{\epsilon}^2\,^2}t}{t^{3/2}} \tag{6.42}$$

The WM has $x(t) = -t^{-1/2}(1-t/T)/\epsilon$, and the asymptotic mortality rate, Eq. (6.42), is constant.

In the Fig. 6.6 we note that, for a simple organism (respect to species presenting a more complex immune system) like a mad-fly, there is a non-negligible fraction of the population which is long lived (many times the mean lifetime). As a consequence, the Gompertz law and our GM model, which is very close to the former, fits only the early period $0 < t < 1.5T$. The WM model takes into account also the long lived fraction of the population $0 < t < 5T$, whereas the very small fraction of the extremely long lived insects $5T < t < 10T$ requires a more sophisticated model where the mortality rate decreases after reaching a constant value. In the human population, we observe that the IM model, intended to explain the behavior of the ANE $CD8^+$ T-lymphocytes, describes correctly the survival curve for $T < t < 2T$. This model gives a mortality rate which decreases after that a maximum at $t \simeq 120$ years is reached.

The inverse problem

The proposed approach allows to infer some properties of the mortality bio-markers starting from demographic data. Indeed, given a survival probability curve, the ratio $\langle\, v(t)\,\rangle/\sigma(t)$, and the value of T can be obtained by computing the inverse of the error function

$$x(t) \equiv -\frac{\langle\, v(t)\,\rangle}{\sigma(t)} = \sqrt{2}\mathrm{Erfc}^{-1}(2\,S(t)) \tag{6.43}$$

Assuming a law for the evolution of the mean $\langle\, v(t)\,\rangle$ of the bio-marker, its variance would be determined by the correspondent survival curve. The comparison between the variance $\sigma(t)$ determined by the experimental values of the bio-marker and the value determined by the survival curves, can be a

reliable test for the accuracy of the correlation between the bio-marker and the mortality rate. The plot of the ratio $x(t)$ is useful to analyze the survival data, and is exempt from the interpolation uncertainties, which affect the computation of the mortality rates from demographic data.

Summary

This Chapter is an attempt to look at ageing highlighting the events characterizing the changing of the IS during the whole lifespan (immunosenescence). We propose a generalization of a standard mathematical scheme to approach the modeling of survival curves and mortality rates of a given population. We focused on stochastic models of demographic data, and we show how important features of ageing can be explained from models describing the T-cell dynamics. Chronic antigenic load explains the spread of antigen experienced T-cells in a given population, and the flattening of the survival probability curves at very advanced ages. Within this scenario, a decrease of the fluctuations of the chronic stimuli implies a reduction of the spread of individual immunological histories around a mean value. Moreover, a decrease of the average value of chronic stimuli corresponds to a decrease of the conversion rate from antigen unexperienced to antigen experienced T-cells. This leads to an increase of the average value of the lifespan. These studies suggest that prevention of chronic antigenic stimuli, such as by prophylactic vaccination might be an effective strategy to prevent declining immune competence in the elderly. Future demographic models on immune system dynamics should reinforce these results, and pave the way to a better understanding of the immunosenescence.

Part IV

Conclusions

In this thesis we drew the attention towards two main facts. First, we show that the kinetics of antigen processing is of outstanding importance for the dynamics of T-cell clones during an IR. T-cell dynamics has been shown to be remarkably influenced by competition for resources and that the IS may take advantage of this events to mount an efficient and effective IR. Second, investigating the long timescale dynamics of the T-cell clones, we suggest that chronic unspecific stimuli can strongly change the homeostasis of clones in peripheral tissue. We evidenced how the antigen presentation and the heterogeneity of antigenic stimuli are both important variable to be taken into consideration for the study of the T-cell response. This thesis provides a scenario for the improvement of vaccination strategies, which are known to suffer for their incapability to deal, at least for the moment, with the very diverse immune cell repertoire at different age and with the very different environmental conditions characterizing each individual. The efficiency of a vaccine is also due to its capability to induce an appropriate diverse T-cell repertoire. Multiple epitope vaccines should therefore be designed with particular care regarding the dynamics of the IR and not only on the specificity of peptides.

The proteasome kinetics

The proteasome is the major protease involved in the intracellular protein degradation. The influx rate of protein substrates and the exit rate of the fragments/products is regulated by the size of the axial channels. Opening the channels is known to increase the overall degradation rate and to change the length distribution of fragments. We develop a mathematical model with a flux that depends on the gate size and a phenomenological cleavage mechanism. The model has Michaelis-Menten kinetics with a $V_{\max}$ that is inversely related to the length of the substrate, as observed in *in vitro* experiments. We study the distribution of fragment lengths assuming that proteasomal cleavage takes place at a preferred distance from the ends of a protein fragment, and find multi-peaked fragment length distributions similar to those found experimentally. Opening the gates in the model increases the degradation rate, increases the average length of the fragments, and increases the peak in the distribution around a length of $8 - 10$ amino acids, as observed with proteasomes equipped with regulatory subunits such as PA28. Finally, we study the effect of re-entry of processed fragments in the degradation kinetics and conclude that re-entry is only expected to affect the cleavage dynamics when short fragments enter the proteasome much faster than the original substrate. In summary, these results capture the known characteristics of

proteasomal degradation, and can therefore help to quantify MHC class I antigen processing and presentation.

Recently, mathematical models have shown how the antigen processing pathway strongly depends upon kinetic parameters [Bulik et al., 2004]. Predictions of epitopes presented on the MHCs are made with the help of algorithms based on the sequence specificity of proteins containing MHC ligand, while algorithms based on the only proteasome cleavage specificity result in a poor predictability. These algorithms perform very well when proteasomal cleavage predictions are combined with TAP transportability prediction algorithms [Tenzer et al., 2005, Kesmir et al., 2002, Kuttler et al., 2000]. Moreover, a recent work suggests that immunoproteasome is not much involved in generating new ligands for the MHC molecules but simply improves the kinetics for those peptides which have a better affinity with the TAP transporter, and therefore a higher immunogenicity [Tenzer et al., 2005]. These algorithms dedicated to the prediction of peptide sequence specificity can also be reliable tools to envisage specific features of the entire peptide distribution characterizing the landscape of the APC surface. Predictions algorithms may therefore ameliorate the kinetic approach, and help to understand more appropriately the mechanisms behind antigen presentation.

The immunoproteasome and the T-cell dynamics

While ultimately described by a steady state equation in which cellular influx equals egress, the fascinating complexities of managing size and composition of lymphocyte populations have proved fertile ground for investigation. Understanding the mechanisms which control the dynamics of cytotoxic T cell response against infectious pathogens is to date a central goal in immunology. Strategical methodology such as the intracellular antigen processing have been evolutionary selected to improve the efficiency of the IR

Mathematical models may help to quantify and predict the main features of this machinery. As a leitmotiv we followed in our approach the concept of competition for resources. T-cells perform their functions and are kept homeostatically in the system only if enough space, food and information to fight or to be quiescent are available.

It has been proposed that changes in the MHC complexes on the surface of APCs could serve as an indicator of a stress-danger for the cell, and therefore a strong and fast signal to alarm the IS [Gleimer and Parham, 2003]. We have shown that the IP may have an immunological role in changing the normal

antigen distribution, and in activating a T-cell response against stressed cells.

Competition, diversity and homeostasis

Lymphocyte diversity associated with polyclonal stimulation may prevent clonal dominance and immune-pathology by a few self-reactive clones. Multiple infections therefore are needed for at least two reasons: to keep the clone repertoire diverse enough to prevent that a pauci-clonal repertoire increases the probability of clonal expansion, and to fixate self-reactive clones, which in absence of competition might become dominant and induce pathology. For instance, there is an inverse correlation between the world incidence of autoimmune diseases and the frequency of infectious diseases. Therefore, it should be stressed that the IS is under continuous re-shaping due to infections. A global re-assessment of the cell repertoire and therefore a strong competition for resources can be an intrinsic and smart way to keep the repertoire diverse and dynamic.

Recently it has been shown that the IS loses its homeostatic size and its functionality by depletion of lymphocytes (lymphopenia caused by chemoterapic treatments or rediations). A strong correlation between the immune replenishment with newly produced lymphocytes and the incidence of autoimmune disease is observed [King et al., 2004]. Clearly, in this condition the organism does not impose a strong limit on the proliferating cells which are somehow licensed to spread without control. Competition is therefore intrinsically related to a functional immune repertoire.

Physiological conditions (ageing) and several pathological situations (HIV infection/highly active antiretroviral therapy (HAART), T-cell leukemia and bone-marrow transplantation) yield different lymphocyte homeostasis and reduced TCR diversity. Phenomenology of these conditions is often similar. T-cell clones, invariably of the T-cell phenotype, tend to expand, forming T-cell clonal expansions that take over the space and thereby reduce diversity of the remainder of the T-cell pool. These states represent potentially informative models to dissect further the relationship between T-cell receptor diversity and T-cell precursor frequency in pathogen resistance and to investigate mechanisms that regulate peripheral maintenance of T-cell diversity. We have shown that competition for resources and immunoproteasome are important mechanisms in shaping the T-cell repertoire and they can be further investigated in the context of these particular states in which T-cell repertoire suffers a different homeostasis and probably a different antigen processing kinetics.

Chronic stimuli are the other side of the coin. The antigen is the first sig-

nal capable of initiate an IR. Costimulatory signals design the power and the timing of an IR. Daily, we face small fluctuating changes in the interactions between our IS and the external environment. Physical entities, hygienic conditions, food, bacteria etc. all contribute to the chronic fluctuating stress. This chronic antigenic stress and the subsequent inflammatory burden have a major impact on survival and frailty. The most important characteristic of immunosenescence is the filling of the immunological space with antigen experienced cells as a consequence of exposure to a variety of antigens. We proposed, even if in a phenomenological way, a possible scenario in which chronic stress can be described from a mathematical point of view. We show that the size of T-cell antigen experienced clones varies between individuals and that it can be strongly influenced by the chronic fluctuations without that any specific restimulation is considered. We believe that this result can at least provoke interest in such a topics and pave the way to new necessary studies. In this regard, one should hold in mind that, to date, one of the strongest limit of vaccination strategies is the incapability to maintain the immunological memory in the whole population, especially in old individuals [Cohen, 2005], which are characterized by a less diverse and more oligoclonal repertoire. We believe that these strategies should account for the effect over long timescale dynamics of chronic antigenic stress which is an important and inevitable issue of ageing.

Finally, there is enormous evidence that the improvement of life quality has strongly elongated the human lifespan. The IS of very old individuals presents a new scenario in the lymphocyte repertoire, in which a partial shrinkage is accompanied with a reshaping of the IS and sometimes even an improvement of some functions [Franceschi et al., 2000a, De Martinis et al., 2005]. It is known that ageing is strongly influenced by the IS activity. In this thesis we have shown how the IS features can be reliable factors for the description of demographic data and that these studies can be improved by the knowledge on the IS.

Closure

Although focused on general aspects of the kinetics of degradation, our work reinforces the message given by the predictions algorithm of epitopes presented by MHCs, which are based on the MHC-peptide processing pathway. We suggest that a more careful and quantitative analysis of the kinetics of antigen processing and presentation should be faced. We highlight the role of the gate of the proteasome in shaping the length distribution of peptides and in regulating the degradation rate of substrates. These studies have inspired

new experiments which are currently under investigation [1]. Preliminary data show how the degradation rate during in vitro degradation depends on the ratio proteasome vs substrate concentration. Moreover, these experiments have confirmed that the degradation rate fairly depends on the substrate length although sequence specificity is an important variable for the prediction of the cleavage sites. We have also evidenced that proteasomes equipped with regulatory particle, such as PA28, perform a fairly different kinetics with respect to the normal 20S proteasome. The influence of the kinetics of degradation, such as the gate opening effect (see Chapter 2) or the immunoproteasome replacement (see Chapter 4) have strong effects on the IS dynamics. Future works should investigate these phenomena in more immunological details. This thesis can be a reliable tool to fuse the kinetics of proteasome degradation with T-cell dynamics, and therefore be a good starting point for a more quantitative and detailed model which investigates the IR and the role that antigen processing kinetics has in this regard.

[1] Together with M. Mishto we performed in vitro experiment in the laboratory of Prof. Kloetzel, Department of Biochemistry, Charite, Berlin. A mathematical model which explains the data is under investigation.

Bibliography

A. N. Akbar, P. C. Beverley, and M. Salmon. Will telomere erosion lead to a loss of T-cell memory? *Nat. Rev. Immunol.*, 4:737–743, 2004.

T. N. Akopian, A. F. Kisselev, and A. L. Goldberg. Processive degradation of proteins and other catalytic properties of the proteasome from Thermoplasma acidophilum. *J. Biol. Chem.*, 272:1791–1798, 1997.

M. J. Allan, R. Callard, J. Stark, and A. Yates. Comparing antigen-independent mechanisms of T cell regulation. *J. theor. Biol.*, 228:81–95, 2004.

A. R. Almeida, B. Rocha, A. A. Freitas, and C. Tanchot. Homeostasis of T cell numbers: from thymus production to peripheral compartmentalization and the indexation of regulatory T cells. *Semin. Immunol.*, 17:239–249, 2005.

R. A. Arnaout and M. A. Nowak. Competitive coexistence in antiviral immunity. *J. theor. Biol.*, 204:431–441, 2000.

R. Arnold, M. Seifert, K. Asadullah, and H. D. Volk. Crosstalk between keratinocytes and T lymphocytes via Fas/Fas ligand interaction: modulation by cytokines. *J. Immunol.*, 162:7140–7147, 1999.

T. P. Arstila, A. Casrouge, V. Baron, J. Even, J. Kanellopoulos, and P. Kourilsky. A direct estimate of the human alphabeta T cell receptor diversity. *Science*, 286:958–961, 1999.

V. P. Badovinac, A. R. Tvinnereim, and J. T. Harty. Regulation of antigen-specific $CD8^+$ T cell homeostasis by perforin and interferon-gamma. *Science*, 290:1354–1358, 2000.

C. Bartholdy, J. P. Christensen, D. Wodarz, and A. R. Thomsen. Persistent virus infection despite chronic cytotoxic T-lymphocyte activation in γ interferon-deficient mice infected with lymphocytic choriomeningitis virus. *J. Virol.*, 74:10304–10311, 2000.

M. Basler, N. Youhnovski, M. Van Den Broek, M. Przybylski, and M. Groettrup. Immunoproteasomes down-regulate presentation of a subdominant T cell epitope from lymphocytic choriomeningitis virus. *J. Immunol.*, 173: 3925–3934, 2004.

C. Bernard. *Introduction a l'etude de la medicine experimentale.* J.-B. Bailliere, Paris, 1865.

S. P. Berzins, R. L. Boyd, and J. F. Miller. The role of the thymus and recent thymic migrants in the maintenance of the adult peripheral lymphocyte pool. *J. Exp. Med.*, 187:1839–1848, 1998.

M. J. Bevan. Cross-priming for a secondary cytotoxic response to minor H antigens with H-2 congenic cells which do not cross-react in the cytotoxic assay. *J. Exp. Med.*, 143:1283–1288, 1976.

J. N. Blattman, D. J. Sourdive, K. Murali-Krishna, R. Ahmed, and J. D. Altman. Evolution of the T cell repertoire during primary, memory, and recall responses to viral infection. *J. Immunol.*, 165:6081–6090, 2000.

M. Bogyo, S. Shin, J. S. McMaster, and H. L. Ploegh. Substrate binding and sequence preference of the proteasome revealed by active-site-directed affinity probes. *Chem. Biol.*, 5:307–320, 1998.

J. A. Borghans, L. S. Taams, M. H. Wauben, and R. J. De Boer. Competition for antigenic sites during T cell proliferation: a mathematical interpretation of in vitro data. *Proc. Natl. Acad. Sci. U.S.A.*, 96:10782–10787, 1999.

A. Brooks, G. J. Lithgow, and T. E. Johnson. Mortality rates in a genetically heterogeneous population of Caenorhabditis elegans. *Science*, 263:668–671, 1994.

S. Bulik, B. Peters, C. Ebeling, and H. Holzhutter. Cytosolic processing of proteasomal cleavage products can enhance the presentation efficiency of MHC-1 epitopes. *Genome. Inform. Ser. Workshop. Genome. Inform.*, 15: 24–34, 2004.

D. H. Busch and E. G. Pamer. T cell affinity maturation by selective expansion during infection. *J. Exp. Med.*, 189:701–710, 1999.

E. C. Butcher and L. J. Picker. Lymphocyte homing and homeostasis. *Science*, 272:60–66, 1996.

R. E. Callard, J. Stark, and A. J. Yates. Fratricide: a mechanism for T memory-cell homeostasis. *Trends Immunol.*, 24:370–375, 2003.

W. Cannon. *The Wisdom of the Body.* W.W. Norton and Company, New York, 1939.

C. Cardozo and C. Michaud. Proteasome-mediated degradation of tau proteins occurs independently of the chymotrypsin-like activity by a nonprocessive pathway. *Arch. Biochem. Biophys.*, 408:103–110, 2002.

C. Cardozo, A. Vinitsky, C. Michaud, and M. Orlowski. Evidence that the nature of amino acid residues in the P3 position directs substrates to distinct catalytic sites of the pituitary multicatalytic proteinase complex (proteasome). *Biochemistry*, 33:6483–6489, 1994.

C. Cardozo, C. Michaud, and M. Orlowski. Components of the bovine pituitary multicatalytic proteinase complex (proteasome) cleaving bonds after hydrophobic residues. *Biochemistry.*, 38:9768–9777, 1999.

J. R. Carey, P. Liedo, D. Orozco, and J. W. Vaupel. Slowing of mortality rates at older ages in large medfly cohorts. *Science*, 258:457–461, 1992.

P. Cascio, C. Hilton, A. F. Kisselev, K. L. Rock, and A. L. Goldberg. 26s proteasomes and immunoproteasomes produce mainly N-extended versions of an antigenic peptide. *EMBO. J.*, 20:2357–2366, 2001.

P. Cascio, M. Call, B. M. Petre, T. Walz, and A. L. Goldberg. Properties of the hybrid form of the 26S proteasome containing both 19S and PA28 complexes. *EMBO. J.*, 21:2636–2645, 2002.

V. Cerundolo, A. Kelly, T. Elliott, J. Trowsdale, and A. Townsend. Genes encoded in the major histocompatibility complex affecting the generation of peptides for TAP transport. *Eur. J. Immunol.*, 25:554–562, 1995.

D. L. Chao, M. P. Davenport, S. Forrest, and A. S. Perelson. A stochastic model of cytotoxic T cell responses. *J. theor. Biol.*, 228:227–240, 2004.

H. D. Chen, A. E. Fraire, I. Joris, M. A. Brehm, R. M. Welsh, and L. K. Selin. Memory $CD8^+$ T cells in heterologous antiviral immunity and immunopathology in the lung. *Nat. Immunol.*, 2:1067–1076, 2001a.

W. Chen, L. C. Anton, J. R. Bennink, and J. W. Yewdell. Dissecting the multifactorial causes of immunodominance in class I-restricted T cell responses to viruses. *Immunity*, 12:83–93, 2000.

W. Chen, C. C. Norbury, Y. Cho, J. W. Yewdell, and J. R. Bennink. Immunoproteasomes shape immunodominance hierarchies of antiviral $CD8(^+)$ T

cells at the levels of T cell repertoire and presentation of viral antigens. *J. Exp. Med.*, 193:1319–1326, 2001b.

J. Cohen. Influenza. Study questions the benefits of vaccinating the elderly. *Science*, 307:1026, 2005.

T. Crough, J. M. Burrows, C. Fazou, S. Walker, M. P. Davenport, and R. Khanna. Contemporaneous fluctuations in T cell responses to persistent herpes virus infections. *Eur. J. Immunol.*, 35:139–149, 2005.

J. G. Cyster. Signaling thresholds and interclonal competition in preimmune B-cell selection. *Immunol. Rev.*, 156:87–101, 1997.

R. De Boer and A. Perelson. Towards a general function describing T cell proliferation. *J. Theor. Biol.*, 175:567–576, 1995.

R. J. De Boer and A. S. Perelson. Competitive control of the self-renewing T cell repertoire. *Int. Immunol.*, 9:779–790, 1997.

R. J. De Boer and A. S. Perelson. T cell repertoires and competitive exclusion. *J. theor. Biol.*, 169:375–390, 1994.

R. J. De Boer, A. A. Freitas, and A. S. Perelson. Resource competition determines selection of B cell repertoires. *J. theor. Biol.*, 212:333–343, 2001a.

R. J. De Boer, M. Oprea, R. Antia, K. Murali-Krishna, R. Ahmed, and A. S. Perelson. Recruitment times, proliferation, and apoptosis rates during the CD8($^+$) T-cell response to lymphocytic choriomeningitis virus. *J. Virol.*, 75:10663–10669, 2001b.

R. J. De Boer, D. Homann, and A. S. Perelson. Different dynamics of $CD4^+$ and $CD8^+$ T cell responses during and after acute lymphocytic choriomeningitis virus infection. *J. Immunol.*, 171:3928–3935, 2003.

M. De Martinis, C. Franceschi, D. Monti, and L. Ginaldi. Inflamm-ageing and lifelong antigenic load as major determinants of ageing rate and longevity. *FEBS. Lett.*, 579:2035–2039, 2005.

G. N. DeMartino and C. A. Slaughter. The proteasome, a novel protease regulated by multiple mechanisms. *J. Biol. Chem.*, 274:22123–22126, 1999.

T. P. Dick, T. Ruppert, M. Groettrup, P. M. Kloetzel, L. Kuehn, U. H. Koszinowski, S. Stevanovic, H. Schild, and H. G. Rammensee. Coordinated dual cleavages induced by the proteasome regulator PA28 lead to dominant MHC ligands. *Cell*, 86:253–262, 1996.

H. Djaballah and A. J. Rivett. Peptidylglutamyl-peptide hydrolase activity of the multicatalytic proteinase complex: evidence for a new high-affinity site, analysis of cooperative kinetics, and the effect of manganese ions. *Biochemistry.*, 31:4133–4141, 1992.

I. Dolenc, E. Seemuller, and W. Baumeister. Decelerated degradation of short peptides by the 20S proteasome. *FEBS. Lett.*, 434:357–361, 1998.

I. T. Dorn, R. Eschrich, E. Seemuller, R. Guckenberger, and R. Tampe. High-resolution AFM-imaging and mechanistic analysis of the 20 S proteasome. *J. Mol. Biol.*, 288:1027–1036, 1999.

H. S. Dunn, D. J. Haney, S. A. Ghanekar, P. Stepick-Biek, D. B. Lewis, and H. T. Maecker. Dynamics of CD4 and CD8 T cell responses to cytomegalovirus in healthy human donors. *J. Infect. Dis.*, 186:15–22, 2002.

R. B. Effros and G. Pawelec. Replicative senescence of T cells: does the Hayflick Limit lead to immune exhaustion? *Immunol. Today*, 18:450–454, 1997.

A. M. Eleuteri, R. A. Kohanski, C. Cardozo, and M. Orlowski. Bovine spleen multicatalytic proteinase complex (proteasome). Replacement of X, Y, and Z subunits by LMP7, LMP2, and MECL1 and changes in properties and specificity. *J. Biol. Chem.*, 272:11824–11831, 1997.

N. P. Emmerich, A. K. Nussbaum, S. Stevanovic, M. Priemer, R. E. Toes, H. G. Rammensee, and H. Schild. The human 26 S and 20 S proteasomes generate overlapping but different sets of peptide fragments from a model protein substrate. *J. Biol. Chem.*, 275:21140–21148, 2000.

F. F. Fagnoni, R. Vescovini, M. Mazzola, G. Bologna, E. Nigro, G. Lavagetto, C. Franceschi, M. Passeri, and P. Sansoni. Expansion of cytotoxic $CD8^+$ CD28- T cells in healthy ageing people, including centenarians. *Immunology.*, 88:501–507, 1996.

F. F. Fagnoni, R. Vescovini, G. Passeri, G. Bologna, M. Pedrazzoni, G. Lavagetto, A. Casti, C. Franceschi, M. Passeri, and P. Sansoni. Shortage of circulating naive $CD8(^+)$ T cells provides new insights on immunodeficiency in aging. *Blood*, 95:2860–2868, 2000.

D. A. Ferrington, H. Sun, K. K. Murray, J. Costa, T. D. Williams, D. J. Bigelow, and T. C. Squier. Selective degradation of oxidized calmodulin by the 20 S proteasome. *J. Biol. Chem.*, 276:937–943, 2001.

A. Forster and C. P. Hill. Proteasome degradation: enter the substrate. *Trends Cell. Biol.*, 13:550–553, 2003.

C. Franceschi and M. Bonafe. Centenarians as a model for healthy aging. *Biochem. Soc. Trans.*, 31:457–461, 2003.

C. Franceschi, D. Monti, P. Sansoni, and A. Cossarizza. The immunology of exceptional individuals: the lesson of centenarians. *Immunol. Today*, 16: 12–16, 1995.

C. Franceschi, S. Valensin, F. Fagnoni, C. Barbi, and M. Bonafe. Biomarkers of immunosenescence within an evolutionary perspective: the challenge of heterogeneity and the role of antigenic load. *Exp. Gerontol.*, 34:911–921, 1999.

C. Franceschi, M. Bonafe, and S. Valensin. Human immunosenescence: the prevailing of innate immunity, the failing of clonotypic immunity, and the filling of immunological space. *Vaccine.*, 18:1717–1720, 2000a.

C. Franceschi, S. Valensin, M. Bonafe, G. Paolisso, A. I. Yashin, D. Monti, and G. De Benedictis. The network and the remodeling theories of aging: historical background and new perspectives. *Exp. Gerontol.*, 35:879–896, 2000b.

A. A. Freitas, M. M. Rosado, A. C. Viale, and A. Grandien. The role of cellular competition in B cell survival and selection of B cell repertoires. *Eur. J. Immunol.*, 25:1729–1738, 1995.

A. A. Freitas, F. Agenes, and G. C. Coutinho. Cellular competition modulates survival and selection of $CD8^+$ T cells. *Eur. J. Immunol.*, 26:2640–2649, 1996.

E. Gaudin, M. Rosado, F. Agenes, A. McLean, and A. A. Freitas. B-cell homeostasis, competition, resources, and positive selection by self-antigens. *Immunol. Rev.*, 197:102–115, 2004.

M. Gleimer and P. Parham. Stress management: MHC class I and class I-like molecules as reporters of cellular stress. *Immunity*, 19:469–477, 2003.

M. H. Glickman. Getting in and out of the proteasome. *Semin. Cell. Dev. Biol.*, 11:149–158, 2000.

R. Glynne, S. H. Powis, S. Beck, A. Kelly, L. A. Kerr, and J. Trowsdale. A proteasome-related gene between the two ABC transporter loci in the class II region of the human MHC. *Nature*, 353:357–360, 1991.

B. Gompertz. On the nature of the function expressive of the law of human mortality, and on the new mode of determining the values of life contingencies. *Philos. Trans. R. Soc. London*, 115:513, 1825.

M. Groettrup, A. Soza, M. Eggers, L. Kuehn, T. P. Dick, H. Schild, H. G. Rammensee, U. H. Koszinowski, and P. M. Kloetzel. A role for the proteasome regulator PA28alpha in antigen presentation. *Nature*, 381:166–168, 1996.

M. Groll and R. Huber. Substrate access and processing by the 20S proteasome core particle. *Int. J. Biochem. Cell. Biol.*, 35:606–616, 2003.

M. Groll, L. Ditzel, J. Lowe, D. Stock, M. Bochtler, H. D. Bartunik, and R. Huber. Structure of 20S proteasome from yeast at 2.4 A resolution. *Nature*, 386:463–471, 1997.

M. Groll, M. Bajorek, A. Kohler, L. Moroder, D. M. Rubin, R. Huber, M. H. Glickman, and D. Finley. A gated channel into the proteasome core particle. *Nat. Struct. Biol.*, 7:1062–1067, 2000.

Z. Grossman, B. Min, M. Meier-Schellersheim, and W. E. Paul. Concomitant regulation of T-cell activation and homeostasis. *Nat. Rev. Immunol.*, 4: 387–395, 2004.

K. P. Hadeler, C. Kuttler, and A. K. Nussbaum. Cleaving proteins for the immune system. *Math. Biosci.*, 188:63–79, 2004.

N. L. Harris, V. Watt, F. Ronchese, and G. Le Gros. Differential T cell function and fate in lymph node and nonlymphoid tissues. *J. Exp. Med.*, 195:317–326, 2002.

J. T. Harty and V. P. Badovinac. Influence of effector molecules on the CD8($^+$) T cell response to infection. *Curr. Opin. Immunol.*, 14:360–365, 2002.

B. F. Haynes, M. L. Markert, G. D. Sempowski, D. D. Patel, and L. P. Hale. The role of the thymus in immune reconstitution in aging, bone marrow transplantation, and HIV-1 infection. *Annu. Rev. Immunol.*, 18:529–560, 2000.

W. Heinemeyer, M. Fischer, T. Krimmer, U. Stachon, and D. H. Wolf. The active sites of the eukaryotic 20 S proteasome and their involvement in subunit precursor processing. *J. Biol. Chem.*, 272:25200–25209, 1997.

S. Heink, D. Ludwig, P. M. Kloetzel, and E. Kruger. IFN-gamma-induced immune adaptation of the proteasome system is an accelerated and transient response. *Proc. Natl. Acad. Sci. U.S.A.*, 0:0, 2005.

R. J. Hodes. Telomere length, aging, and somatic cell turnover. *J. Exp. Med.*, 190:153–156, 1999.

L. Hoffman and M. Rechsteiner. Nucleotidase activities of the 26 S proteasome and its regulatory complex. *J. Biol. Chem.*, 271:32538–32545, 1996.

P. D. Holler and D. M. Kranz. T cell receptors: affinities, cross-reactivities, and a conformer model. *Mol. Immunol.*, 40:1027–1031, 2004.

H. G. Holzhutter and P. M. Kloetzel. A kinetic model of vertebrate 20S proteasome accounting for the generation of major proteolytic fragments from oligomeric peptide substrates. *Biophys. J.*, 79:1196–1205, 2000.

G. L. Hortin and J. Murthy. Substrate size selectivity of 20S proteasomes: analysis with variable-sized synthetic substrates. *J. Protein. Chem.*, 21: 333–337, 2002.

H. A. Huffman, M. Sadeghi, E. Seemuller, W. Baumeister, and M. F. Dunn. Proteasome-cytochrome c interactions: a model system for investigation of proteasome host-guest interactions. *Biochemistry.*, 42:8679–8686, 2003.

S. Hutschenreiter, A. Tinazli, K. Model, and R. Tampe. Two-substrate association with the 20S proteasome at single-molecule level. *EMBO. J.*, 23: 2488–2497, 2004.

S. C. Jameson. Maintaining the norm: T-cell homeostasis. *Nat. Rev. Immunol.*, 2:547–556, 2002.

S. C. Jameson. T cell homeostasis: Keeping useful T cells alive and live T cells useful. *Semin. Immunol.*, 17:231–237, 2005.

C. A. Janeway, P. Travers, M. Walport, and M. Shlomchik. *Immunobiology. The Immune System in Health and Disease.* Garland Publications, New York, London, 5 edition, 2001.

S. M. Kaech and R. Ahmed. Memory $CD8^+$ T cell differentiation: initial antigen encounter triggers a developmental program in naive cells. *Nat. Immunol.*, 2:415–422, 2001.

R. M. Kedl, J. W. Kappler, and P. Marrack. Epitope dominance, competition and T cell affinity maturation. *Curr. Opin. Immunol.*, 15:120–127, 2003.

A. Kelly, S. H. Powis, R. Glynne, E. Radley, S. Beck, and J. Trowsdale. Second proteasome-related gene in the human MHC class II region. *Nature*, 353:667–668, 1991.

C. Kesmir, A. K. Nussbaum, H. Schild, V. Detours, and S. Brunak. Prediction of proteasome cleavage motifs by neural networks. *Protein. Eng.*, 15: 287–296, 2002.

C. Kesmir, V. Van Noort, R. J. De Boer, and P. Hogeweg. Bioinformatic analysis of functional differences between the immunoproteasome and the constitutive proteasome. *Immunogenetics.*, 55:437–449, 2003.

S. Khan, M. Van den Broek, K. Schwarz, R. De Giuli, P. A. Diener, and M. Groettrup. Immunoproteasomes largely replace constitutive proteasomes during an antiviral and antibacterial immune response in the liver. *J. Immunol.*, 167:6859–6868, 2001.

C. King, A. Ilic, K. Koelsch, and N. Sarvetnick. Homeostatic expansion of T cells during immune insufficiency generates autoimmunity. *Cell*, 117: 265–277, 2004.

A. F. Kisselev, T. N. Akopian, and A. L. Goldberg. Range of sizes of peptide products generated during degradation of different proteins by archaeal proteasomes. *J. Biol. Chem.*, 273:1982–1989, 1998.

A. F. Kisselev, T. N. Akopian, K. M. Woo, and A. L. Goldberg. The sizes of peptides generated from protein by mammalian 26 and 20 S proteasomes. Implications for understanding the degradative mechanism and antigen presentation. *J. Biol. Chem.*, 274:3363–3371, 1999.

A. F. Kisselev, Z. Songyang, and A. L. Goldberg. Why does threonine, and not serine, function as the active site nucleophile in proteasomes? *J. Biol. Chem.*, 275:14831–14837, 2000.

A. F. Kisselev, D. Kaganovich, and A. L. Goldberg. Binding of hydrophobic peptides to several non-catalytic sites promotes peptide hydrolysis by all active sites of 20 S proteasomes. Evidence for peptide-induced channel opening in the alpha-rings. *J. Biol. Chem.*, 277:22260–22270, 2002.

P. M. Kloetzel. The proteasome and MHC class I antigen processing. *Biochim. Biophys. Acta*, 1695:225–233, 2004a.

P. M. Kloetzel. Generation of major histocompatibility complex class I antigens: functional interplay between proteasomes and TPPII. *Nat. Immunol.*, 5:661–669, 2004b.

A. Kohler, P. Cascio, D. S. Leggett, K. M. Woo, A. L. Goldberg, and D. Finley. The axial channel of the proteasome core particle is gated by the Rpt2 ATPase and controls both substrate entry and product release. *Mol. Cell.*, 7:1143–1152, 2001.

P. H. Krammer. CD95's deadly mission in the immune system. *Nature*, 407: 789–795, 2000.

C. C. Ku, M. Murakami, A. Sakamoto, J. Kappler, and P. Marrack. Control of homeostasis of $CD8^+$ memory T cells by opposing cytokines. *Science*, 288:675–678, 2000.

C. C. Ku, J. Kappler, and P. Marrack. The growth of the very large $CD8^+$ T cell clones in older mice is controlled by cytokines. *J. Immunol.*, 166: 2186–2193, 2001.

U. Kuckelkorn, T. Ruppert, B. Strehl, P. R. Jungblut, U. Zimny-Arndt, S. Lamer, I. Prinz, I. Drung, P. M. Kloetzel, S. H. Kaufmann, and U. Steinhoff. Link between organ-specific antigen processing by 20S proteasomes and $CD8(^+)$ T cell-mediated autoimmunity. *J. Exp. Med.*, 195:983–990, 2002.

C. Kuttler, A. K. Nussbaum, T. P. Dick, H. G. Rammensee, H. Schild, and K. P. Hadeler. An Algorithm for the Prediction of Proteasomal Cleavages. *J. Mol. Biol.*, 298:417–429, 2000.

A. Lanzavecchia and F. Sallusto. Dynamics of T lymphocyte responses: intermediates, effectors, and memory cells. *Science*, 290:92–97, 2000.

C. Lee, S. Prakash, and A. Matouschek. Concurrent translocation of multiple polypeptide chains through the proteasomal degradation channel. *J. Biol. Chem.*, 277:34760–34765, 2002.

C. W. Liu, M. J. Corboy, G. N. DeMartino, and P. J. Thomas. Endoproteolytic activity of the proteasome. *Science*, 299:408–411, 2003.

J. Lowe, D. Stock, B. Jap, P. Zwickl, W. Baumeister, and R. Huber. Crystal structure of the 20S proteasome from the archaeon T. acidophilum at 3.4 A resolution. *Science*, 268:533–539, 1995.

F. Luciani. The role of the immunoproteasome during the clonal expansion of cytotoxic t cell clones. *Poster presentation at 6th Workshop on Proteasomes.*, Clermont Ferrand (France), April., 2005.

F. Luciani. Stochastic processes in immunology: T cell dynamics and immunosenescence. *Contributed talk in "Stochastic processes in Immunology", First International MTBio Workshop on Function and Regulation of Cellular Systems: Experiments and Models.*, Dresden, January, 2001.

F. Luciani. A mathematical model for proteasome degradation: channel configuration regulates the fragment length distribution. *Invited Talk: Conference on Computational and Mathematical Population Dynamics.*, Trento (Italy), June, 2004a.

F. Luciani. Kinetics of proteasome degradation: Immunoproteasome as an open channel proteasome. *Invited Talk: Workshop: Proteasomes: Theory, Experiment and Immunological aspects.*, Tuebingen (Germany), July., 2003.

F. Luciani. T cell clonal expansion: Homeostasis and chronic stress. *Contributed talk in BIOCOMP 2002.*, Vietri sul Mare (Italy), June., 2002a.

F. Luciani. A mathematical model for proteasome degradation: channel configuration regulates the fragment length distribution. *Invited Talk: Joint meeting between the Department of Biochemistry and the Theoretical Immunology Group of the Humboldt University Berlin Germany.*, March 2004, 2004b.

F. Luciani. A mathematical model for proteasome degradation. *Poster presentation at 5th ESMTB Conference: Mathematical Modeling and Computing in Biology and Medicine;*, Milano (Italy), July, 2002b.

F. Luciani. A mathematical model for proteasome degradation: channel configuration regulates the fragment length distribution. *Invited Talk: Neuntes Herbstseminar "Strukturbildung in Chemie und Biophysik".*, Salzwedel, Germany. 3-5 October, 2004c.

F. Luciani. *Modelli fisico-matematici per la memoria immunologica e l'immunosenescenza*. Master thesis,Univ. Bologna, 2000.

F. Luciani and M. Or-Guil. The clonal expansion of cytotoxic t cell clones: a possible immunological role for the immunoproteasome. *In preparation*, 2005.

F. Luciani, G. Turchetti, C. Franceschi, and S. Valensin. A mathematical model for the immunosenescence. *Riv. Biol.*, 94:305–318, 2001a.

F. Luciani, S. Valensin, R. Vescovini, P. Sansoni, F. Fagnoni, C. Franceschi, M. Bonafe, and G. Turchetti. A stochastic model for CD8(+)T cell dynamics in human immunosenescence: implications for survival and longevity. *J. theor. Biol.*, 213:587–597, 2001b.

F. Luciani, S. Valensin, M. Bonafe, G. Turchetti, and C. Franceschi. A stochastic model for the clonal expansion of cytotoxic t lymphocytes. *Scientia Mathematicae Japonicae SCMJ*, 2:439–453, 2003.

F. Luciani, C. Kesmir, M. Mishto, M. Or-Guil, and R. J. De Boer. A mathematical model of protein degradation by the proteasome. *Biophys. J.*, 88: 2422–2432, 2005.

M.Abramowitz and I. Stegun, editors. *Handbook of Mathematical Functions*. Dover, New York, 1972.

R. Macarthur and R. Levins. Competition habitat selection and character displacement in a patchy environment. *Proc. Natl. Acad. Sci. U.S.A.*, 51: 1207–1210, 1964.

L. Mariani. *Modelli matematici per l'immunosenescenza*. Master thesis,Univ. Bologna, 2001.

L. Mariani, G. Turchetti, and C. Franceschi. Chronic antigenic stress, immunosenescence and human survivorship over the 3 last centuries: heuristic value of a mathematical model. *Mech. Ageing Dev.*, 124:453–458, 2003.

D. R. Marshall, S. J. Turner, G. T. Belz, S. Wingo, S. Andreansky, M. Y. Sangster, J. M. Riberdy, T. Liu, M. Tan, and P. C. Doherty. Measuring the diaspora for virus-specific $CD8^+$ T cells. *Proc. Natl. Acad. Sci. U.S.A.*, 98:6313–6318, 2001.

C. K. Martinez and J. J. Monaco. Homology of proteasome subunits to a major histocompatibility complex-linked LMP gene. *Nature*, 353:664–667, 1991.

A. R. McLean, M. M. Rosado, F. Agenes, R. Vasconcellos, and A. A. Freitas. Resource competition as a mechanism for B cell homeostasis. *Proc. Natl. Acad. Sci. U.S.A.*, 94:5792–5797, 1997.

L. Michaelis. Untersuchungen uber eiweissprazipitine. *Dtsch. Med. Wschr.*, 28:733, 1902.

L. Michaelis. Weitere untersuchungen uber eiweis-sprazipitine. *Dtsch. Med. Wschr.*, 30:1240, 1904.

J. F. Miller. Effect of thymectomy in adult mice on immunological responsiveness. *Nature*, 208:1337–1338, 1965.

R. A. Miller. The aging immune system: primer and prospectus. *Science*, 273:70–74, 1996.

N. A. Mitchison. Specialization, tolerance, memory, competition, latency, and strife among T cells. *Annu. Rev. Immunol.*, 10:1–12, 1992.

S. Morel, F. Levy, O. Burlet-Schiltz, F. Brasseur, M. Probst-Kepper, A. L. Peitrequin, B. Monsarrat, R. Van Velthoven, J. C. Cerottini, T. Boon, J. E. Gairin, and B. J. Van den Eynde. Processing of some antigens by the standard proteasome but not by the immunoproteasome results in poor presentation by dendritic cells. *Immunity*, 12:107–117, 2000.

K. Murali-Krishna, J. D. Altman, M. Suresh, D. J. Sourdive, A. J. Zajac, J. D. Miller, J. Slansky, and R. Ahmed. Counting antigen-specific CD8 T cells: a reevaluation of bystander activation during viral infection. *Immunity*, 8:177–187, 1998.

K. Murali-Krishna, L. L. Lau, S. Sambhara, F. Lemonnier, J. Altman, and R. Ahmed. Persistence of memory CD8 T cells in MHC class I-deficient mice. *Science*, 286:1377–1381, 1999.

Y. N. Naumov, E. N. Naumova, K. T. Hogan, L. K. Selin, and J. Gorski. A fractal clonotype distribution in the $CD8^+$ memory T cell repertoire could optimize potential for immune responses. *J. Immunol.*, 170:3994–4001, 2003.

J. Nikolich-Zugich. T cell aging: naive but not young. *J. Exp. Med.*, 201: 837–840, 2005.

C. C. Norbury and L. J. Sigal. Cross priming or direct priming: is that really the question? *Curr. Opin. Immunol.*, 15:82–88, 2003.

M. A. Nowak, R. M. May, R. E. Phillips, S. Rowland-Jones, D. G. Lalloo, S. McAdam, P. Klenerman, B. Koppe, K. Sigmund, C. R. Bangham, et al. Antigenic oscillations and shifting immunodominance in HIV-1 infections. *Nature*, 375:606–611, 1995a.

M. A. Nowak, R. M. May, and K. Sigmund. Immune responses against multiple epitopes. *J. theor. Biol.*, 175:325–353, 1995b.

A. K. Nussbaum, T. P. Dick, W. Keilholz, M. Schirle, S. Stevanovic, K. Dietz, W. Heinemeyer, M. Groll, D. H. Wolf, R. Huber, H. G. Rammensee, and H. Schild. Cleavage motifs of the yeast 20S proteasome β subunits deduced from digests of enolase 1. *Proc. Natl. Acad. Sci. U.S.A.*, 95:12504–12509, 1998.

M. Orlowski, C. Cardozo, M. C. Hidalgo, and C. Michaud. Regulation of the peptidylglutamyl-peptide hydrolyzing activity of the pituitary multicatalytic proteinase complex. *Biochemistry.*, 30:5999–6005, 1991.

P. A. Osmulski and M. Gaczynska. Nanoenzymology of the 20S proteasome: proteasomal actions are controlled by the allosteric transition. *Biochemistry.*, 41:7047–7053, 2002.

E. G. Pamer. Antigen presentation in the immune response to infectious diseases. *Clin. Infect. Dis.*, 28:714–716, 1999.

G. Pawelec, A. Akbar, C. Caruso, R. Effros, B. Grubeck-Loebenstein, and A. Wikby. Is immunosenescence infectious? *Trends Immunol.*, 25:406–410, 2004.

B. Peters, K. Janek, U. Kuckelkorn, and H. G. Holzhutter. Assessment of proteasomal cleavage probabilities from kinetic analysis of time-dependent product formation. *J. Mol. Biol.*, 318:847–862, 2002.

L. L. Pewe, J. M. Netland, S. B. Heard, and S. Perlman. Very diverse CD8 T cell clonotypic responses after virus infections. *J. Immunol.*, 172:3151–3156, 2004.

L. Piantanelli, G. Rossolini, A. Basso, A. Piantanelli, M. Malavolta, and A. Zaia. Use of mathematical models of survivorship in the study of biomarkers of aging: the role of heterogeneity. *Mech. Ageing Dev.*, 122: 1461–1475, 2001.

C. M. Pickart and A. P. VanDemark. Opening doors into the proteasome. *Nat. Struct. Biol.*, 7:999–1001, 2000.

M. J. Pinkoski, N. M. Droin, T. Lin, L. Genestier, T. A. Ferguson, and D. R. Green. Nonlymphoid Fas ligand in peptide-induced peripheral lymphocyte deletion. *Proc. Natl. Acad. Sci. U.S.A.*, 99:16174–16179, 2002.

C. Realini, C. C. Jensen, Z. Zhang, S. C. Johnston, J. R. Knowlton, C. P. Hill, and M. Rechsteiner. Characterization of recombinant REGalpha, REGbeta, and REGgamma proteasome activators. *J. Biol. Chem.*, 272: 25483–25492, 1997.

M. Rechsteiner, C. Realini, and V. Ustrell. The proteasome activator 11 S REG (PA28) and class I antigen presentation. *Biochem. J.*, 345:1–15, 2000.

J. Reidlinger, A. M. Pike, P. J. Savory, R. Z. Murray, and A. J. Rivett. Catalytic properties of 26 S and 20 S proteasomes and radiolabeling of MB1, LMP7, and C7 subunits associated with trypsin-like and chymotrypsin-like activities. *J. Biol. Chem.*, 272:24899–24905, 1997.

E. Reits, A. Griekspoor, J. Neijssen, T. Groothuis, K. Jalink, P. Van Veelen, H. Janssen, J. Calafat, J. W. Drijfhout, and J. Neefjes. Peptide diffusion, protection, and degradation in nuclear and cytoplasmic compartments before antigen presentation by MHC class I. *Immunity*, 18:97–108, 2003.

E. Reits, J. Neijssen, C. Herberts, W. Benckhuijsen, L. Janssen, J. W. Drijfhout, and J. Neefjes. A Major Role for TPPII in Trimming Proteasomal Degradation Products for MHC Class I Antigen Presentation. *Immunity*, 20:495–506, 2004.

H. Risken. *The Fokker-Planck equation.* Springer Verlag, Berlin, 1989.

B. Rocha and H. Von Boehmer. Peripheral selection of the T cell repertoire. *Science*, 251:1225–1228, 1991.

K. L. Rock, I. A. York, and A. L. Goldberg. Post-proteasomal antigen processing for major histocompatibility complex class I presentation. *Nat. Immunol.*, 5:670–677, 2004.

T. Saric, C. I. Graef, and A. L. Goldberg. Pathway for degradation of peptides generated by proteasomes: A key role for thimet oligopeptidase and other metallopeptidases. *J. Biol. Chem.*, 0:0, 2004.

P. A. Savage, J. J. Boniface, and M. M. Davis. A kinetic basis for T cell receptor repertoire selection during an immune response. *Immunity*, 10: 485–492, 1999.

A. Scherer and S. Bonhoeffer. Epitope down-modulation as a mechanism for the coexistence of competing T-cells. *J. theor. Biol.*, 233:379–390, 2005.

G. Schmidtke, S. Emch, M. Groettrup, and H. G. Holzhutter. Evidence for the existence of a non-catalytic modifier site of peptide hydrolysis by the 20 S proteasome. *J. Biol. Chem.*, 275:22056–22063, 2000.

E. Seemuller, A. Lupas, D. Stock, J. Lowe, R. Huber, and W. Baumeister. Proteasome from Thermoplasma acidophilum: a threonine protease. *Science*, 268:579–582, 1995.

L. K. Selin, M. Y. Lin, K. A. Kraemer, D. M. Pardoll, J. P. Schneck, S. M. Varga, P. A. Santolucito, A. K. Pinto, and R. M. Welsh. Attrition of T cell memory: selective loss of LCMV epitope-specific memory CD8 T cells following infections with heterologous viruses. *Immunity*, 11:733–742, 1999.

Y. Shinkai, G. Rathbun, K. P. Lam, E. M. Oltz, V. Stewart, M. Mendelsohn, J. Charron, M. Datta, F. Young, A. M. Stall, et al. RAG-2-deficient mice lack mature lymphocytes owing to inability to initiate V(D)J rearrangement. *Cell*, 68:855–867, 1992.

A. J. Sijts, T. Ruppert, B. Rehermann, M. Schmidt, U. Koszinowski, and P. M. Kloetzel. Efficient generation of a hepatitis B virus cytotoxic T lymphocyte epitope requires the structural features of immunoproteasomes. *J. Exp. Med.*, 191:503–514, 2000.

M. Skoberne and G. Geginat. Efficient in vivo presentation of Listeria monocytogenes- derived CD4 and CD8 T cell epitopes in the absence of IFN-gamma. *J. Immunol.*, 168:1854–1860, 2002.

M. K. Slifka and J. L. Whitton. Functional avidity maturation of CD8($^+$) T cells without selection of higher affinity TCR. *Nat. Immunol.*, 2:711–717, 2001.

R. L. Stein, F. Melandri, and L. Dick. Kinetic characterization of the chymotryptic activity of the 20S proteasome. *Biochemistry.*, 35:3899–3908, 1996.

R. Stohwasser, U. Salzmann, J. Giesebrecht, P. M. Kloetzel, and H. G. Holzhutter. Kinetic evidences for facilitation of peptide channelling by the proteasome activator PA28. *Eur. J. Biochem.*, 267:6221–6230, 2000.

M. W. Su, S. Pyarajan, J. H. Chang, C. L. Yu, Y. J. Jin, Y. D. Stierhof, P. Walden, and S. J. Burakoff. Fratricide of CD8$^+$ cytotoxic T lymphocytes is dependent on cellular activation and perforin-mediated killing. *Eur. J. Immunol.*, 34:2459–2470, 2004.

C. D. Surh and J. Sprent. Regulation of naive and memory T-cell homeostasis. *Microbes. Infect.*, 4:51–56, 2002.

C. Tanchot and B. Rocha. The peripheral T cell repertoire: independent homeostatic regulation of virgin and activated $CD8^+$ T cell pools. *Eur. J. Immunol.*, 25:2127–2136, 1995.

C. Tanchot, F. A. Lemonnier, B. Perarnau, A. A. Freitas, and B. Rocha. Differential requirements for survival and proliferation of CD8 naive or memory T cells. *Science*, 276:2057–2062, 1997.

S. Tenzer, L. Stoltze, B. Schonfisch, J. Dengjel, M. Muller, S. Stevanovic, H. G. Rammensee, and H. Schild. Quantitative analysis of prion-protein degradation by constitutive and immuno-20S proteasomes indicates differences correlated with disease susceptibility. *J. Immunol.*, 172:1083–1091, 2004.

S. Tenzer, B. Peters, S. Bulik, O. Schoor, C. Lemmel, M. M. Schatz, P. M. Kloetzel, H. G. Rammensee, H. Schild, and H. G. Holzhutter. Modeling the MHC class I pathway by combining predictions of proteasomal cleavage,TAP transport and MHC class I binding. *Cell. Mol. Life. Sci.*, 62: 1025–1037, 2005.

D. Tilman. *Resource Competition and Community Structure*. Princeton University Press, Princeton, 1982.

R. E. Toes, A. K. Nussbaum, S. Degermann, M. Schirle, N. P. Emmerich, M. Kraft, C. Laplace, A. Zwinderman, T. P. Dick, J. Muller, B. Schonfisch, C. Schmid, H. J. Fehling, S. Stevanovic, H. G. Rammensee, and H. Schild. Discrete cleavage motifs of constitutive and immunoproteasomes revealed by quantitative analysis of cleavage products. *J. Exp. Med.*, 194:1–12, 2001.

D. F. Tough, P. Borrow, and J. Sprent. Induction of bystander T cell proliferation by viruses and type I interferon in vivo. *Science*, 272:1947–1950, 1996.

D. F. Tough, S. Sun, X. Zhang, and J. Sprent. Stimulation of memory T cells by cytokines. *Vaccine.*, 18:1642–1648, 2000.

G. Turchetti, L. Mariani, and F. Luciani. A stochastic model of immune system aging. In N. Stramaglia, editor, *Proceeding of the workshop Modeling Biomedical signals*, pages 80–89, New Jersey, 2002. World Scientific.

G. Turchetti, F. Luciani, and L. Mariani. Environmental randomness and survival probability. In P. L. V. C. e. The MIRIAM Project Series, editor,

Mathematical Modeling in Biology and medicine, 5th ESMTB Conference., pages 403–409, Bologna, Italy, 2003. ESCULAPIO Pub. Co.

T. Van Hall, A. Sijts, M. Camps, R. Offringa, C. Melief, P. M. Kloetzel, and F. Ossendorp. Differential influence on cytotoxic T lymphocyte epitope presentation by controlled expression of either proteasome immunosubunits or PA28. *J. Exp. Med.*, 192:483–494, 2000.

J. W. Vaupel and B. Jeune. *Exceptional longevity: From Prehistory to the Present*. Odense University Press, 1996.

H. Veiga-Fernandes, U. Walter, C. Bourgeois, A. McLean, and B. Rocha. Response of naive and memory $CD8^+$ T cells to antigen stimulation in vivo. *Nat. Immunol.*, 1:47–53, 2000.

R. Wang, B. T. Chait, I. Wolf, R. A. Kohanski, and C. Cardozo. Lysozyme degradation by the bovine multicatalytic proteinase complex (proteasome): evidence for a nonprocessive mode of degradation. *Biochemistry.*, 38: 14573–14581, 1999.

J. S. Weitz and H. B. Fraser. Explaining mortality rate plateaus. *Proc. Natl. Acad. Sci. U.S.A.*, 98:15383–15386, 2001.

T. Wenzel, C. Eckerskorn, F. Lottspeich, and W. Baumeister. Existence of a molecular ruler in proteasomes suggested by analysis of degradation products. *FEBS. Lett.*, 349:205–209, 1994.

E. J. Wherry, V. Teichgraber, T. C. Becker, D. Masopust, S. M. Kaech, R. Antia, U. H. Von Andrian, and R. Ahmed. Lineage relationship and protective immunity of memory CD8 T cell subsets. *Nat. Immunol.*, 4: 225–234, 2003.

F. G. Whitby, E. I. Masters, L. Kramer, J. R. Knowlton, Y. Yao, C. C. Wang, and C. P. Hill. Structural basis for the activation of 20S proteasomes by 11S regulators. *Nature*, 408:115–120, 2000.

G. Wick, P. Jansen-Durr, P. Berger, I. Blasko, and B. Grubeck-Loebenstein. Diseases of aging. *Vaccine.*, 18:1567–1583, 2000.

D. Wodarz and A. R. Thomsen. Does programmed CTL proliferation optimize virus control? *Trends Immunol.*, 26:305–310, 2005.

E. Z. Wolpert, P. Grufman, J. K. Sandberg, A. Tegnesjo, and K. Karre. Immunodominance in the CTL response against minor histocompatibility antigens: interference between responding T cells, rather than with presentation of epitopes. *J. Immunol.*, 161:4499–4505, 1998.

A. Yashin, I. Iachine, and A. Begun. Mortality rate modeling : a review. *Math. Pop. Biol.*, 8:305–332, 2000.

A. Yates and R. Callard. Cell death and the maintenance of immunological memory. *Discr. Cont. Dynam Sys. B*, 1:43, 2001.

J. W. Yewdell. Not such a dismal science: the economics of protein synthesis, folding, degradation and antigen processing. *Trends Cell. Biol.*, 11:294–297, 2001.

J. W. Yewdell and J. R. Bennink. Immunodominance in major histocompatibility complex class I-restricted T lymphocyte responses. *Annu. Rev. Immunol.*, 17:51–88, 1999.

J. W. Yewdell and M. Del Val. Immunodominance in TCD8$^+$ responses to viruses: cell biology, cellular immunology, and mathematical models. *Immunity*, 21:149–153, 2004.

J. W. Yewdell, E. Reits, and J. Neefjes. Making sense of mass destruction: quantitating MHC class I antigen presentation. *Nat. Rev. Immunol.*, 3: 952–961, 2003.

M. Zhang, A. I. MacDonald, M. A. Hoyt, and P. Coffino. Proteasomes begin ornithine decarboxylase digestion at the carboxy terminus. *J. Biol. Chem.*, 0:0, 2004.

W. Zhong and E. L. Reinherz. In vivo selection of a TCR Vbeta repertoire directed against an immunodominant influenza virus CTL epitope. *Int. Immunol.*, 16:1549–1559, 2004.

Part V

Appendices

Appendix A

Proteasome

A.1 Simplified model of proteasome degradation

To simplify the mathematical model given in Chapter 2, let N be the concentration of substrate outside and n the concentration of substrate inside the CP. The length of the substrate is L. Define p as the total product concentration present at time t in the CP. For simplicity, assume that the length of these products is always smaller than θ, so the efflux of products can be assumed to not depend strongly on the product lengths. The equations for the substrate dynamics are

$$\begin{aligned} \frac{dN}{dt} &= -\hat{a}(1-(p+n)vL)N + \epsilon n \\ \frac{dn}{dt} &= \hat{a}(1-(p+n)vL)N - cn - \epsilon n \\ \frac{dp}{dt} &= cn - \bar{e}p \end{aligned} \tag{A.1}$$

where $\hat{a}$ is the influx rate of the substrate, c is the cleavage rate, v is the scaling factor for the volume of the proteasome (see Table 4.1). Let ϵ be the slow exit rate of the substrate. Long substrates hardly exit the proteasome without being cleaved, i.e. $\epsilon = 0$, however, for short substrates ϵ can be larger than zero. This simplified model resembles the full model given that the average efflux rate of the fragments is $\bar{e}$ (see Section 2.3). Assuming that the substrate and the products inside the CP are in the quasi steady state (i.e., $dn/dt = dp/dt = 0$), one obtains

$$n_q = \frac{\bar{e}\hat{a}N}{\hat{a}vL(c+\bar{e})N + \bar{e}(c+\epsilon)}\ , \qquad p_q = \frac{c\hat{a}N}{\hat{a}vL(c+\bar{e})N + \bar{e}(c+\epsilon)},$$

where n_q and p_q are the quasi steady state concentrations of the substrate and the products, respectively. This leads to:

$$\frac{dN}{dt} = -\frac{c\hat{a}\bar{e}N}{\hat{a}vL(c+\bar{e})N + \bar{e}(c+\epsilon)} \tag{A.2}$$

which is a Michaelis-Menten function with a maximum degradation rate $V_{max} = \frac{\bar{e}c}{vL(c+\bar{e})}$ when $N \to \infty$, and approaches to $\hat{a}\frac{c}{c+\epsilon}$ if $N << K_m$. If the exit rate of substrate is equal to the cleavage rate, the degradation is reduced by 50%. The Michaelis-Menten constant, i.e., the substrate concentration at which dN/dt is half of the maximum, is $K_m = \frac{\bar{e}(c+\epsilon)}{\hat{a}vL(c+\bar{e})}$. For long substrates, $\epsilon \to 0$ holds and we obtain $K_m \simeq V_{max}/\hat{a}$ and the linear dependence $dN/dt \simeq \hat{a}N$ for low substrate concentrations.

Appendix B

T-cell dynamics

B.1 Reaction scheme for the T-cell-MHCp kinetics

In Chapter 4 the equations for the T cell dynamics are derived from the following reaction scheme

$$N_i + F_j \quad \underset{k^d}{\overset{k^a}{\rightleftharpoons}} \; {C^N}_{ij} \overset{{k_p}^N}{\rightarrow} {T^*}_i + F_j \tag{B.1}$$

$$E_i + F_j \quad \underset{k^d}{\overset{k^a}{\rightleftharpoons}} \; {C^E}_{ij} \overset{{k_p}^E}{\rightarrow} 2E_i + F_j \tag{B.2}$$

$$T^* \quad \overset{k^*}{\rightarrow} 2\phi N_i + 2(1-\phi)E_i \tag{B.3}$$

i, j are indexes for the T cell and for the MHCp specificity. F_j is the amount of free sites j, ${C^N}_{i,j}$ and ${C^E}_{i,j}$ are the complexes formed between T-cell and MHC-peptide complex for the N and E pool respectively. The kinetics of complex formation are described by the reaction kinetics with association and dissociation constant ${k^a}_{i,j}$ and ${k^d}_{i,j}$ respectively. For simplicity we consider the same complex formation kinetics for both the Naive and Effector pool. Effector cells proliferate with the rate ${k_p}^E > {k_p}^N$.

Following De Boer and Perelson [1997, 1994] we can obtain the equations for $\frac{dN_i}{dt}$ and $\frac{dE_i}{dt}$ with a Quasi Steady State (QSS) approximation applied to the kinetics of the complex formation, namely $\frac{d{C^N}_{i,j}}{dt} = \frac{d{C^E}_{i,j}}{dt} = 0$.

$$\frac{{C^N}_{ij}}{dt} = -{k_p}^N\,{C^N}_{ij} + {k^a}_{i,j}F_j\,N_i - {k^d}_{i,j}{C^N}_{ij} \quad \text{(B.4)}$$

$$\frac{{C^E}_{ij}}{dt} = -{k_p}^E\,{C^E}_{ij} + {k^a}_{i,j}F_j\,E_i - {k^d}_{i,j}{C^E}_{ij} \quad \text{(B.5)}$$

With the QSS assumption we get

$${C^N}_{ij} = \frac{{k^a}_{i,j}}{{k_p}^N + {k^d}_{i,j}}\,F_j\,N_i \quad \text{(B.6)}$$

$${C^E}_{ij} = \frac{{k^a}_{i,j}}{{k_p}^E + {k^d}_{i,j}}\,F_j\,E_i \quad \text{(B.7)}$$

we can then define the reaction constant ${K^N}_{i,j}$ and ${K^E}_{i,j}$

$${K^N}_{i,j} = \frac{{k^a}_{i,j}}{{k_p}^N + {k^d}_{i,j}} \qquad {K^E}_{i,j} = \frac{{k^a}_{i,j}}{{k_p}^E + {k^d}_{i,j}} \quad \text{(B.8)}$$

In the next step, we assume that the kinetics of the activated cells ${T^*}_i$ is faster than the other reactions. Therefore, we can consider the activation - differentiation process in only one reaction

$$N_i + F_j \rightleftharpoons {C^N}_{i,j} \rightarrow 2\phi N_i + 2(1-\phi)E_i + F_j \quad \text{(B.9)}$$

We can now write

$$\frac{dN_i}{dt} = 2\phi\,{k_p}^N \sum_{j=1}^{N_{pep}} {C^N}_{ij} + \sum_{j=1}^{N_{pep}} ({k^d}_{i,j}{C^N}_{ij} - {k^a}_{i,j}F_jN_i) \quad \text{(B.10)}$$

$$\frac{dE_i}{dt} = 2(1-\phi)\,{k_p}^N \sum_{j=1}^{N_{pep}} {C^N}_{ij} + \sum_{j=1}^{N_{pep}} (2{k^E}_p{C^E}_{ij} + {k^d}_{i,j}{C^E}_{ij} - {k^a}_{i,j}F_jE_i) \quad \text{(B.11)}$$

Substituting Eqs. (B.6-B.7) into Eqs. (B.10-B.11), and adding the death terms δ_N and δ_E, and the thymic output H_i we finally have

$$\frac{dN_i}{dt} = H_i + (2\phi - 1)\,{k_p}^N \sum_{j=1}^{N_{pep}} {K^N}_{ij}\,F_jN_i - \delta_N N_i \quad \text{(B.12)}$$

$$\frac{dE_i}{dt} = 2(1-\phi)\,{k_p}^N \sum_{j=1}^{N_{pep}} {K^N}_{ij}\,F_jN_i + \sum_{j=1}^{N_{pep}} {k^E}_p\,{K^E}_{ij}\,F_jE_i - \delta_E E_i \quad \text{(B.13)}$$

B.2 The kinetics of peptides

Peptides are generated intracellularly by the degradation of intracellular proteins via the proteasome machinery. Moreover, these proteasome products are processed further in the ER, where they bind to MHC molecules. We assume that peptides are processed intracellularly by the APCs at the site of infection. The homing mechanism of the APC from the site of infection to the secondary lymphoid tissue is considered to evolve with a fast kinetics. This hypothesis allows to consider only a generic APC presenting all peptides on its surface. We can then write

$$P_i + E \underset{k_-}{\overset{k_+}{\rightleftharpoons}} S_i \tag{B.14}$$

$$Z = M_T - \sum_{j=1}^{N_{pep}} S_j \tag{B.15}$$

where $k = \frac{k^-{}_j}{k^+{}_j}$, M_T is the total amount of MHC molecules available in the intracellular environment of APCs. S_i is the total number of MHCp complexes which mount the peptide i. P_i is the available peptide abundance, and Z is the number of free MHC molecules. The equation for MHC-peptide complexes is obtained from Eq. (B.14)

$$\frac{dS_i}{dt} = k_1 * P_i(M_T - \sum_{j=1}^{N_{pep}} S_j) - k_{-1}S_i) \tag{B.16}$$

Substituting the last equation in the Eq. (B.15), and considering the QSS approximation $\frac{dS_i}{dt} = 0$ the following equation is obtained

$$S_i = \frac{k_i P_i M_T}{\sum k_j P_j + 1} \tag{B.17}$$

Finally, the number of free sites can be written as

$$F_j = S_j - \sum_{j=1}^{N_{clone}} (C^N{}_{i,j} + C^E{}_{i,j}) \tag{B.18}$$

Substituting in the last relation the steady state values for $C^N{}_{i,j}$ and $C^E{}_{i,j}$ (Eqs. (B.6-B.7), the equation for the free MHC-peptide complex F_j read

$$F_j = \frac{S_j}{1 + \sum_{l=1}^{N_{clone}} (K^N{}_{l,j} N_l + K^E{}_{l,j} E_l)} \tag{B.19}$$

Appendix C

Clonal expansion

C.1 Fokker-Planck equation for the Ornstein-Uhlembeck process

The Fokker Planck equation for the Ornstein Uhlembeck [Risken, 1989] read

$$\frac{\partial p}{\partial t} - \frac{\partial kxp}{\partial x} = \frac{D}{2}\frac{\partial^2 p}{\partial x^2} \tag{C.1}$$

writing

$$x = v' \qquad k = 1 \qquad D = \gamma^2\sigma^2 T \tag{C.2}$$

$$p(x, t; x_0, t_0) = \rho \tag{C.3}$$

we obtain

$$\frac{\partial \rho}{\partial t'} - \frac{\partial v'\rho}{\partial v'} = \frac{\gamma^2 T\sigma^2}{2}\frac{\partial^2 \rho}{\partial v'^2} \tag{C.4}$$

Let consider the following initial condition

$$p(x, t_0; x_0, t_0) = \delta(x - x_0) \tag{C.5}$$

The solution can be easily obtained writing the characteristic function for the joint probability p defined as the average value of the variable e^{isx}

$$\phi(t, s) = \langle e^{(isx)} \rangle = \int_{-\infty}^{+\infty} p(x)e^{isx}dx \tag{C.6}$$

The Fokker Planck equation written for $\phi(s, t)$ now is

$$\frac{\partial \phi}{\partial t} + ks\frac{\partial \phi}{\partial s} = -\frac{1}{2}Ds^2\phi \tag{C.7}$$

This is obtained from the following property of the Fourier operator F

$$F(\frac{\partial^n p}{\partial x^n}) = -is^n F(p) \tag{C.8}$$

We are now left with a hyperbolic partial differential equation of the first order. We can therefore apply the method of the characteristic equation. Consider the space S defined from the variables s, t, ϕ, and two manifolds defined by

$$u(s,t,\phi) = a \qquad v(s,t,\phi) = b \tag{C.9}$$

Writing $J(s,t,\phi) = \theta(s,t) - \phi$ the solution of Eq. (C.7) can be found in an implicit form solving the equation

$$J(s,t,\phi) = 0 \tag{C.10}$$

namely the solution is found through all the manifolds $\phi(t,s) = F(u,v)$, which are defined in the generic point $P(t,s,\phi)$ of the space S in the tangent plane π

$$\begin{gathered} d\frac{\partial\phi}{\partial t} + e\frac{\partial\phi}{\partial s} = c \\ d = 1 \\ e = ks \\ c = -\tfrac{1}{2}Ds^2\phi \end{gathered} \tag{C.11}$$

Imposing the invertibility of the function J, the linear relation between the normal versors to the two manifolds defined by u e v, and using the equation for the tangent plane, we obtain

$$\frac{dt}{1} = \frac{ds}{ks} = -\frac{d\phi}{\frac{1}{2}Ds^2\phi} \tag{C.12}$$

he integrals of these equations are

$$s(t) = ae^{kt} \qquad \phi(s) = be^{\frac{Ds^2}{4k}} \tag{C.13}$$

We note that the dependence of the characteristic curves $t(x), s(x)$ with x is not explicit, therefore, we can take as evolution parameters the two generic surface u e v. Supposing a generic relation $v = g(u)$ we obtain

$$\phi(s,t) = e^{-\frac{Ds^2}{4k}} g\left[se^{-kt}\right] \tag{C.14}$$

the function g is determined by the initial condition on p

$$p(x, 0|x_0, 0) = \delta(x - x_0) \tag{C.15}$$

this implies

$$\phi(s, 0) = e^{ix_0 s} \tag{C.16}$$

$$g(s) = e^{\frac{Ds^2}{4k} + ix_0 s} \tag{C.17}$$

Substituting the last equation in Eq. (C.14)

$$\phi(s, t) = \exp\left[-\frac{Ds^2}{4k}\left(1 - e^{-2kt}\right) + isx_0 e^{-kt}\right] \tag{C.18}$$

The solution is a Gaussian function in the space defined by the variable s. Anti-transforming ϕ, a Gaussian function is found as well, characterized by

$$\begin{aligned} \langle x(t)\rangle &= x_0 e^{-kt} \\ \sigma^2(t) &= \frac{D}{2k}\left[1 - e^{-2kt}\right] \end{aligned} \tag{C.19}$$

we can now write the solution for the vitality v

$$\rho(v) = \frac{\exp - \frac{(v - <v>(t))^2}{2\sigma^2(t)}}{\sqrt{2\pi\sigma^2(t)}} \tag{C.20}$$

clearly, the stationary solution is obtained in the limit $t \to \infty$. the mean of the vitality and its standard deviation are then 0 e $\frac{D}{2k}$

$$\begin{aligned} \sigma^2(t) &= \gamma^2\sigma^2\frac{T}{2}(1 - e^{-2t/T}) \\ < v > (t) &= v_\infty + (1 - v_\infty)e^{-t/T} \end{aligned} \tag{C.21}$$

C.2 Strong damping approximation

Such approximation for the proposed deterministic model

$$\frac{dx}{dt} = v \tag{C.22}$$

$$\frac{dv}{dt} = -\beta v + F(t) - V'(x) \tag{C.23}$$

consists in neglecting the term dv/dt when β^{-1} is small with respect to a typical time scale of the system without damping. We have chosen both $F(t)$ and $V(x)$ proportional to ω^2, where ω^{-1} defines such a scale. Indeed if $F = 0$ the period of oscillations around the minima scales as ω^{-1}. If $V = 0$ such a scale is given by the pulse duration T, as one can check directly by solving the linear equation, and we choose T of order ω^{-1}.

When $\beta \gg \omega$ the equations (C.23) are approximated by the first order equation

$$\beta \frac{dx}{dt} = F(t) - V'(x) \tag{C.24}$$

Taking into account the definition for $F(t)$ and $V(t)$ given in Chapter 5, introducing the rescaled time $t' = t\,\omega^2/\beta$ and pulse duration $T' = T\,\omega^2\beta$ equation (C.24) reads

$$\begin{aligned} \frac{dx}{dt'} &= \begin{cases} \sigma(x) + F_0 & t' < T' \\ \sigma(x) & t' > T' \end{cases} \\ \sigma(x) &= \begin{cases} -1 & 2n-2 < x < 2n-1 \\ 1 & 2n-1 < x < 2n \end{cases} \end{aligned} \tag{C.25}$$

Solving with initial condition $x(0) = 0$ we obtain

$$x(t') = (F_0 - 1)\,t' \qquad 0 < t \le t'_1 = \frac{1}{F_0 - 1} \tag{C.26}$$

$$x(t') = 1 + (F_0 - 1)\,(t' - t'_1) \qquad t'_1 < t \le t'_2 = t'_1 + \frac{1}{F_0 + 1} \tag{C.27}$$

$$x(t') = 2 + (F_0 + 1)\,(t' - t'_2) \qquad t'_2 < t \le t'_3 = t'_2 + \frac{1}{F_0 - 1} \tag{C.28}$$

where $x(t'_1) = 1$, $x(t'_2) = 2$, $x(t'_3) = 3$ and so on until some n such that $t'_{2n-1} < T' < t'_{2n+1}$. Then, for $T' < t'_{2n}$, the point reaches $x = 2n$ and stops; in the last interval $[x(T'), 2n]$ the points slows down changing its speed to 1. Instead, for $T' > t'_{2n}$, the point overcomes the equilibrium point and after reaching $x(T') > 2$ comes back, with speed 1, to the equilibrium point. In Fig. C.1 we show the piecewise linear trajectories which can be followed to reach a minimum of $V(x)$.

The times at which the maxima $2n - 1$ and the minima $x = 2n$ of $V(x)$ are reached are given by the recurrence

$$t'_{2n-1} = t'_{2n-2} + \frac{1}{F_0 - 1} \qquad t'_{2n} = t'_{2n-1} + \frac{1}{F_0 + 1} \tag{C.29}$$

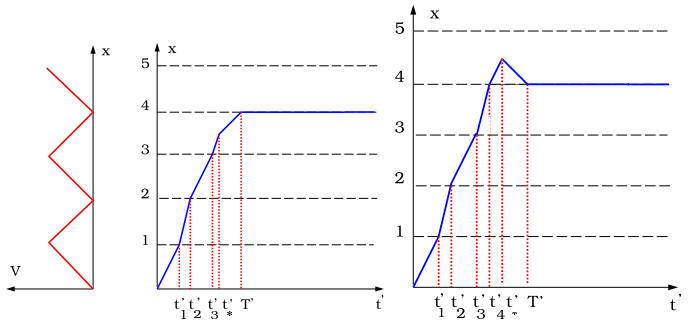

Figure C.1: Sawtooth landscape and time evolution $x(t)$. Left panel : $t'_3 < T' < t'_4$ the second minimum is not overcome. Left panel : $t'_4 < T' < t'_5$ the second minimum is overcome and it is reached after an expansion up to a larger value. For this figure $\omega = 1$ has been chosen.

whose solution reads

$$t'_{2n} = \frac{n}{F_0 - 1} + \frac{n}{F_0 + 1} \qquad t'_{2n+1} = \frac{n+1}{F_0 - 1} + \frac{n}{F_0 + 1} \tag{C.30}$$

so that the condition for the trajectory to end in the interval $[2n-1,\, 2n+1]$ stopping at the minimum $x = 2n$ is $t'_{2n-1} < T' < t'_{2n+1}$ from which equations (C.26-C.28) follow.

Weak damping approximation

An analytical study of the the problem is still possible in the weak damping approximation ($\beta \ll \omega$), which is basically a first order perturbative expansion in β. We show only how to construct the solution in the interval $0 < x < 1$, starting with initial conditions $x(0) = v(0) = 0$. The equations are

$$\begin{aligned} \frac{dx}{dt} &= v \\ \frac{dv}{dt} &= -\beta v + \omega^2 (F_0 - 1) \qquad 0 < x < 1 \end{aligned} \tag{C.31}$$

In order to compute the solution, the function H wis introduced, which satisfies the following equation

$$H = \frac{v^2}{2} - \omega^2 (F_0 - 1)\, x \qquad \frac{dH}{dt} = -\beta v^2 \tag{C.32}$$

The unperturbed solution, $\beta = 0$, reads $x(t) = \frac{1}{2}\omega^2 \,(F_0 - 1)\, t^2$, and the time to reach $x = 1$ is $t_1 = \omega^{-1} \sqrt{2/(F_0 - 1)}$. The first order of the perturbative

expansion is computed according to

$$\begin{aligned} H(x,v) - H(0,0) &\equiv \frac{v^2}{2} - \omega^2(F_0-1)x = -\beta \int_0^t \omega^4 \,(F_0-1)^2\, t'^2\, dt' \\ &= -\beta\, \omega^4 (F_0-1)^2 \frac{t^3}{3} \end{aligned} \tag{C.33}$$

where t is expressed in terms of x using the unperturbed solution. As a consequence

$$v = \omega\sqrt{2(F_0-1)}\, x^{1/2}\, 1 - \frac{4}{3}\,\frac{\beta\, x^{1/2}}{\omega\sqrt{2(F_0-1}}\left(1 - \frac{4}{3}\,\frac{\beta\, x^{1/2}}{\omega\sqrt{2(F_0-1}}\right)^{1/2} \tag{C.34}$$

$$\simeq \omega\sqrt{\underline{2(F_0-1)}}\, x^{1/2} - \frac{2}{3}\beta x \tag{C.35}$$

Solving $dx/dt = v(x)$ by separation of variables we find at the first order in β the solution $x(t)$ and the time t_1 at which the first maximum is reached (provided that $T_1 < T$)

$$x = \frac{\omega^2}{2}\,(F_0-1)\,t^2 - \frac{3}{4}\,\beta\, t^3\left(t^2 - \frac{3}{4}\,\beta\, t^3\right) \qquad t_1 = \frac{1}{\omega}\,\sqrt{\frac{2}{F_0-1}} + \frac{3}{4}\,\frac{\beta}{\omega(F_0-1)} \tag{C.36}$$

Appendix D

Ageing

D.1 Asymptotic expansions

The survival probability is 1/2 at the time T where the average of the vitality vanishes.

$$S(T) = \frac{1}{2}\,\mathrm{Erf}(0) = \frac{1}{2} \qquad \langle\, v(T)\,\rangle = 0 \tag{D.1}$$

The next properties are related to the as asymptotic behavior of $S(t)$ for $t \to 0$ and $t \to +\infty$. In order to obtain them we need asymptotic expansion of the error function $E(x)$ [M.Abramowitz and Stegun, 1972] for $x \to +\infty$

$$E(x) \equiv \frac{1}{\sqrt{2\pi}} \int_x^{+\infty} e^{-u^2/2}\, du = \frac{e^{-x^2/2}}{x\,\sqrt{2\pi}}\, 1 - \frac{1}{x^2} + \frac{3}{x^4} + \ldots \left(1 - \frac{1}{x^2} + \frac{3}{x^4} + \ldots\right) \tag{D.2}$$

and for $x \to -\infty$

$$E(x) = 1 - E(-x) = 1 + \frac{e^{-x^2/2}}{x\,\sqrt{2\pi}}\, 1 - \frac{1}{x^2} + \frac{3}{x^4} + \ldots \left(1 - \frac{1}{x^2} + \frac{3}{x^4} + \ldots\right) \tag{D.3}$$

When t approaches 0 the survival $S(t)$ approaches 1 with an horizontal tangent. The mortality rate exponentially goes to zero ($exp(-1/t)$). In order to prove it, we notice that the mean value of $v(t)$ tends to a constant, whereas the variance is $\sigma(t) = \epsilon\sqrt{t}$. This behavior is also found in a Wiener process when t tends to 0. As a consequence writing $S(t) = E(x(t)$ where

$$x(t) = -\frac{\langle\, v\,\rangle}{\sigma(t)} \simeq -\frac{v_0}{\epsilon\sqrt{t}} \tag{D.4}$$

and using the asymptotic expansion Eq. (D.2), we have

$$S(t) = 1 - \frac{\exp(-\frac{{v_0}^2}{\epsilon^2 t})}{2\pi\frac{v_0}{\epsilon\sqrt{t}}} \tag{D.5}$$

The mortality rate for $t \to 0$ is given by

$$R(t) \simeq -\frac{\dot{S}}{S} = \frac{\epsilon v_0}{2\sqrt{2\pi}} \frac{\exp(-\frac{{v_0}^2}{\epsilon^2 t})}{t^{3/2}} \tag{D.6}$$

Curriculum vitae

Personal data

Dottore in Fisica Fabio Luciani
Invalidenstr. 143
D-10115 Berlin
Tel.: (+49) (30) 24 63 2004
E-mail: f.luciani@biologie.hu-berlin.de

Date of birth: April 18$^{\text{th}}$, 1974
Place of birth: Lanciano, Italy
Citizenship: italian

Degree

M.Sc. in Physics, Bologna University, Bologna, Italy

Diploma thesis: *Modelli fisico-matematici per la memoria immunological e l'immunosenescenza*
Final exam date: June. 12$^{\text{th}}$, 2000
Final exam grade: very good (110/110 *summa cum laude*)

Education

July 2002 – June 2005	PhD student in the Institute for Theoretical Biology, Humboldt University, Berlin, Germany Group of Dr. Michal Or-Guil
Sept. 2001 – June 2005	PhD student in the Max Planck Institute for the physics of Complex System, Dresden, Germany Group of Prof. Marcus Baer
Sept. 1995 – June 2000	Student of Electrical Engineering at the Univerista degli studi Federico II, Napoli, Italy
Oct. 1993 – June 1995	Student of Physics at the Bologna University, Bologna, Italy
Sep. 1988 – Jun. 1993	High School "Liceo Scientifico G. Galilei", Lanciano, Italy

Fellowships

Jan. 2004 – Feb. 2004	Utrecht University, Utrecht (Niederland), cooperation (7 weeks) with the group of Prof. Rob J. de Boer
Feb. 2003 – Mar. 2003	Utrecht University, Utrecht (Niederland), cooperation (7 weeks) with the group of Prof. Rob J. de Boer
Sept. 2001	Winner of the national competition for grants awarded by the Bank "Banca Popolare di Lanciano e Sulmona" to recent graduates for the best Laurea thesis with marks *Summa cum laude*, (Lanciano, Italy)
Nov. 2000	Winner of the national competition "Premio Lando Caiani ", awarded by SISSA, International School for Advanced Studies, Trieste (Italy): best Laurea thesis in Theoretical Physics of the year 2000, in the field of statistical physics and complex systems. (Trieste, Italy)

List of publications

Luciani et al. [2001b]
Luciani et al. [2001a]
Turchetti et al. [2002]
Luciani et al. [2003]
Turchetti et al. [2003]
Luciani et al. [2005]
Luciani and Or-Guil [2005]

Poster and Talks

Luciani [2001]
Luciani [2002a]
Luciani [2002b]
Luciani [2003]
Luciani [2004c]
Luciani [2004a]
Luciani [2004b]
Luciani [2005]

Abbreviations

Abbreviation	Description
IS	Immune System
IR	Immune Response
APC	Antigen Presenting Cell
DC	Dentritic cell
TCR	T-Cell Receptor
ER	Endoplasmatic Reticulum
MHC	Major Histocompatibility Complex
MHCp	MHC-Peptide Complex
COP	Core Particle
CIS	Chronic Immune Stress
AE	Antigen Experienced
ANE	Antigen Non-Experienced
LCMV	Lymphocytes Choriomeningitis Virus
CP	Constitutive Proteasome
IP	Immunoproteasome

Acknowledgments

First of all, it is a pleasure to thank Dr. Michal Or-Guil for giving me the opportunity to work in a very free environment on my Ph.D. at the Institute for Theoretical Biology, Humboldt University Berlin. Michal showed a lot of patience with my “wild style" of science, and she trusted on me during some difficulties I encountered during these four years of work in her lab. Now I am much more focused and less chaotic: thanks!

My Family again played a fundamental role: “Vi ringrazio con affetto Mamma, Papa e Marcella: senza di voi non ci sarei mai riuscito."

The Volkswagen Foundation is acknowledged for the financial support.

Special thanks to Rob de Boer and Can Kesmir for their important help and experience in theoretical immunology. They have been also good friends. I want to thank my best friends Pierluigi, Bubetto, Luciano, Margherita and Barbara: they were extremely important for me to keep in contact with my traditions and to be equilibrated during my permanence in Berlin. Special thanks go to my “Berlin friends" Maurizio, who gave me the necessary psycological support, and to Bianca, Elisa and Alberta. Many thanks to Alberta for helping me with the german language: “Grazie tante!". I also want to thank Luca and Riccardo, which are following my steps: “ragazzi non copiate la mia vita berlinese!". I would never forget my sport-friends, and in particular Tom Krüger: "Danke, Ich werde euch niemals vergessen!".

I am very greatful to Prof. Claudio Franceschi and Prof. Giorgio Turchetti: they introduced me to the field of theoretical immunology six years ago!

I en joyed great discussions with Michele Mishto, Niels Blüthgen, Hanspeter Herzel, George Carneiro, Victor Tapia, Nicole Wittenbrink, Nicole Bruni, and Christian Waltermann.

Last but not least, I would like to thank Francesca who gave me the necessary support: “Cara Franci, sai bene quanto sia stato difficile la nostra relazione in questi anni...ma ce l’abbiamo fatta!"

Figure Acknowledgements

The permission to adapt and reproduce the following figures is greatfully acknowledged: Fig. 1.2 from Yewdell et al., 2003, copyright 2003 by Nature Publisher; Fig. 3.3 from Arnaout and Nowak, 2000, copyright 2000 by Elsevier Publisher.

Selbständigkeitserklärung

Hiermit erkläre ich, dass alle verwendeten Hilfsmittel und Hilfen in dieser Arbeit angegeben worden sind. Ich versichere, dass die Dissertation auf dieser Grundlage von mir selbständig erarbeitet und verfasst wurde.

Berlin, 11. Juli 2005

Fabio Luciani